OPTIMIZATION OF INJECTION INTO VAPOR-DOMINATED GEOTHERMAL RESERVOIRS CONSIDERING ADSORPTION

A Report Submitted to the Department of Petroleum Engineering and the Committee on Graduate Studies of Stanford University in Partial Fulfillment of the Requirements for the Degree of Master of Science

by

Roman B. Sta. Maria

May 1996

I certify that I have read this report and that in my opinion it is fully adequate, in scope and in quality, as a project report for the degree of Master of Science.

_____

Roland N. Horne
(Adviser)

Abstract

Physical adsorption and capillary pressure are major factors governing the behavior of vapor-dominated geothermal reservoirs. These mechanisms affect both the estimation of the reserves and the production performance of the field. The effectiveness of water injection programs to sustain the field's productivity is also affected. This study investigated the influence of adsorption and capillary pressure on injection into vapor-dominated reservoirs. The objective was to determine the most effective injection strategy once these two effects are considered.

Geothermal reservoir simulators that account for the effects of adsorption and curved interface thermodynamics are now available. Hence, simulation was adopted as the analysis tool. It was determined that the hysteresis and temperature dependence of the adsorption and capillary properties are issues that still need to be addressed in available simulators.

Water injection into a vapor-dominated reservoir may increase the prevailing reservoir pressure. Although this improves field productivity, injection also increases the water retention capacity of the reservoir rocks through adsorption and capillary condensation. Thus it was found that increasing the injection rate will result in a greater fraction of injectate remaining unproduced when the same pressure drawdown is imposed.

It was determined that the most effective strategy will be to constrain the water injection rate so that breakthrough of injectate in the production area is delayed as long as possible. Because of the costs associated with injection, optimizing an injection program involves not only maximizing the energy yield from the resource but also the net present worth of the project.

It was found that comparable energy yield can be attained for injection programs that are initiated at various stages of the field's development. Higher injection rate is desirable when the injection program starts later in the productive life of the field. Considering the economics of the project, it is best

to implement the injection program during the later stages of the field's development. This way, a greater fraction of the injectate can become available for production and at the same time optimize the present worth of the project.

Acknowledgments

I would like to express my sincere gratitude to Prof. Roland Horne. His guidance during the course of my research and his confidence in allowing me to explore my ideas have broadened my understanding of various aspects of geothermal exploitation technology.

I also want to thank Shaun Fitzgerald (Stanford Geothermal Program), Willis Ambusso (Stanford Geothermal Program), Al Pingol (UNOCAL), Mike Shook (INEL), and Kok-Thye Lim (ARCO E&P Technology) for their helpful suggestions and comments.

Special thanks to Unocal Corporation and Philippine Geothermal Incorporated for the encouragement and moral support they have extended to me.

Last but not least, I would like the acknowledge the support given by U.S. Department of Energy, Geothermal Division.

Table of Contents

List of Tables

List of Figures

1. Introduction

1.1 Objectives

The ability to model the effect of water injection into vapor-dominated reservoirs is of great interest to the geothermal industry. Experience has shown that vapor-dominated systems are prone to run out of water even though vast amounts of heat still remain in the reservoir. It has been established through research and field studies that water injection into the reservoir can provide artificial mass recharge to improve steam production from the field (Enedy et al, 1991). However, if done incorrectly injection may have detrimental effects on production (Barker et al., 1991). Clearly, an appropriate injection program is a major component of resource management for vapor-dominated systems.

Adsorption and capillary pressure are major factors affecting the behavior of vapor-dominated geothermal reservoirs. These mechanisms affect both the estimation of the reserves and the production performance of the field. The effectiveness of water injection programs to sustain the field's productivity is also affected. Hence the optimization of an injection strategy should include consideration of these effects.

A major motivation for the study of the effects of adsorption in geothermal reservoirs is the phenomenon known as "The Geysers Paradox". Data from The Geysers geothermal field suggests that even though the reservoir is vapor-dominated some liquid water must be stored in the reservoir. This was an apparent paradox because the phenomenon can be observed even though the prevailing reservoir pressure and temperature suggest superheated conditions. According to conventional concepts of flat interface equilibrium thermodynamics, liquid water and steam can coexist only under saturated conditions.

Physical adsorption of steam onto rocks and the thermodynamics of curved interfaces prevailing in the pore spaces of the rock matrix can explain the apparent paradox. These mechanisms make it

possible for water and steam to coexist under conditions we normally refer to as “superheated” based on our concept of flat interface thermodynamics (i.e., the Steam Table).

Studies in the past have shown that the performance of a vapor-dominated geothermal reservoir can be strongly affected by adsorption (Hornbrook, 1994). The adsorbed condensed phase represents most of the fluid mass in the reservoir. Thus, this adsorbed phase sustains production beyond what might be expected for a reservoir filled only with vapor. While this is beneficial in terms of resource longevity, adsorption complicates the analysis of the reservoir because the condensed phase is “invisible” (Horne et al., 1995).

Furthermore, the effectiveness of water injection to sustain production of a vapor-dominated reservoir may also be affected by adsorption. Understanding how adsorption and capillarity affect water injection is particularly relevant at this time because of the plans to increase water injection into The Geysers geothermal field. Although water injection has been ongoing for many years, injection rates will increase significantly when water from Lake County, and possibly the city of Santa Rosa, becomes available for injection. An accurate prediction of the performance of the reservoir under this new condition is desired by the field operators.

Numerical simulation is an effective method to forecast the performance of a geothermal reservoir. Until recently, simulators have used flat interface thermodynamics to define the phase of the reservoir. However, the development of new simulation codes has enabled the effects of adsorption and curved interface thermodynamics to be incorporated. This study makes use of these new simulators to investigate the effects of adsorption and capillary pressure on water injection into vapor-dominated geothermal reservoirs. The ultimate objective of this study is to optimize water injection into a hypothetical vapor-dominated geothermal field.

1.2 Overview of the Report

This report begins with a review of the previous work done in the development of the theory regarding steam adsorption in geothermal reservoirs. The basic concepts pertaining to the applicability of flat interface and curved interface thermodynamics to describe the physics prevailing in the reservoir will be covered. The mechanics of physical adsorption and capillary condensation, and their influence on geothermal exploitation will be discussed.

The results of the preliminary work performed will be discussed. Two simulation codes were evaluated, TETRAD and GSS. Using similar models, the production performances of the models were simulated using both TETRAD and GSS. Cases with and without adsorption and capillary pressure were considered. The results of this preliminary study and the reasons for choosing TETRAD over GSS will be explained.

Another preliminary study about the effects of adsorption on production and injection operations was conducted. Using simple reservoir models, the process of injection and production to and from vapor-dominated reservoirs were investigated.

A hypothetical field-scale model of a vapor-dominated reservoir was then constructed. Using this model, various injection strategies to maximize steam production from the reservoir were considered. The parameters that were investigated in this study are: 1) how much water to inject; and, 2) when to inject it.

An economic model using an incremental cashflow method was constructed for the various injection schemes. Cost functions for capital and operating expenses for the injection project were established. Another optimization was performed with the objective of maximizing the net present worth of the injection project.

Finally the conclusions from this study are presented.

2. Previous Work

Steam adsorption in geothermal reservoirs and its effects on geothermal field performance during exploitation have been an area of active research for several years. Much of our understanding of the phenomena has been gained through the results of adsorption experiments on geothermal reservoir rocks. However, the use of this information to forecast geothermal field performance has been possible only recently. The following discussion covers previous done work on adsorption theory and its implementation in geothermal reservoir simulation codes.

2.1 Theory

Physical adsorption is the phenomenon by which molecules of steam adhere to the surfaces of a porous medium. This phenomenon is caused mainly by Van der Waals forces. Desorption is the opposite of adsorption; it occurs when the adsorbed phase vaporizes due to pressure reduction. When sufficient deposition has taken place, a capillary interface may form and deposition due to capillary condensation becomes more significant. The transition from adsorption to capillary condensation is continuous. Both mechanisms cause vapor to condense onto the solid surface and reduces the apparent vapor pressure.

In addition to mass storage, adsorption affects other aspects of geothermal exploitation. The surface between the vapor and the liquid phases in a porous medium is not flat. It is a well-recognized phenomenon that the vapor pressure above the curved surface of a liquid is a function of the curvature of the liquid-vapor interface. Thus, curved interface thermodynamics is more appropriate than flat interface thermodynamics. The curvature of the surface gives rise to vapor pressure lowering (VPL), thus allowing liquid and vapor to coexist in equilibrium at pressures that are less than the saturation pressure.

Sorption (adsorption and desorption) and capillary condensation are affected by temperature. The general behavior is that the amount of the adsorbed phase increases as the temperature increases, and vice versa (Shang et al., 1993). In experiments performed at Stanford University, the amount of steam

condensing onto rocks is measured as a function of the relative vapor pressure (p_v/p_{sat}). This relationship, which is measured at a specific temperature, is called an adsorption isotherm. The desorption isotherm is measured when the process is reversed and the condensed phase vaporizes as the pressure is reduced.

Experiments show that adsorption and desorption are not exactly reversible processes. Measurements of adsorption and desorption isotherms show hysteresis. Rock heterogeneity effects on capillary condensation and irreversible changes in the rock pore structure during adsorption are the likely causes of this hysteresis (Shang et al., 1993). Because of this, the adsorption isotherm is different from the desorption isotherm.

2.2 Implementation

There are two main schools of thought about the implementation of curved interface thermodynamics in reservoir simulation. One focuses on capillary pressure while the other focuses on the adsorbed mass in reservoir rocks.

The focus on capillary pressure follows the work of Calhoun et al. (1949). Experimental studies were conducted to measure vapor pressure lowering and capillary retention of water in porous solid. The primary principle is described by Kelvin equation:

$$p_c = \frac{RT\rho_l}{M_w} \ln\left(\frac{p_{sat}}{p_v}\right) \qquad \textit{(Equation 2.1)}$$

where R is the universal gas constant, T is absolute temperature, ρ_l is water density, M_W is the water molecular weight, p_{sat} is the equilibrium vapor pressure (from the Steam Table) and p_v is the lowered vapor pressure. In the original formulation, 'p_c' denotes the capillary pressure. In recent published literature (Pruess et al., 1992), suction pressure (p_{suc}) is defined as numerically equal to p_c but with a negative sign. The term 'suction pressure' is preferred because it is recognized that the phenomenon

being observed involves not only capillarity but also adsorption. The suction pressure is the same mechanism that promotes imbibition of water into the pores of dry rocks.

Works by Pruess and O'Sullivan (1992) and Shook (1994) follow this line of thought and are now being implemented on the simulators TOUGH2 (Lawrence Berkeley National Laboratory), STAR (S-Cubed), and TETRAD Version 12 (also known as ASTRO).

The simulator TETRAD (Version 12) was used in this study. TETRAD is a commercial simulator that has been modified to account for vapor pressure lowering. Version 12 of the code use the generalized vapor pressure lowering algorithm developed in the Idaho National Engineering Laboratory (Shook, 1993). The algorithm follows on the earlier work by Holt and Pingol (1992) to modify the standard steam tables to account for vapor pressure lowering.

The other approach follows the work of Hsieh and Ramey (1978). It focuses on the measurement of the amount of adsorbed mass in reservoir rocks. If the dominant mechanism for liquid storage is adsorption, then measurement of sorption isotherms of water on reservoir rocks is deemed necessary.

Experimental data suggest that sorption isotherms may follow a Langmuir-type behavior, as described by a modified form of the Langmuir equation:

$$X = d\left\{\frac{c\left(\frac{p_v}{p_{sat}}\right)}{1+(c-1)\left(\frac{p_v}{p_{sat}}\right)}\right\} \qquad \textit{(Equation 2.2)}$$

where the parameters 'd' and 'c' represent the magnitude and the curvature of the adsorption isotherm (Hornbrook et al., 1994). The parameter 'X' is the mass adsorbed per unit mass of rock. The quantity (p_v/p_{sat}) is often denoted by the symbol β, referred to as the relative vapor pressure or the vapor pressure lowering factor. The isotherm that describes the relationship between sorption and relative vapor-pressure

accounts for both adsorption and capillary condensation. Several studies using this approach have been conducted by the Stanford Geothermal Program (work synopsis given by Horne et al., (1995)).

The implementation of this approach into a numerical simulator was accomplished in GSS (Geothermal Sorption Simulator), a simulator recently developed in Stanford University (Lim, 1995). GSS was specially developed to take into account adsorption and curved interface thermodynamics.

3. Preliminary Work

One of the initial steps taken in this study was to choose the simulator to be used in the injection optimization study. The simulators TETRAD and GSS were evaluated to compare results when using different formulations to account for adsorption as described in the preceding chapter. A simple reservoir model was constructed. Production forecasts were generated for cases with and without adsorption.

3.1 Choice of Simulator

3.1.1 TETRAD Versus GSS

The data required to incorporate vapor pressure lowering in numerical simulations is either a capillary pressure relationship (p_c versus S_w) or an adsorption isotherm (X versus β). TETRAD requires a capillary pressure relation. GSS requires an adsorption isotherm.

Figure 3.1 shows a plot of the Langmuir equation with coefficients of c=0.1 and d=0.0128. This adsorption isotherm is based on measurements conducted on some core samples from The Geysers geothermal field. The main difference of this Langmuir isotherm from the actual adsorption isotherm is the end value of adsorbed mass when the relative pressure is equal to 1.0. Actual measurements of adsorption isotherms do not reach this point, as measurements can only reach pressures which remain below saturation (for example, P_v/P_{sat} = 0.95).

Figure 3.2 shows the plot of the capillary pressure relation based on the adsorption isotherm. The two sets of data shown in Figure 3.1 and Figure 3.2 are equivalent. The conversion from one to the other is conducted through the Kelvin equation and an intermediate relation for X versus S_w. This relation is given by the equation:

$$S_w = \left(\frac{1-\phi}{\phi}\right)\left(\frac{\rho_r}{\rho_w}\right)X \qquad \textit{(Equation 3.1)}$$

where ϕ is the rock matrix porosity and ρ_r is the rock grain density.

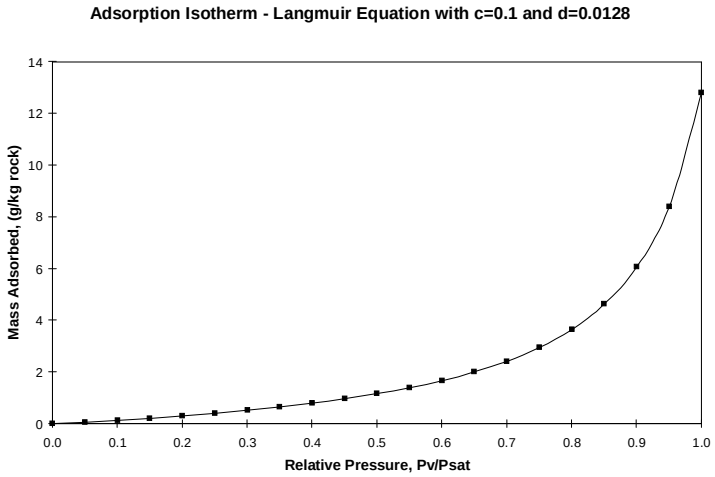

Figure 3.1: Typical Geysers adsorption isotherm.

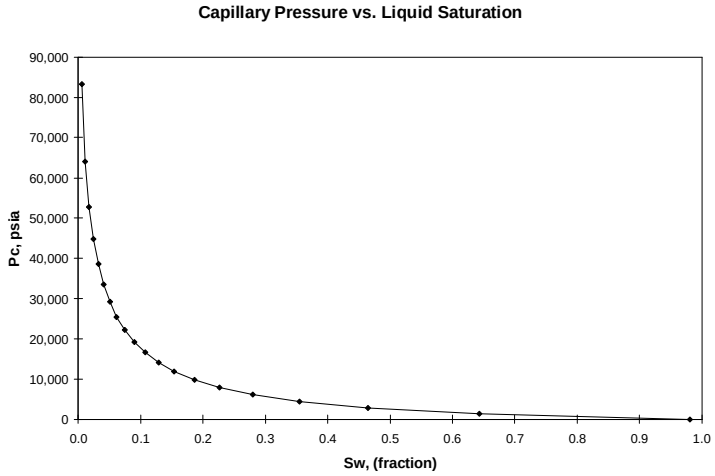

Figure 3.2: Adsorption isotherm in Figure 3.1 converted to a capillary pressure relationship.

The resulting p_c versus S_w relationship can be approximated by the van Genuchten equation (Pruess et al, 1994). This equation is expressed as follows:

$$p_c = p_o \left[S_{ef}^{-\frac{1}{\lambda}} - 1 \right]^{1-\lambda} \qquad \textit{(Equation 3.2)}$$

where $S_{ef} = (S_w - S_{wr})/(1-S_{wr})$ is the normalized (effective) liquid saturation. The term 'S_{wr}' is the residual liquid saturation and, P_o and λ are fitting parameters (Pruess et al., 1992).

Neither the Langmuir nor the van Genuchten equations can represent the empirical data over the entire range of relative pressure. The Langmuir equation breaks down over the range where capillary condensation is dominant (e.g. $\beta > 0.9$). On the other hand, the van Genuchten equation breaks down when water saturation is low (e.g., $S_w < 0.1$) and adsorption is dominant. Therefore, even if a simulator has the capability of using data in a parametric equation form, it is also important to have the ability to use data in tabular form. Both TETRAD and GSS have this capability.

One of the big advantages of GSS is that it is able to utilize the sorption isotherms from the experiments almost directly. The only data conversion needed is the translation of the isotherm measured in the laboratory to the appropriate reservoir temperature. It must be pointed out that the sorption experiments being conducted by the Stanford Geothermal Program do not exceed 300°F because of equipment limitations. Actual geothermal reservoir temperature far exceeds this value (e.g., > 450°F). Although not done in this study, the adsorption isotherm can be translated to the appropriate temperature by recognizing the temperature-invariant relationship between the adsorbed mass (X) and the activity coefficient (A) . The activity coefficient is defined as (Hsieh and Ramey, 1983):

$$A = RT \ln\left(\frac{1}{\beta}\right) \qquad \textit{(Equation 3.3)}$$

GSS uses this invariance relation to adjust the adsorption isotherm as the reservoir temperature changes as a result of exploitation (Lim, 1995).

The simplest way to enter a p_c versus S_w relationship into TETRAD is by using analytical functions of relative permeability and capillary pressure as a function of liquid saturation. However, the built-in analytical expression for capillary pressure,

$$p_c = a\left[1 - S_w\right]^b \qquad \textit{(Equation 3.4)}$$

where 'a' and 'b' are fitting parameters, is insufficient to represent the converted adsorption data. The van Genuchten expression is also available but was not used in this study. Instead, tabular input of relative permeability and capillary pressure relations were used.

3.1.2 The Evaluation Model

A simple model of a vapor-dominated reservoir was developed. The model has dual-porosity. Low permeability matrix blocks provide most of the storage while the fracture system provides the large scale permeability. In the initial state all liquid saturation resides in the matrix. Relative permeability is defined such that steam is the only mobile phase at the given liquid saturation. Adsorption property is patterned after those typically observed in The Geysers field. The data shown in Figure 3.1 and Figure 3.2 were used.

The reservoir model is comprised of a horizontal layer 100 feet thick and with lateral dimensions of 1,000 feet on both sides . A uniform 5-by-5 Cartesian grid with a total of 50 (dual porosity) gridblocks was used. The geometry of the model is illustrated in Figure 3.3.

Gridblock Dimensions: 200 ft x 200 ft x 100 ft

PROD				
				INJ

Figure 3.3: The model geometry used in the simulations.

3. PRELIMINARY WORK

The petrophysical properties (porosity, absolute permeability, sorption, and capillarity) for all the 25 fracture gridblocks and 25 matrix gridblocks are uniform. Initial thermodynamic state (pressure, temperature, and saturation) is also uniform throughout the model. The model reservoir properties are given in Table 3.1.

PROPERTY	MATRIX	FRACTURE
Porosity	4%	1%
Permeability	0.01 md	100 md
Initial liquid saturation	29%	0%
Initial reservoir pressure	400 psia	400 psia
Initial reservoir temperature	evaluated	evaluated
Rock density	165 lbs/cu-ft	N/A
Rock specific heat	0.245 Btu/lb-F	N/A
Adsorption isotherm	Modified Langmuir c = 0.1 and d = 0.0128	none
Relative permeability function	$k_{rl} = S_w^{*4}$ $k_{rv} = (1-S_w^{*2})(1-S_w^{*})^2$	same

Table .3.1: Dual porosity model properties.

The relative permeability function is based on the work of Sorey (1980). The parameter S_w^* is normalized to $S_{wc} = 0.35$ such that $S_w^* = \frac{(S_w - S_{wc})}{(1 - S_{wc})}$. The appropriate reservoir temperature is evaluated based on the reservoir pressure, phase saturation, and the magnitude of the vapor pressure lowering.

The model is essentially a closed tank. The model boundaries are closed to mass and heat flows. The only way mass and energy can flow in and out of the systems are through the wells. A production well was placed in one corner of the model and an injection well was placed in the corner diagonally opposite. The maximum production rate of the well is constrained to 10,000 lbs/day. The minimum flowing bottomhole pressure was constrained to 100 psia. The water injection rate can be imposed arbitrarily.

The initial state of the model was checked for equilibrium by running the model for 10,000 days without production and injection. Equilibrium was confirmed by the stable thermodynamic properties

through time. All of the subsequent predictive simulations are run for 10,000 days. Production and injection operations always begin at day zero and terminate at 10,000 days.

The model described above was constructed using both TETRAD and GSS. The TETRAD model and the GSS model are only approximately similar because there are differences in input formats of the two simulators. The simulation data decks of the TETRAD and GSS evaluation models are listed in Appendix A and Appendix B, respectively. Zero timestep runs were performed for the models to check the consistency of their initial mass and energy in-place. It was immediately apparent that although the masses in-place are consistent, the heats in-place are not. GSS computed an initial heat-in-place that is about 33.5% greater than TETRAD's calculation. A manual calculation of the heat in-place verified the result of TETRAD. A cursory inspection of the GSS source codes did not reveal an obvious source of error.

It was decided that the heat in-place discrepancy of the two simulators can be ignored for this phase of the study. The production rates are low enough such that only a small fraction of the initial heat in-place will evolve during a 10,000 days simulation (less than 5%). The models were simulated with production operation only. The objective was to investigate the differences in production, reservoir pressure, reservoir temperature, and matrix water saturation through time with and without adsorption and vapor pressure lowering.

3.1.3 Without Adsorption and Vapor Pressure Lowering

Figures 3.4, 3.5, 3.6, and 3.7 show the results of TETRAD and GSS with the model undergoing production. The thermodynamic state of the model is governed by the flat interface thermodynamics (i.e., no vapor pressure lowering).

Figure 3.4 shows the comparison of steam production rates though time. The results are practically identical. Both simulators predicted a drastic decline of production as the reservoir dries-out at about 6,000 days.

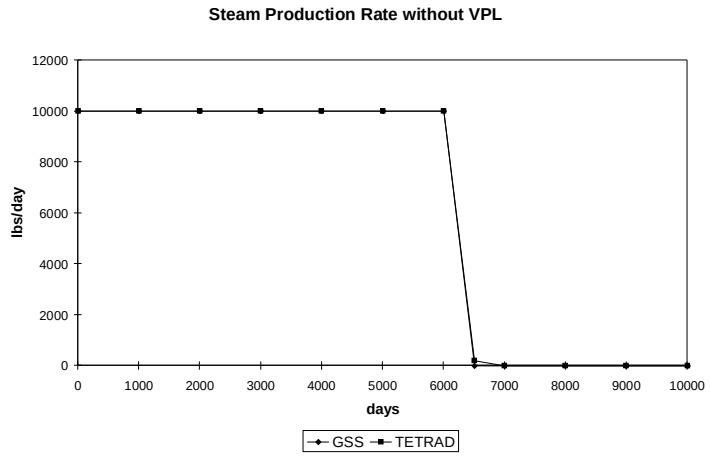

Figure 3.4: Comparison of steam production rates through time without VPL.

Figure 3.5 shows the comparison of reservoir pressure behavior. After a very gradual decline, the reservoir pressure dropped drastically as the reservoir dried-out.

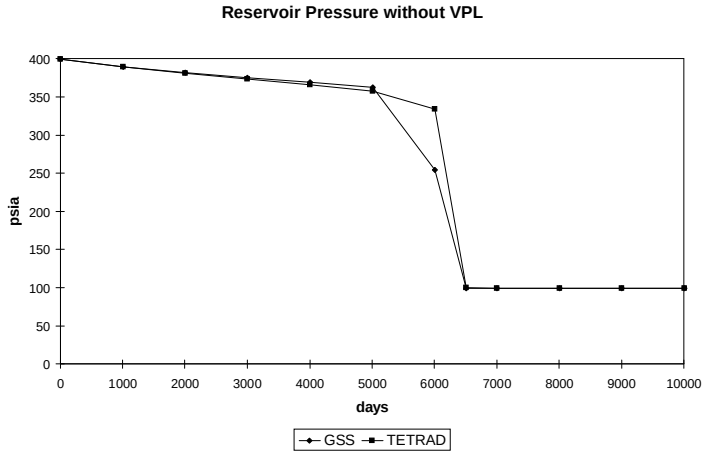

Figure 3.5: Comparison of reservoir pressure through time without VPL.

Figure 3.6 shows the comparison of reservoir temperature. Although the two models started with the same reservoir temperature of 445^{o}F (this is the saturation temperature at 400 psia reservoir pressure), significant deviations can be observed in the later stages of the simulation. The GSS model ends up being hotter than the TETRAD model. This temperature deviation can be attributed to the greater heat in-place being calculated by GSS.

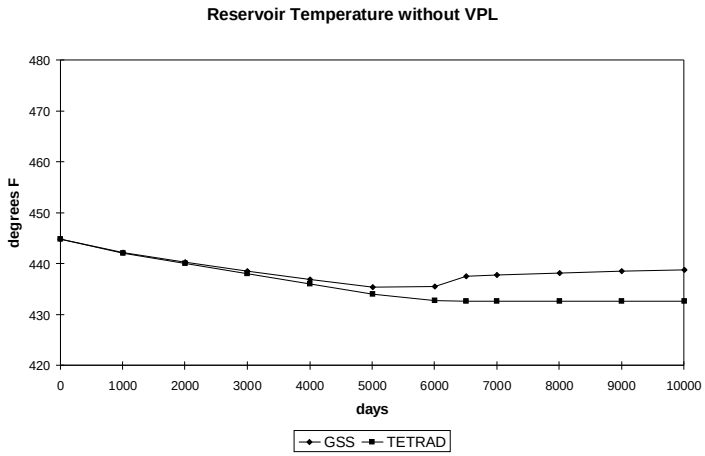

Figure 3.6: Comparison of reservoir temperature through time without VPL.

Figure 3.7 shows the comparison of matrix water saturation through time. The results are close and show that the reservoir will be completely dry after 6,000 days of production.

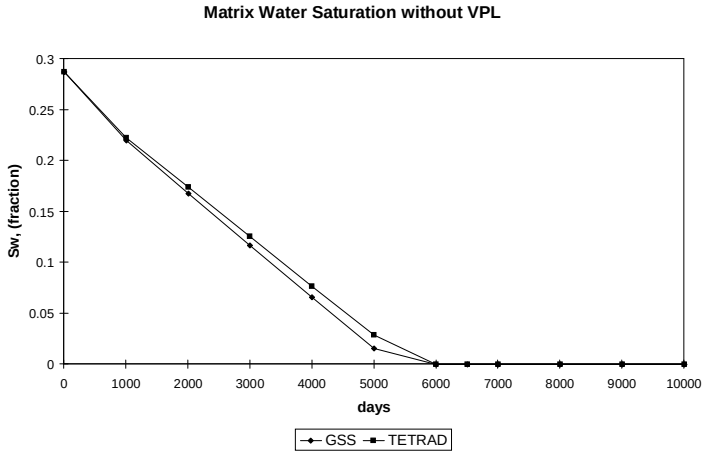

Figure 3.7: Comparison of matrix water saturation through time without VPL.

These results show the classic behavior of a system governed by flat interface thermodynamics. Gradual productivity decline followed by catastrophic decline when the reservoir dries-out are expected. The complete dry-out of the matrix is also an expected behavior. Ignoring the obvious discrepancy in heat-in-place and reservoir temperature, for the purpose of this study the TETRAD and GSS models can be considered equivalent.

3.1.4 With Adsorption and Vapor Pressure Lowering

Figures 3.8, 3.9, 3.10, and 3.11 illustrate the results of TETRAD and GSS with the model undergoing production and the state of the system is governed by curved interface thermodynamics (i.e., with vapor pressure lowering).

Figure 3.8 shows the comparison of steam production rates though time. The results are quite close. Both simulators predicted a decline of well productivity starting at about 5,000 days. Note that the decline was observed about 1,000 days earlier than the previous case.

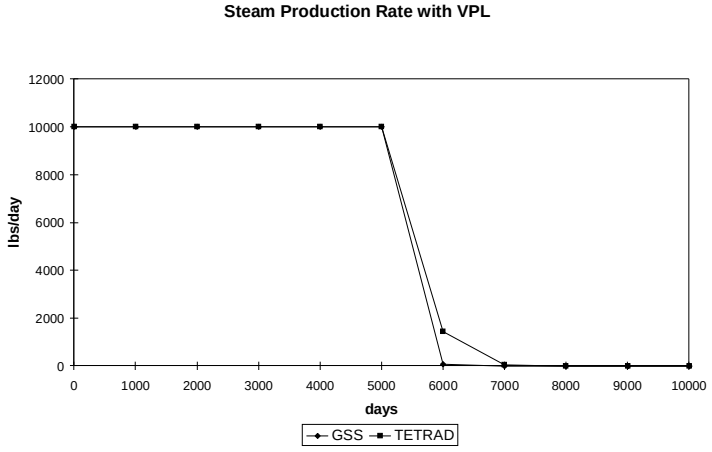

Figure 3.8: Comparison of steam production rates through time with VPL.

Figure 3.9 shows the comparison of reservoir pressure behavior. The results shows a gradual decline of reservoir pressure until the minimum flowing bottomhole pressure of 100 psia was reached.

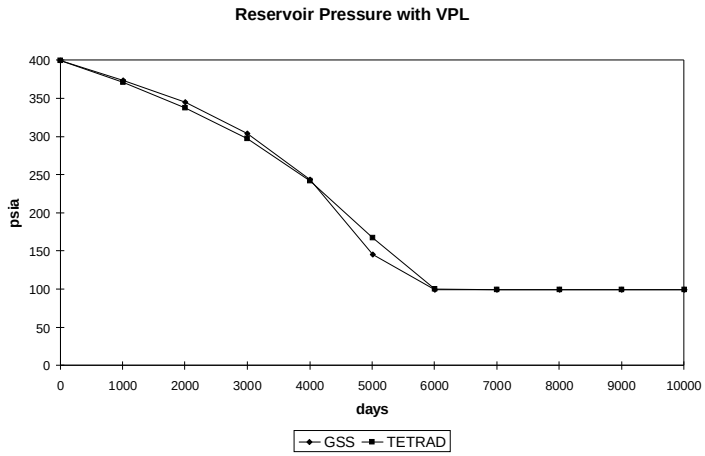

Figure 3.9: Comparison of reservoir pressure through time with VPL.

Figure 3.10 shows the comparison of reservoir temperatures. Again, the two models started with the same reservoir temperature. However, the initial reservoir temperature is 466°F, not the original 445°F. With vapor pressure lowering, maintaining the reservoir pressure at 400 psia will require a higher temperature than what saturated condition dictates. This implies that the model with vapor pressure lowering is no longer equivalent to the original model in terms of initial heat-in-place. Comparing TETRAD and GSS, significant deviation can be observed in the later stages of the simulation. This temperature deviation is attributed to the greater heat in-place calculated by GSS.

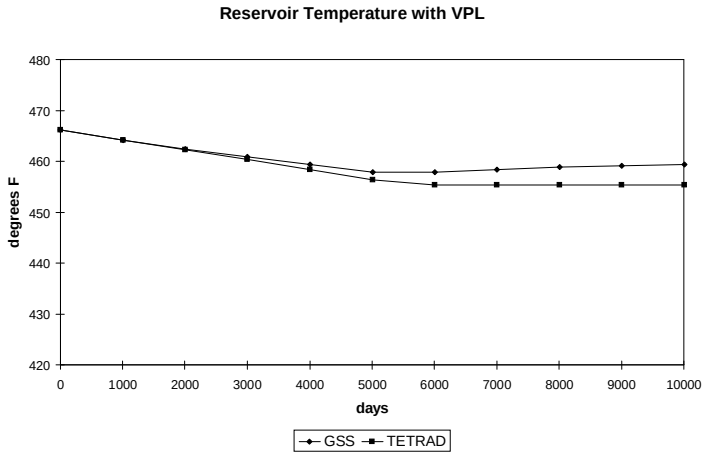

Figure 3.10: Comparison of reservoir temperature through time with VPL.

Figure 3.11 shows the comparison of matrix water saturation through time. The results are again close and it shows that the reservoir will never completely dry-out. With an abandonment pressure of 100 psia, about 2.5% water saturation will be retained in the rock matrix.

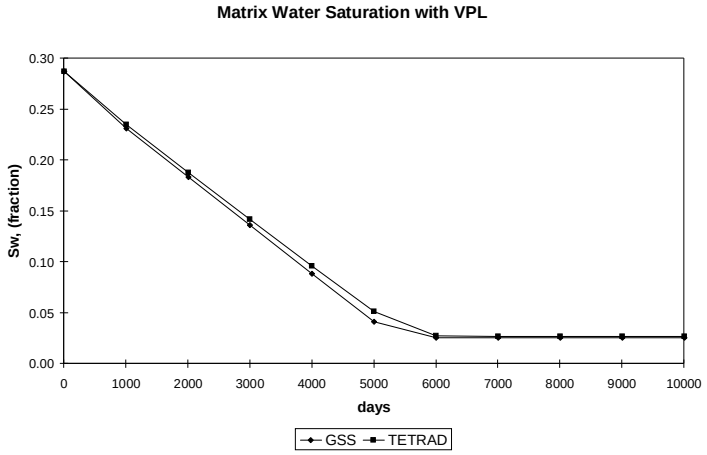

Figure 3.11: Comparison of matrix water saturation through time with VPL.

3.1.5 Discussion of Results

The main weakness of TETRAD is its inability to adjust the p_c versus S_w relationship as the reservoir temperature changes in response to exploitation. This is only possible if the built-in analytical expression for capillary pressure is used. This means that the p_c versus S_w relationship used in this study remains constant even when parts of the reservoir are cooled by production and water injection.

On the other hand, GSS also has problems. First, GSS is not robust. Even with the simple model used in this study, numerical non-convergence was a problem. In particular, the oscillating transition of wells from rate-control to pressure-control was very troublesome. Another major problem is an apparent error in the heat-in-place computation. Comparison of heat-in-place calculated manually, by GSS, and by TETRAD revealed a significant error in GSS.

The common major weakness of GSS and TETRAD is their inability to handle the adsorption/desorption hysteresis (Figure 3.12). Although any number of sorption isotherms or p_c versus S_w relationships can be assigned to different gridblocks, only one sorption isotherm or p_c versus S_w relationship can be specified for a particular gridblock. The matrix blocks may undergo both adsorption and desorption in response to injection and production operations.

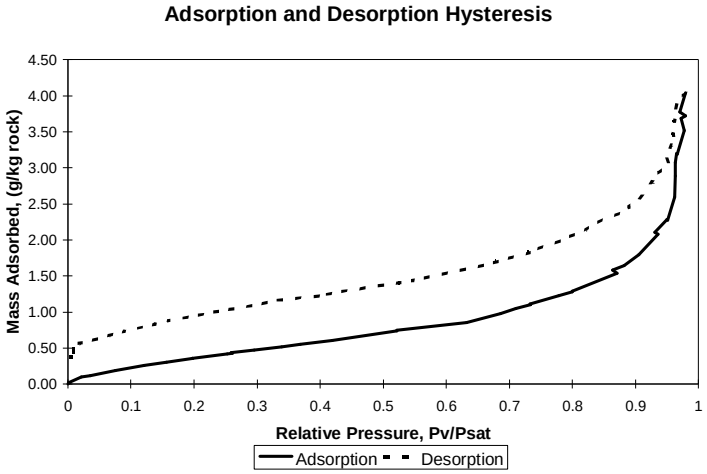

Figure 3.12: Example of adsorption and desorption isotherms hysteresis.

3.2 Effects of Adsorption on Injection

3.2.1 The Evaluation Models

Two vapor-dominated reservoir models (with simple geometry) were developed to investigate the effects of adsorption and capillarity on injection. The geometry of these models is illustrated in Figure 3.13 and Figure 3.14. The basic properties used in both models are listed in Table 3.2. The relative permeability function used allows steam as the only mobile phase at the given initial water saturation (S_w is 30%); water becomes mobile when S_w is greater than 35%. Adsorption properties are patterned after those typically observed in The Geysers (Figures 3.1 and 3.2).

The model shown in Figure 3.13 is comprised of a horizontal layer 1,000 feet long, 200 feet wide, and 100 feet thick. A uniform Cartesian grid with five uniform gridblocks was used. The porosity, permeability, sorption properties, and capillary pressure relations are uniform for all gridblocks. Initial thermodynamic state is also uniform. An injection well and a production well are located at the opposite ends of the model. The simulation data deck is listed in Appendix C.

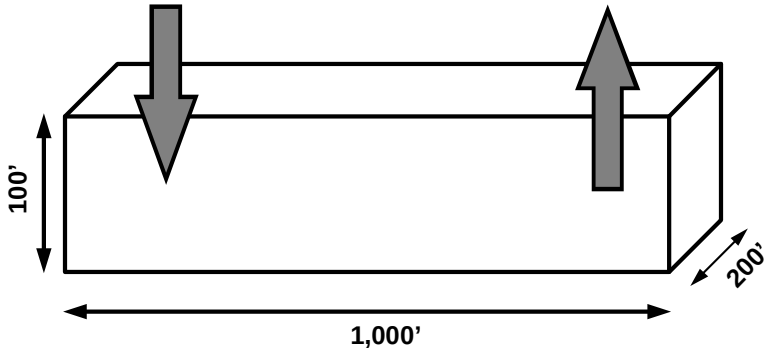

Figure 3.13: One-dimensional model with a pair of injection and production wells.

The second model shown in Figure 3.14 uses a uniform radial grid. The model is horizontal, 100 feet thick, and 1,000 feet in diameter. This model uses the same properties used in the Cartesian model. In this case however, the production and injection wells are both located in the center gridblock. The simulation data deck is listed in Appendix D.

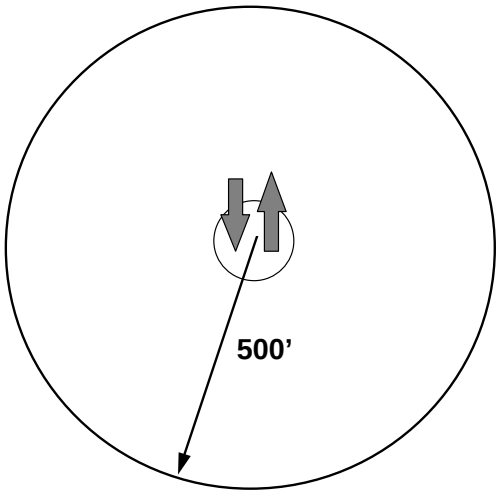

Figure 3.14: Two-dimensional model with production and injection wells at the center.

PROPERTIES	VALUES
Porosity	5%
Permeability	20 md
Initial liquid saturation	30%
Initial reservoir pressure	400 psia
Reservoir temperature	Evaluated

Table 3.2: Properties of the Cartesian and radial model.

The two models described above are essentially closed tanks. The model boundaries are closed to mass and heat flows. Mass and energy can flow in and out of the systems only though the production and injection wells.

For clarity, the "reservoir pressure" of 400 psia shown in the table above is equal to the pressure of the vapor phase. Note that the reservoir temperature needs to be evaluated based on the given reservoir pressure and the prevailing phase saturation in the reservoir. At the given initial condition where S_w is 30% the appropriate reservoir temperature is about 465^{o}F. If we had been using flat interface thermodynamics, the appropriate temperature would have been 445^{o}F. In a conventional sense the models we are using are superheated by about 20^{o}F at the initial condition.

3.2.2 Modeling Injection

Working with the one-dimensional Cartesian model, we investigated the effects of water injection into a vapor-dominated reservoir when adsorption and vapor pressure lowering are included. We compared the predicted behavior to the case when adsorption and vapor pressure lowering are ignored.

We perturbed the reservoir by injecting cold water (90^{o}F). Figure 3.15 below shows that 20 lbs/h of water is injected during the first 10,000 days.

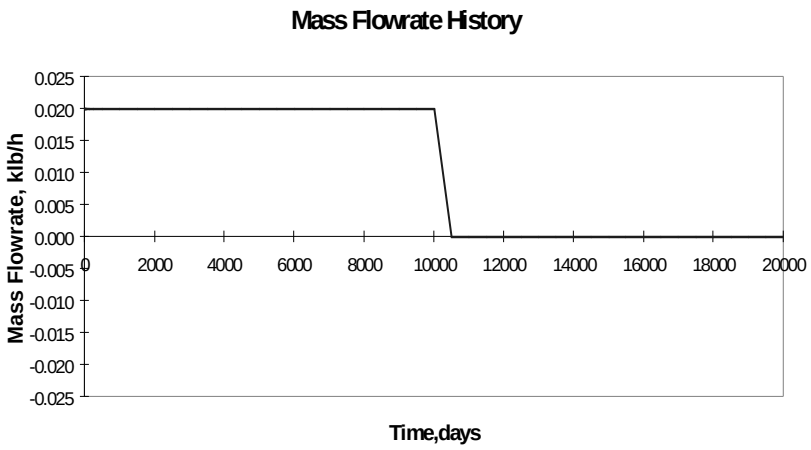

Figure 3.15: Water injection for 10,000 days into the one-dimensional Cartesian model.

Figures 3.16, 3.17, and 3.18 contrast the behavior of the reservoir if it is modeled with and without adsorption and vapor pressure lowering. Shown in these plots are the reservoir pressure, reservoir temperature, and phase saturation measured in the injection gridblock.

Figure 3.16 shows the reservoir pressure through time. With no adsorption the pressure measured in the injection gridblock is observed to decline. With adsorption the opposite effect is observed. Instead of declining, the pressure is observed to rise in response to injection.

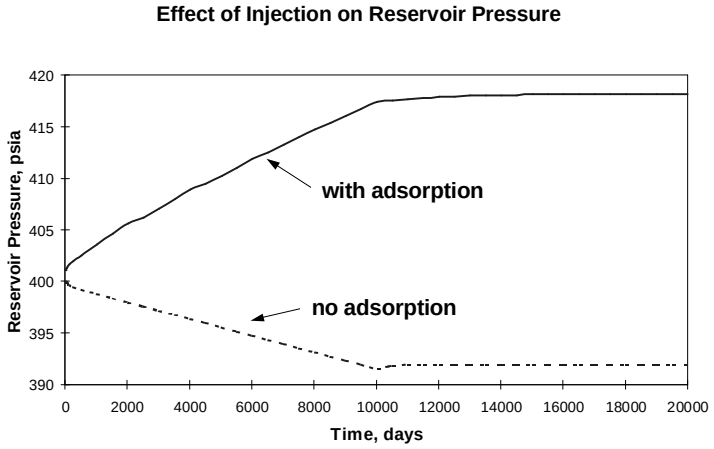

Figure 3.16: Pressure responses of the injection gridblock.

Figure 3.17 shows the reservoir temperature through time. As mentioned earlier, the use of pressure as the independent parameter to specify the thermodynamic state of the reservoir results in different temperatures for models with and without vapor pressure lowering. Without adsorption, the reservoir temperature is about 445°F; this is the saturation temperature at 400 psia if the vapor/liquid interface is flat. With vapor pressure lowering, 400 psia actually corresponds to a lowered vapor pressure across a curved vapor/liquid interface. With the water saturation initially at 30%, the given adsorption isotherm dictates the appropriate reservoir temperature to be about 465°F. Thus, in terms of initial heat in-place the models with and without adsorption are not equivalent. The differences are not limited to the heat in-place but also include the temperature variation of each gridblock. Without adsorption, the temperature declines monotonically for all gridblocks. With adsorption, gridblocks adjacent to the injection gridblock initially exhibit increases of temperature before starting to decline (not shown in Figure 3.17).

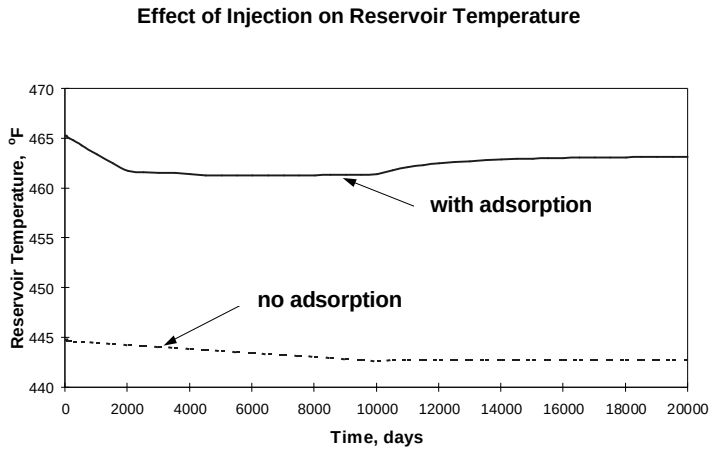

Figure 3.17: Temperature responses of the injection gridblock.

Figure 3.18 shows the vapor saturation of the injection gridblock through time. The difference between the curves (with and without adsorption) can be attributed to the differences in the pressure and temperature profiles.

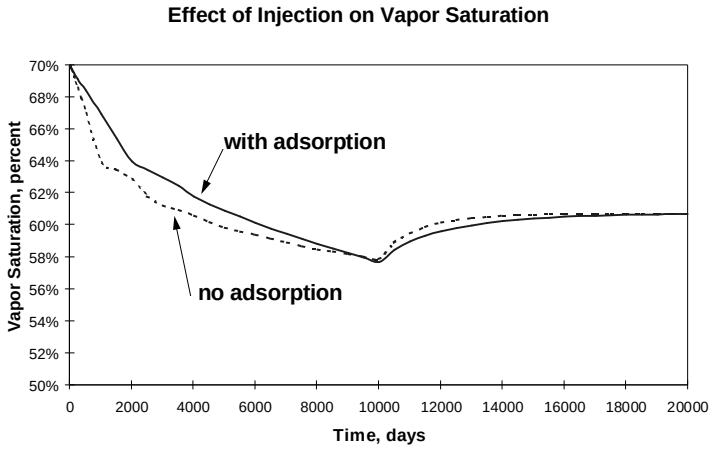

Figure 3.18: Vapor saturation changes of the injection gridblocks.

A curious behavior of the reservoir pressure is illustrated in Figure 3.19. Shown in this figure are the reservoir pressures measured in the injection and production gridblocks through time.

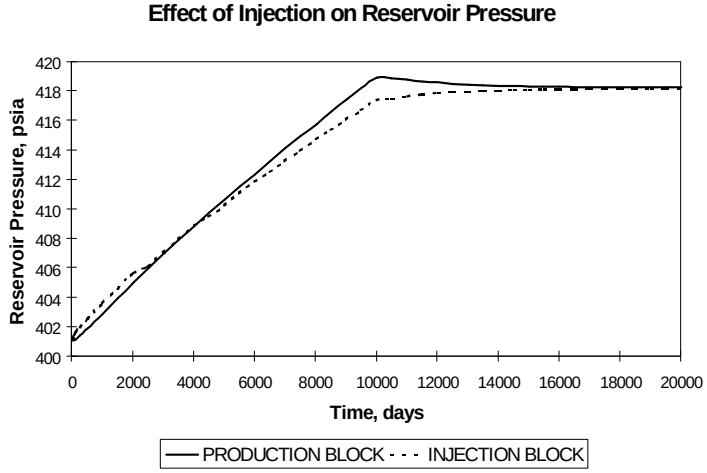

Figure 3.19 Pressure responses of the injection and production gridblocks.

The pressure in the injection gridblock was initially higher than the production gridblock. However, beyond 4,000 days the situation is reversed, the production block have a higher pressure than the injection block. Through the injection period there is a net mass flowing away from the injection block towards the production block. The apparent contradiction in pressure gradient and mass flow is explained by keeping in mind that the pressure of the vapor and liquid phases are different. As defined

earlier, the reservoir pressure shown in Figure 3.19 is the pressure of the vapor phase. Thus, initially steam is migrating away from the injection gridblock. At a later time the pressure gradient is reversed and steam will migrate towards the injection block. On the other hand, liquid water will continuously move away from the injection gridblock towards the production gridblock.

The pressure of the water phase is always higher in the injection gridblock compared to the production gridblock and any other blocks adjacent to it. This can be explained if we consider the saturation variation between gridblocks as shown in Figure 3.20. The vapor saturation of the injection gridblock is less than the production gridblock. From Figure 3.2 we know that the capillary pressure increases as the vapor saturation increases (i.e., decreasing liquid water saturation). Capillary imbibition draws water from the injection area towards the production area. Eventhough there is a counter-flow of steam and water, the net mass flow is still moving away from the injection area.

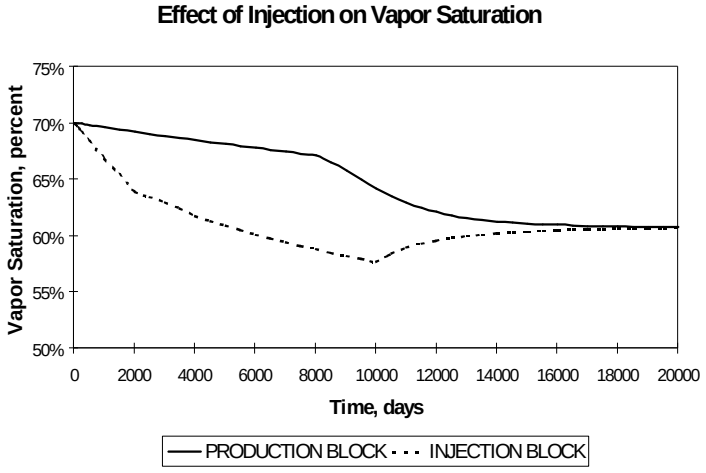

Figure 3.20: Vapor saturation changes measured in the injection and production gridblocks.

To complete the picture of the effects of injection, Figure 3.21 shows the reservoir temperature measured in the injection and production gridblocks.

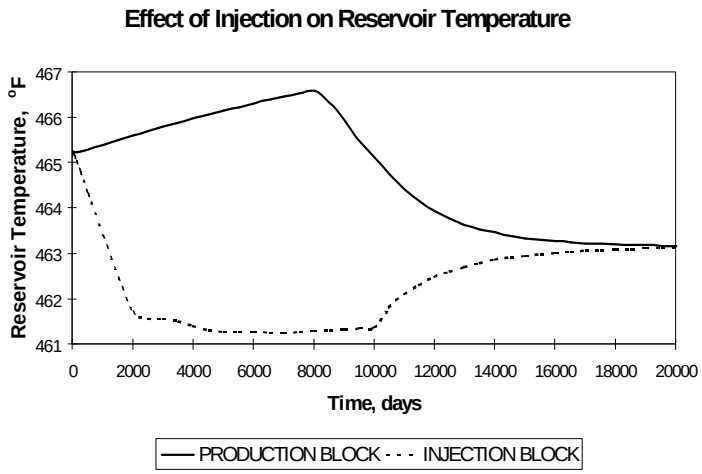

Figure 3.21: Temperature responses of the injection and production gridblocks.

The next step taken was to use the two-dimensional radial model to investigate the behavior of the reservoir when we try to produce the injected water. To do this, we imposed adsorption and vapor pressure lowering on the model. During water injection, the reservoir pressure was raised above the initial reservoir pressure. After terminating injection the production well was opened.

Figure 3.22 shows the reservoir pressure measure in the central gridblock throughout the 30,000 days simulation period.

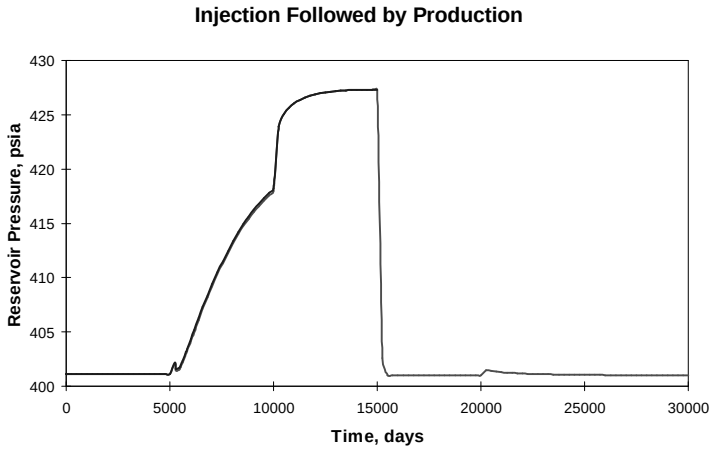

Figure 3.22: Pressure of the central block in response to injection followed by production.

Cold water was injected at a constant rate of 30 lbs/h beginning at 5,000 days through 10,000 days. The production well was opened beginning at 15,000 days. The production well was allowed to flow as long as it could sustain production based on given constraints. Production was constrained such that the maximum production rate did not exceed 30 lbs/h and the well is able to produce only down to the point when the reservoir pressure is restored to its value before injection. As expected, injection raised the reservoir pressure. Production caused rapid drawdown in the central gridblock.

Figure 3.23 shows the resulting mass flowrate history of the model. We used a sign convention such that injection is denoted by a positive mass flow while production is denoted by negative mass flow. It is apparent from the plot below that the production rate declines rapidly in response to the decline of the reservoir pressure.

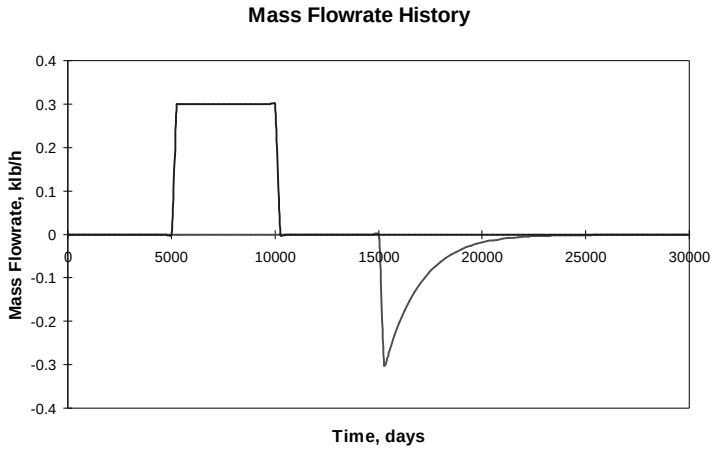

Figure 3.23: Injection and production rate history.

Figure 3.24 the same information as the previous plot but in terms of cumulative production and injection through time. The total mass injected into the reservoir was 36×10^6 lbs. The total mass produced afterwards was about 13.82×10^6 lbs. The total mass produced amounts to only 38.4% of the mass injected. The mass difference of over 22×10^6 lbs was retained in the reservoir and can be produced only if the reservoir pressure is allowed to decline below 400 psia.

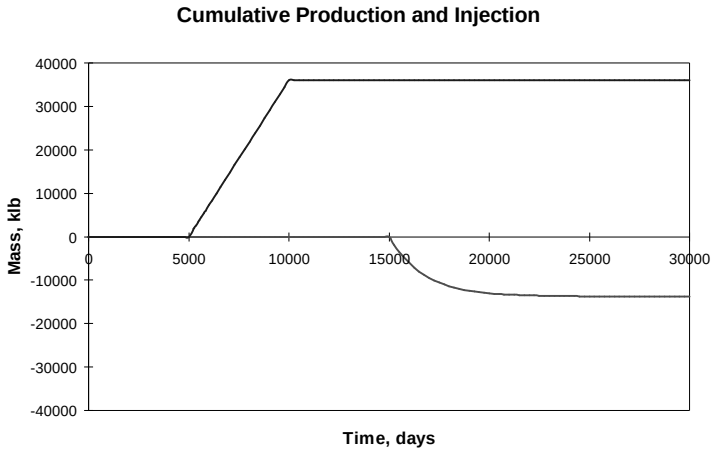

Figure 3.24: Cumulative masses produced and injected.

3.2.3 Discussion of Results

It is clear from the preceding results that the forecasted behavior of a vapor-dominated reservoir is different when we consider adsorption and capillary pressure. Calculations of mass and energy in-place are affected, as well as the thermodynamic behavior of the reservoir during exploitation. An excellent illustration of this point is the increase of reservoir pressure in response to water injection. If we do not consider adsorption we observe the opposite effect; reservoir pressure is decreased. Because the goal of water injection is to sustain reservoir productivity, using the appropriate physics to make forecasts is crucial.

Another revealing result of this study is the interdependence of pressure, temperature, and saturation in a geothermal reservoir. With flat interface thermodynamics, water saturation in the rock matrix is independent of pressure and temperature for a system at saturation condition. Because saturation is one of the major unknown quantities in reservoir modeling, it is often considered as a "calibrating" parameter. However, this is not the case with curved interface thermodynamics. If the measured reservoir pressure and temperature are close to saturation conditions, this implies that vapor pressure lowering is negligible and a high liquid saturation is appropriate. On the other hand, if a

substantial vapor pressure lowering (i.e., superheating) is observed, liquid saturation must be small and it can be evaluated if the sorption properties of the reservoir rocks are known.

Adsorption and desorption hysteresis is a major issue that needs to be addressed. Sorption experiments at Stanford University using cores from The Geysers field show that the adsorption and desorption isotherms can be very different. For vapor-dominated reservoirs, hysteresis can cause injected water to be retained in the rock matrix instead of becoming available for immediate production. This will have an impact on forecasting the effectiveness of injection in sustaining production. In the preceding simulations, although it was assumed that adsorption and desorption follow the same isotherm, it was apparent that the water retention property of the reservoir rock is significant. Apparently water injection causes localized increase in reservoir pressure, thus promoting adsorption rather than production of the injected water. If an actual desorption isotherm was used, water retention will be further increased, thus resulting in an even lower mass recovery from injection operations.

Capillary pressure is a major factor affecting the propagation of injectate into the reservoir. The high magnitude of suction pressure (of the order of 10^4 psia) of rocks with low water saturation will cause injectate to be imbibed into the rock matrix. If injection is targeted in depleted areas with high degree of superheat, imbibition of water into the rocks may minimize the detrimental effects to production that is associated with injection breakthrough.

4. Optimization of Injection

A field-scale model of a geothermal reservoir is necessary to study the optimization of water injection projects. The objective of this study was to determine the appropriate injection strategy that would result in an optimum energy yield from the geothermal resource while maximizing the net present worth of the injection project. There are two main questions that were addressed in this study: how much water to inject; and, when to start injecting?

4.1 Methodology

4.1.1 The Reservoir Model

A field-scale model of a hypothetical vapor-dominated geothermal reservoir was developed. The lateral extent of the reservoir was arbitrarily defined to be 7,000 feet by 7,000 feet. The vertical extent of the reservoir is 7,200 feet. The top of the reservoir is located at 2,000 feet below the surface.

The basic properties of the reservoir model are listed in Table 4.1.

PROPERTIES	VALUES
Porosity	5%
Lateral permeability	40.008 md
Vertical permeability	20.004 md
Initial liquid saturation	35%
Initial reservoir pressure	400 psia
Reservoir temperature	Evaluated

Table 4.1: Reservoir properties of the full-field model.

A single porosity formulation was used to construct the reservoir model. Comparison of models constructed using single and dual porosity formulations showed that there is no significant difference in model performance during production. For the dual porosity model, it was assumed that the fractures also have adsorption properties identical to the matrix. This assumption was necessary to have an initial mass

in-place in the dual porosity model that was equal to that of the single porosity model. Another reason was to enable the use of curved interface thermodynamics in both the matrix and fracture gridblocks. However, the issue of how fractures should be treated with respect to adsorption property is still a question. Therefore, the single porosity formulation was used to simplify the model and avoid the complications associated with the dual porosity formulation.

The lateral permeability value of 40.008 md given in Table 4.1 is equivalent to that of a fractured system with a matrix permeability of 0.01 md (4% bulk porosity) and a fracture permeability of 200 md (1% bulk porosity). The vertical permeability was arbitrarily defined as 50% of the lateral permeability.

The relative permeability functions used were based of the work of Sorey (1980). The liquid and vapor permeability functions are defined as follows:

$$k_{rl} = S_w^{*4}; \text{ and,} \qquad \textit{(Equation 4.1)}$$

$$k_{rv} = \left(1 - S_w^{*2}\right)\left(1 - S_w^{*}\right)^2, \qquad \textit{(Equation 4.2)}$$

where $S_w^* = \dfrac{\left(S_w - S_{wc}\right)}{\left(1 - S_{wc}\right)}$ and $S_{wc} = 0.35$.

The initial liquid saturation of the reservoir was set to 35%, so only steam is mobile while the liquid water is initially immobile. The mass of liquid water can become available for production by evaporation or if it becomes mobile when the liquid saturation rises above 35% through steam condensation or influx of additional water through injection.

Similar to the previous evaluation models, the field-scale model is essentially a closed tank. The model boundaries are closed to heat and mass flows. The only way heat and mass can flow to and from the reservoirs is through the production and injection wells.

4.1.2 The Field Model

The installed generating capacity of the model field is 75 MW(e). Assuming a plant capacity factor of 90%, the average gross generating capacity is 67.5 MW(e). The steam usage is 18.5 klb/h per MW(e). Thus, the required average production rate to sustain full generating capacity is about 1,250 klb/h. It was assumed that a minimum flowing bottomhole pressure of 100 psia is required to deliver steam to a power plant.

The model field is located at an elevation of 2,000 feet above the source of water for injection. All injection water comes from this source. A 10-mile water pipeline brings water from the lowland source to the hypothetical geothermal field.

4.1.3 Injection Optimization Scheme

Instead of modeling the whole field, a symmetry element 1/50th the size of the whole reservoir was modeled. This symmetry element has dimensions of 1,400 feet by 1,400 feet laterally and 3,600 feet thick. If the full-scale reservoir is gridded into 5-by-5-by-2 layers, one gridblock will be represented by the symmetry element.

The symmetry element was further gridded into 7-by-7-by-9 layers. Each gridblock has dimensions of 200-by-200 feet and 400 feet thick. A pair of production and injection well were placed on diagonally opposite corners of the element. The injection well was completed in layer 5. The production well was completed in layers 4, 5, and 6. An observation well was placed in the center of the element and completed in layer 5. This production/injection well pattern implies that the field was developed with a 5-spot injection pattern. The model's symmetry element is illustrated in Figure 4.1.

Assuming that mass is produced uniformly throughout the reservoir, the field's total average production rate of 1,250 klbs/h translates to a production rate of 25 klbs/h for each symmetry element. For all simulation runs, the production rate of 25 klbs/h will be referred to here as the peak production

rate. The reported water injection rates are scaled relative to this production rate. The base case simulation data deck for this model is listed in Appendix E.

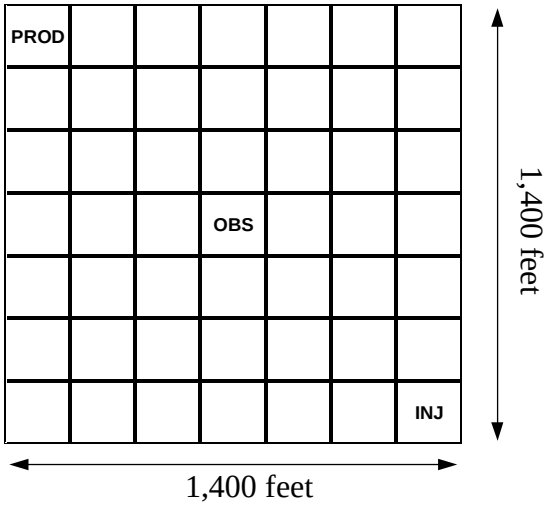

Figure 4.1: Symmetry element of the reservoir model.

To investigate the issue regarding when water injection should start during the field's development, seven cases were considered. For all cases, production begins at time t=0 years while the injection operation begins at various stages of the field's exploitation. The cases considered are the following:

Case I: Injection begins at t = 0 year;

Case II: Injection begins at t = 5 years;

Case III: Injection begins at t = 10 years;

Case IV: Injection begins at t = 15 years;

Case V: Injection begins at t = 20 years;

Case VI: Injection begins at t = 25 years; and,

Case VII: Injection begins at t = 30 years.

4. OPTIMIZATION OF INJECTION

For each of the preceding cases, the effects of injecting water at different rates were further investigated. These sub-cases are the following:

Sub-case A: Base case - no injection;

Sub-case B: Inject 20% of the peak production rate;

Sub-case C: Inject 40% of the peak production rate;

Sub-case D: Inject 60% of the peak production rate;

Sub-case E: Inject 80% of the peak production rate;

Sub-case F: Inject 100% of the peak production rate;

Sub-case G: Inject 120% of the peak production rate; and,

Sub-case H: Optimum case - injection rate causing water breakthrough at t = 50 years.

The cases described above required a total of 50 permutations. The optimum case (Case H) uses water breakthrough in the production well at t = 50 years (18,250 days) as the optimization criteria. The optimum injection rate may be less than or greater than the rate used in Case G (120% of peak rate).

4.2 Results

The first simulation performed was intended to establish the base case production performance of the reservoir. The production well was opened at t = 0 days and allowed to flow for 20,000 days. The production rate was constrained to a maximum of 25 klb/h. The production well's bottomhole flowing pressure was constrained to a minimum of 100 psia. The base case production performance is illustrated in Figures 4.2, 4.3, 4.4, and 4.5.

Figure 4.2 shows that the reservoir can sustain the peak production rate for about 7,000 days, or 19 years. After 19 years, the steam production rate declines exponentially with a nominal rate of about 0.12 per year. After 50 years (18,250 days), the steam production rate is nil.

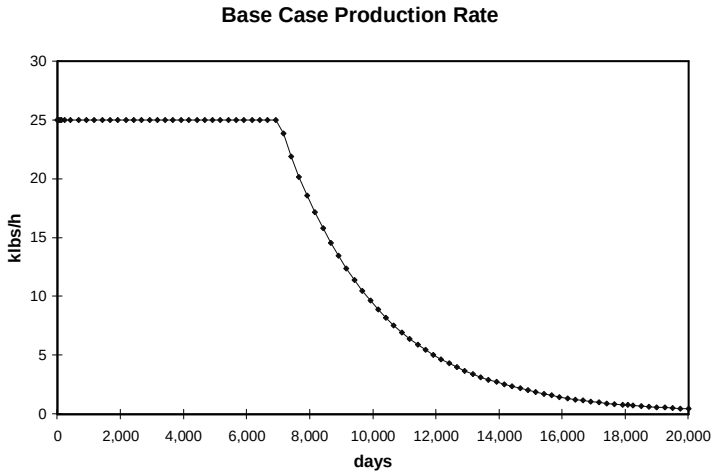

Figure 4.2: Base case production rate.

Figure 4.3 shows the reservoir pressure in the production gridblock through time. After a rapid drawdown, the reservoir pressure declined gradually as steam from the neighboring areas migrated into the production area. The flowing bottomhole pressure constraint of 100 psia was reached after 19 years of production.

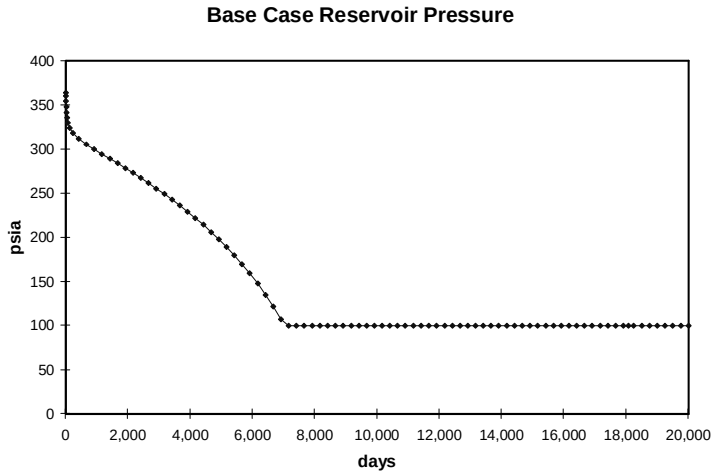

Figure 4.3: Base case reservoir pressure in the production gridblock.

Figure 4.4 shows the measured reservoir temperature in the production gridblock through time. Consistent with the pressure response, the temperature declined in response to production.

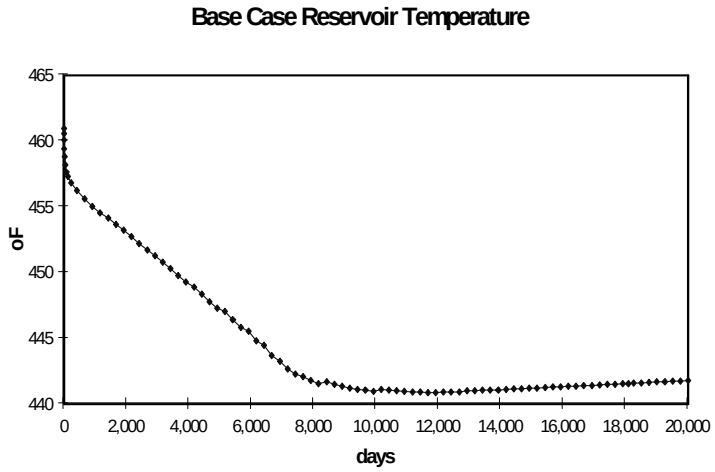

Figure 4.4: Base case reservoir temperature in the production gridblock.

Figure 4.5 shows the steam saturation measured in the production gridblock through time. The residual liquid phase saturation after 20,000 days of production is about 3.38%. This remaining liquid mass is not available for steam production unless the flowing bottomhole pressure is allowed to be less than 100 psia.

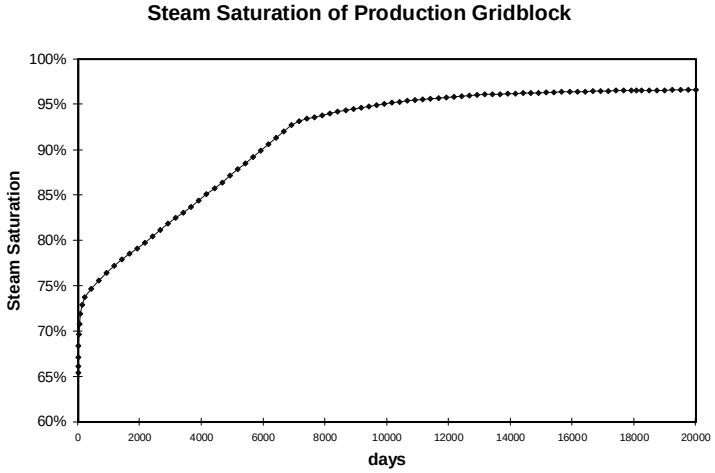

Figure 4.5: Base case steam saturation of the production gridblock.

4. OPTIMIZATION OF INJECTION

To illustrate the production optimization process, the following plots show results for Case I. For this case, injection and production begins at the same time at t=0 years.

Figure 4.6 and Figure 4.7 are plots of the reservoir pressures through time measured in the production and observation gridblocks, respectively. In this case, the optimum injection rate is 93% of the peak production rate. It is clear from these plots that higher injection rates provide greater support to the reservoir pressure. Injecting water with the optimum rate of 23.25 klb/h, the flowing bottomhole pressure is maintained above 100 psia beyond 16,000 days. Injecting with rates that are greater than 93% of the peak production rate can sustain the pressure even longer (e.g., 100% and 120% of peak production rate). However, it will be shown later that these cases actually yield lower total production compared to the optimum case.

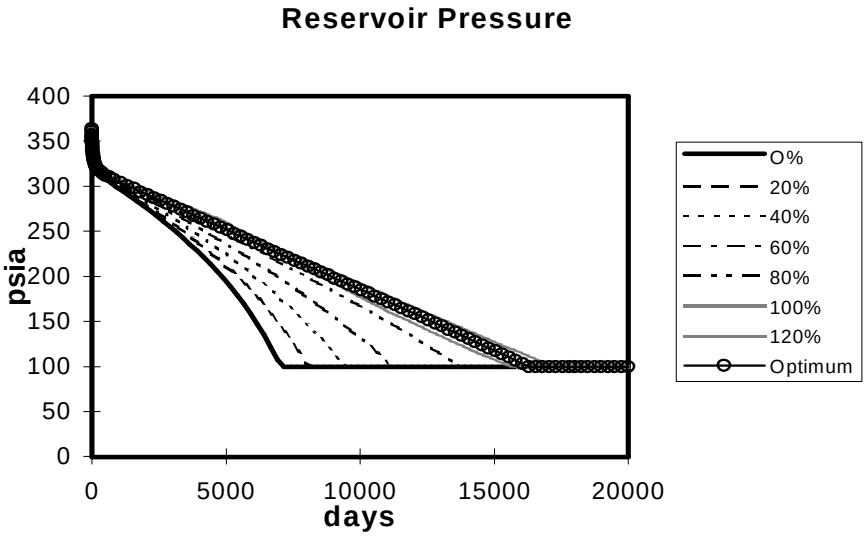

Figure 4.6: Case I - Reservoir pressures measured at the production gridblock.

The pressures measured in the observation gridblock as shown in Figure 4.7 essentially present the same information. However, the influences of injection and production operations are diminished because of its distance from the wells. Thus, the properties measured in the observation gridblock better represent the average reservoir properties.

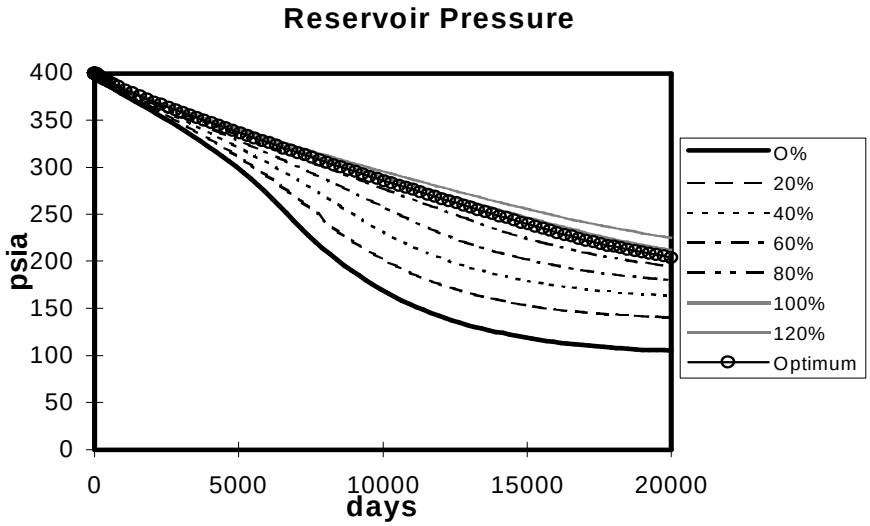

Figure 4.7: Case I - Reservoir pressures measured at the observation gridblock.

Pressure support from injection translates to increased deliverability. Figure 4.8 shows that with injection the steam production rate of 25 klb/h can be sustained much longer than in the base case. Thus, the cumulative production is also greater. This is illustrated in Figure 4.9.

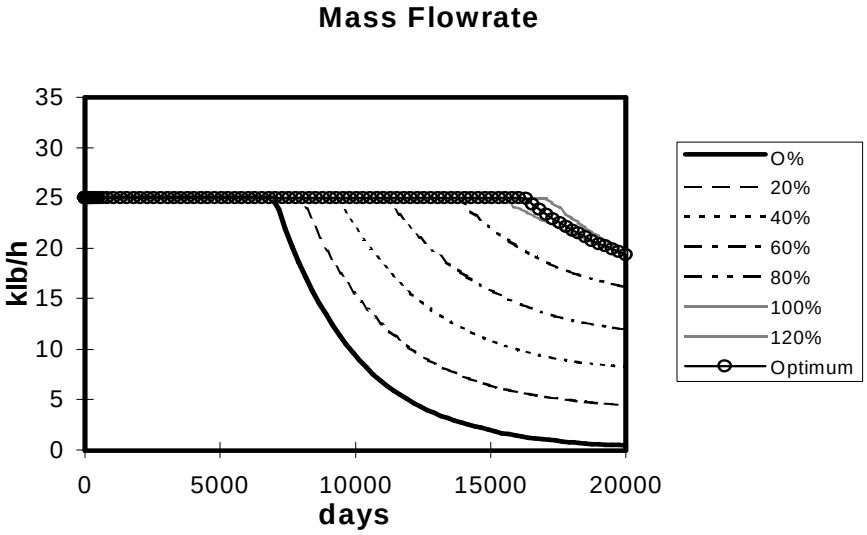

Figure 4.8: Case I - Steam production rates.

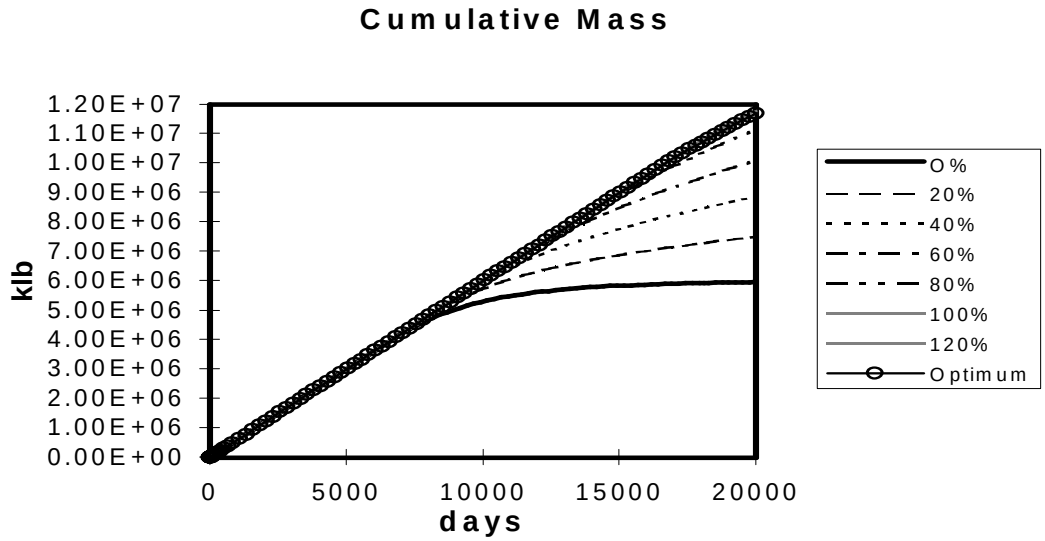

Figure 4.9: Case I - Cumulative mass produced.

Figures 4.10 and 4.11 show the temperatures measured through time in the production and observation gridblocks, respectively.

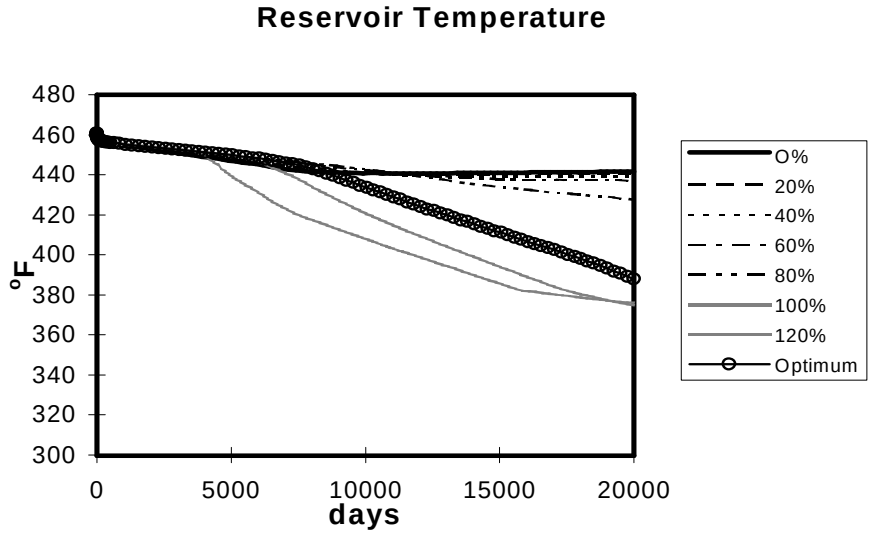

Figure 4.10: Case I - Reservoir temperatures measured at the production gridblock.

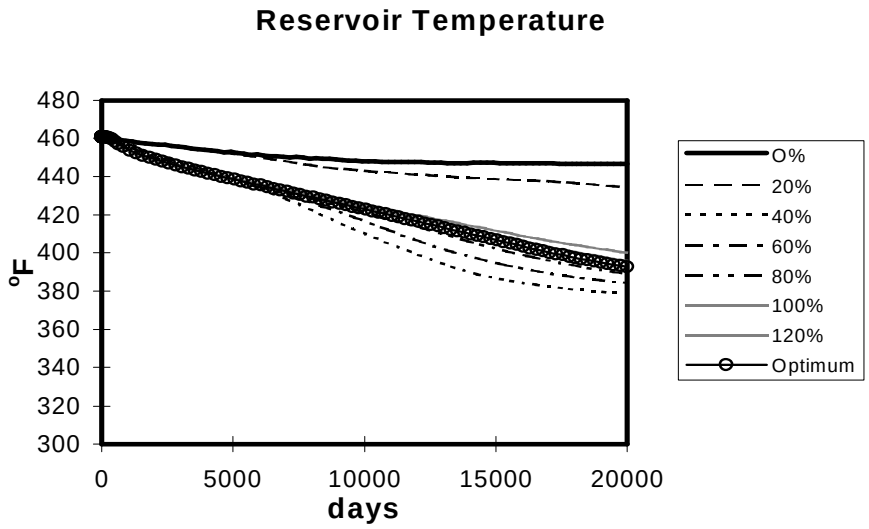

Figure 4.11: Case I - Reservoir temperatures measured in the observation gridblock.

Figures 4.12 and 4.13 show the steam saturation through time measured in the production and injection gridblocks, respectively.

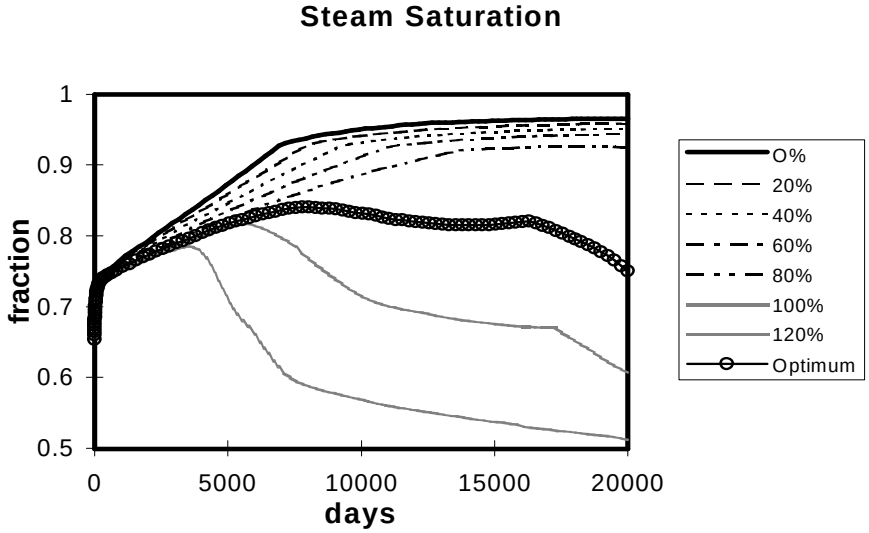

Figure 4.12: Case I - Steam saturations of the production block.

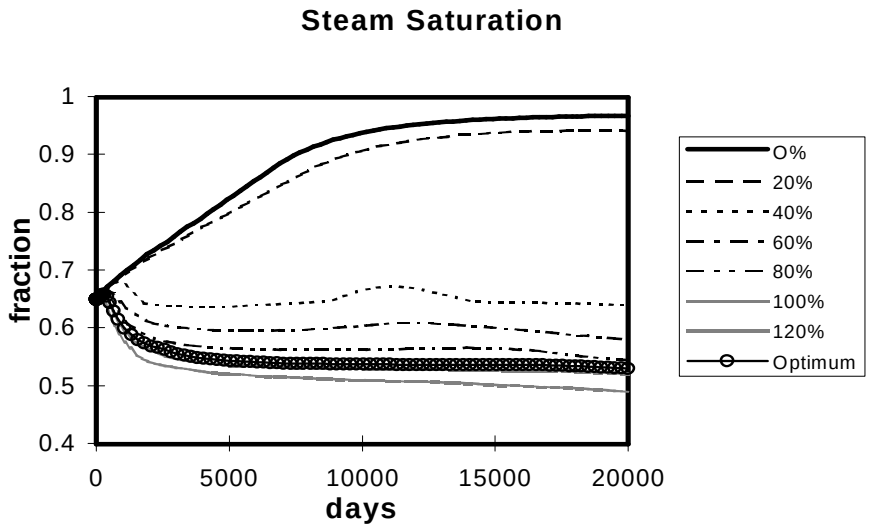

Figure 4.13: Case I - Steam saturations of the observation gridblock.

As mentioned earlier, the criterion used to determine the optimum injection rate is the onset of water breakthrough in the production well at the 50th year. Figure 4.14 shows the water production rates for various injection rates of Case I. Injection rates equal to 100% and 120% of the peak production rate caused early breakthroughs. Injecting 93% of the peak production rate satisfied the optimum criterion.

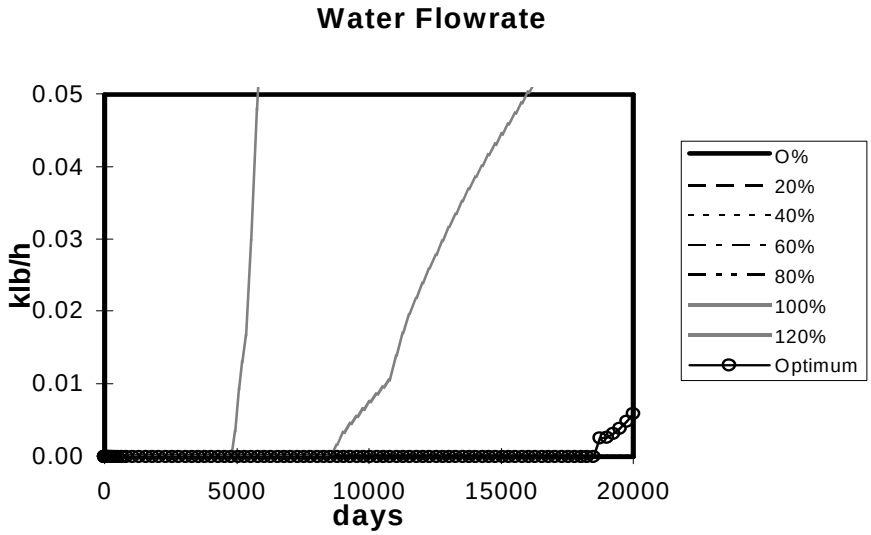

Figure 4.14: Case I - Water production rates.

4. OPTIMIZATION OF INJECTION

The plots of the results for all cases considered in this study are shown in Appendices F through L. Of special interest are cases where the injection program started after the field's steam production was already on a decline (i.e., later than the 19th year). A good example is Case VI (Appendix K). In this case, water injection started on the 25th year (9,125 days) of production. The optimum injection rate is 190% of the peak production rate. Figure 4.15 shows the reservoir pressure through time in the production gridblock. Injecting the optimum rate, the flowing bottomhole pressure of the production well was observed to increase.

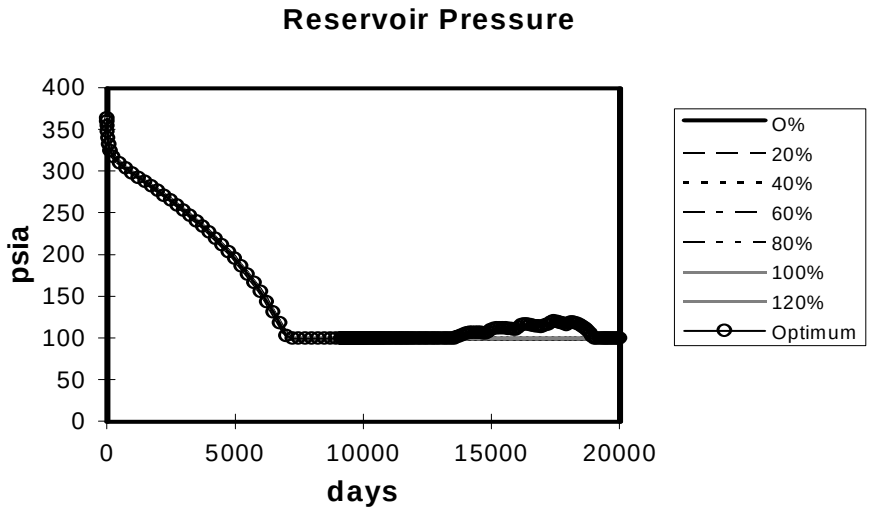

Figure 4.15: Case VI - Reservoir pressures measured at the production gridblock.

The pressures measured in the observation gridblock are more illustrative. These are shown in Figure 4.16. Injecting at the rate of 60% of the peak production rate maintained the prevailing reservoir pressure during the start of injection. Injecting at rates greater than 60% actually caused the reservoir pressure to increase above the reservoir pressure at the start of injection.

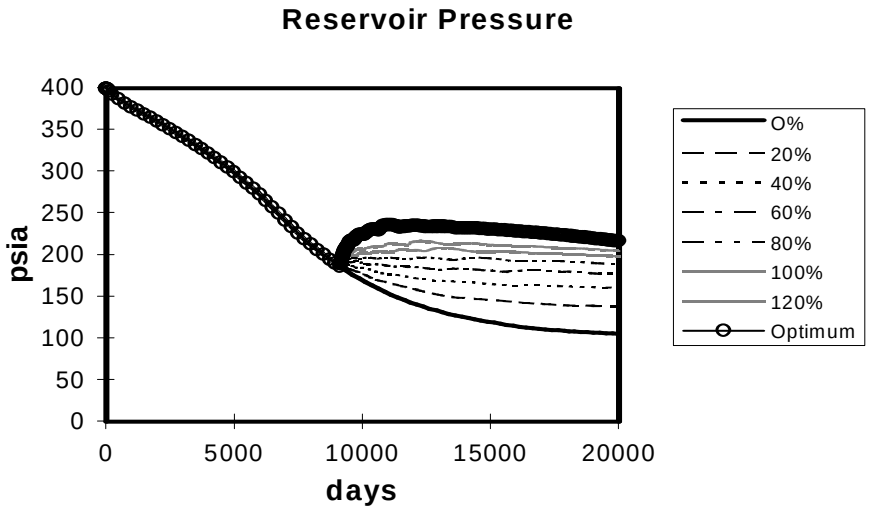

Figure 4.16: Case VI - Reservoir pressures measured at the observation gridblocks.

The resulting mass flowrates are shown in Figure 4.17. Injecting with a rate between 60% and 80% of the peak production rate approximately maintains the production rate at the start of the injection project. Injecting at a rate greater than 80% causes the production rate to increase. Injecting at the optimum rate actually resulted to a production rate that is equal to the peak rate. The dip in production near the end of the simulation period is caused by injection breakthrough.

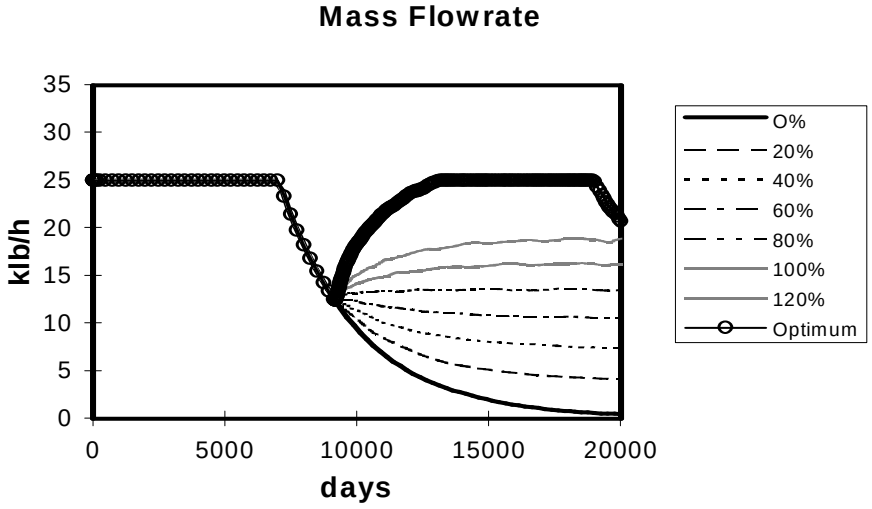

Figure 4.17: Case VI - Production rates.

The optimum injection rates for all seven cases are shown graphically in Figure 4.18. There is a clear trend that starting water injection later in the field's development results in higher allowable injection rates. For example, Case VII where injection started in the 30th year of production, the optimum injection rate is 224% of the peak production rate.

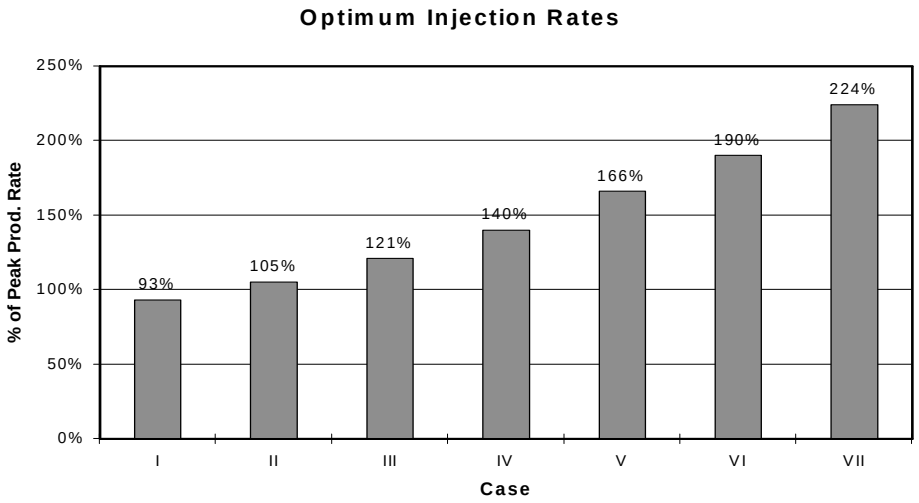

Figure 4.18: Optimum injection rates relative to the peak production rate.

The resulting optimum incremental cumulative production within 50 years for each of the cases are shown in Figure 4.19. Except for Case VI and Case VII, the incremental cumulative production is in excess of 80% of the base case. The lower incremental cumulative productions for Case VI and Case VII are good examples of how injecting too fast can actually diminish the ultimate production from the reservoir. Higher reservoir pressures and heat transfer limitations between the reservoir rocks and the injected water are conditions that tend to promote early injection breakthrough. Also, the short production periods after the start of injection for Cases VI and VII leave greater amounts of injectate unproduced in the reservoir. This is illustrated in Figure 4.20 in terms of the reservoir pressure measured at the observation gridblock on the 50th year.

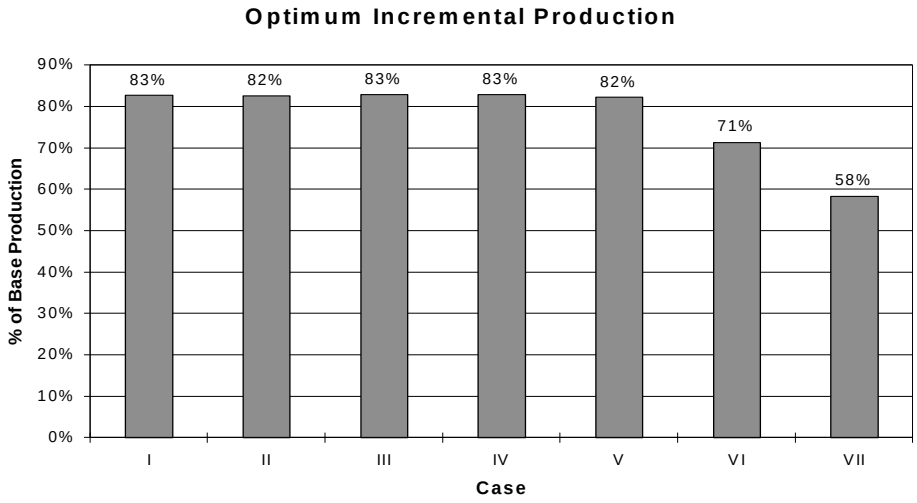

Figure 4.19: Optimum incremental cumulative production relative to the base production.

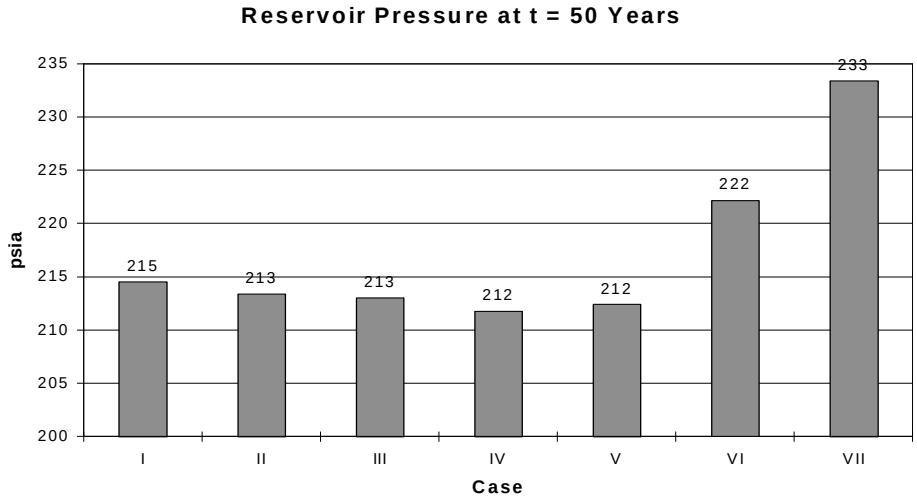

Figure 4.20: Reservoir pressure measured at the observation gridblock for optimum cases.

Another interesting parameter is how much of the injected water is eventually produced. Injectate recovery is defined as the incremental mass produced within 50 years (with injection) divided by the base case production. The injectate recoveries for all the cases are shown in Figure 4.21. It is clear from this graph that injection recoveries are lower for higher injection rates. In Case IV, injecting 20% (Sub-case B) results in a recovery of about 57%. Injecting 120% (Sub-case G) leads to a recovery of 48%. For the optimum case (Sub-case H), injecting 140% results in a recovery of only about 46%.

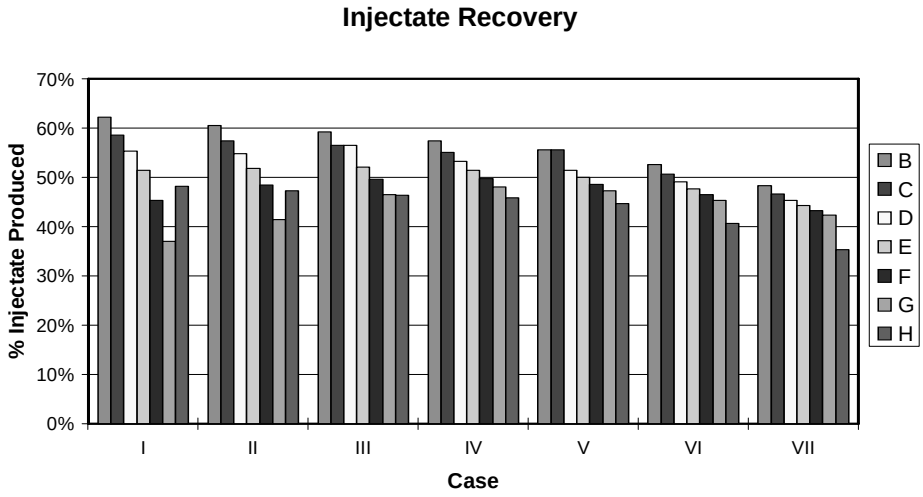

Figure 4.21: Injectate recovery for all cases.

The details regarding injectate recovery for various the cases and various injection rates can be found in Appendix M and Appendix N.

4.3 Economic Optimum

Several assumptions about the field model were necessary to construct an economic model. The economic model was used generate a cashflow value that results from the injection project. This process was performed for all cases to determine which one yields the maximum present worth. Only the incremental costs and benefits of the injection project were considered. The costs and revenues that are associated with the base case are common to all cases, and thus can be factored out.

The revenue stream that results from the injection project was based on the incremental steam production. The steam production performance when there is injection was compared to the base case production performance of the reservoir. The observed difference in steam production was attributed to the injection project. The incremental steam production was then converted to incremental electricity generation using a steam usage rate of 18.5 kilopounds per MWh (net). The income for the operator

from this incremental generation was calculated using an assumed gross income of $25 per MWh. The incremental revenue stream throughout the entire 50 years period was generated this way.

As mentioned earlier, the geothermal field is located at an elevation of 2,000 feet above the lowland water source. All injection water comes from this source through a 10-mile water pipeline. This information was used to evaluate the capital expense required to build the water pipeline and the pumping facilities. It was assumed that construction of the pipeline cost $12 per diameter inch-feet (installed). The capital cost for the pump was assumed to be $1,341 per kW ($1,000/hp). The necessary structures, controls, and power supply for the pumps cost an additional $2,682 per kW ($2,000/hp).

The injection rate for the whole field ranges from 250 klb/h to 3,000 klb/h. These rates correspond to 20% and 240% of the peak steam production rate (1,250 klb/h). With a choice of using either a 6, 12, 18, 24, or 30-inch diameter pipe, the pumping power required to deliver water to the field at a given flow rate was evaluated. The elevation head and the pressure drop in the pipeline due to friction were considered. Figure 4.22 shows the pumping power that is required for various injection rates and pipeline sizes.

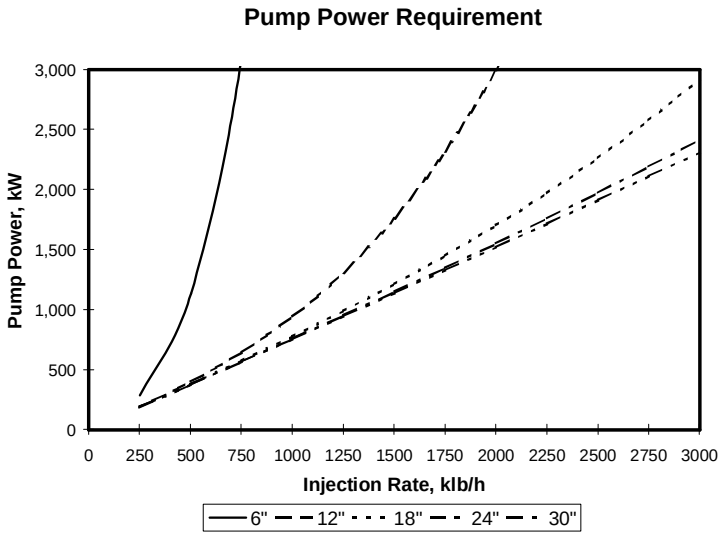

Figure 4.22: Pump power requirement for various injection rates and pipeline sizes.

4. OPTIMIZATION OF INJECTION

The optimum combination of pump and pipeline size was evaluated. The objective was to minimize the required capital expense for a given injection rate. This process is illustrated in Figure 4.23.

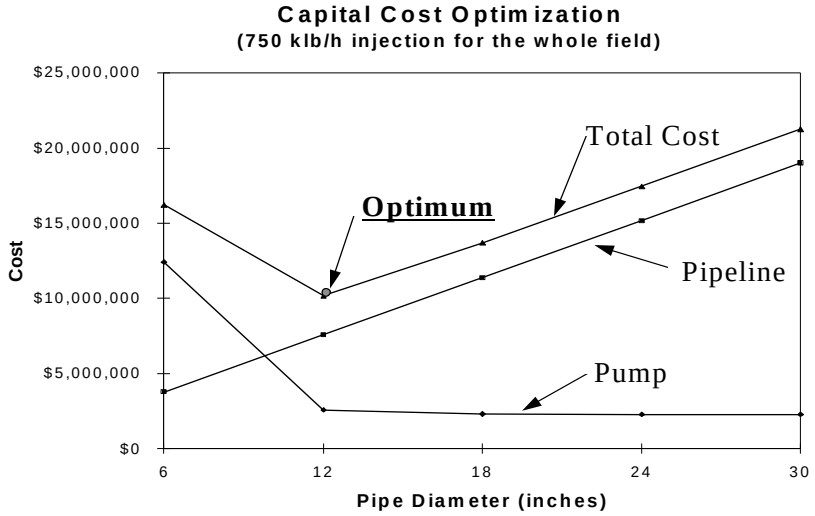

Figure 4.23: Illustration of capital cost optimization.

Table 4.2 lists the total capital cost for various combinations of injection rate and pipeline size. The total capital cost (sum of pumping facilities and pipeline costs) shown is scaled to the size of the symmetry element (1/50 of the whole field).

% Injection Rate	Pipeline Internal Diameter (inches)				
	6	12	18	24	30
20%	$99	$167	$243	$319	$395
40%	$167	$184	$259	$334	$410
60%	$325	$204	$274	$350	$426
80%	$616	$228	$291	$365	$441
100%	$1,086	$257	$308	$381	$456
120%	$1,777	$294	$326	$397	$472
140%	$2,735	$339	$345	$413	$487
160%	$4,004	$393	$365	$429	$503
180%	$5,628	$459	$387	$446	$518
200%	$7,652	$537	$411	$463	$534
220%	$10,118	$629	$436	$481	$550
240%	$13,073	$736	$463	$499	$566

Table 4.2: Total capital cost (k$) for various injection rates and pipeline sizes.

The optimum cost cases for different injection rates are given in Table 4.3. The given pipeline size and pumping power are for the whole field. The given total capital cost is for a symmetry element.

% Injection	Pipe Size (Inches)	Pump Power (kW)	Capital Cost (k$)
20%	6	285	99
40%	6	1,132	167
60%	12	645	204
80%	12	942	228
100%	12	1,308	257
120%	12	1,762	294
140%	12	2,318	339
160%	18	1,704	365
180%	18	1,975	387
200%	18	2,267	411
220%	18	2,582	436
240%	18	2,922	463

Table 4.3: Optimum pump and pipeline facilities.

There are two other pieces of information required to complete the economic model. These are the operating cost of the injection system and the cost of drilling the injection wells. The cost of the pipelines to distribute water among the injection wells was ignored in this study.

The operating cost was estimated as a function of the total mass of injected water. By making assumptions about the cost of electricity to operate the pumps, an operating cost function of $0.11 per kilopound of injectate was determined. Additional costs associated with manpower requirements and injection facilities maintenance were ignored.

It was also assumed that a total of six injection wells were required to fully develop the field. This assumption was applied to all cases regardless of the injection rate. This was done to remain consistent with using the same injection pattern for all cases. If the average cost of drilling a well is $1.5 million, the total cost of the six injection wells is $9 million. Scaling this amount to the symmetry element (i.e., 1/50 of the field), the cost attributed to the symmetry element was $180,000.

A cashflow was generated in each of the cases considered previously. The capital expenses were entered at the start of injection. The operating expenses and revenues were entered as they were incurred

and earned, respectively. The present value (at t=0 years) of the cashflow was evaluated using an assumed discount rate of 10% per year.

Figure 4.24 shows the graph of the present worth of the injection project for all the cases. The detailed plots for each case are presented in Appendix O. Except for Case VII-B (present worth of minus $17,000), all of the other cases yielded positive present worth. Case VI-B (present worth of $2,500) and Case VII-B are good examples of injecting "too little, too late." Apparently, excluding the extreme cases, a water injection project into a vapor-dominated geothermal field is almost always a good investment.

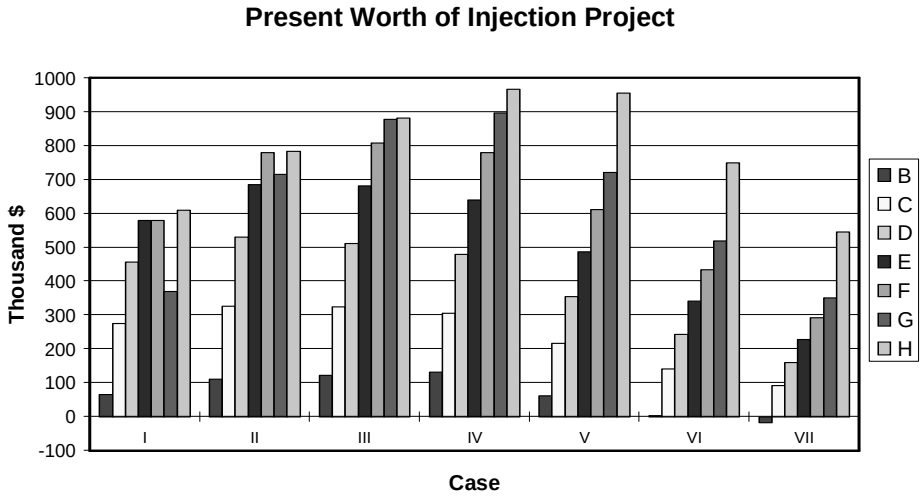

Figure 4.24: Present worth of the injection project for all cases (symmetry element).

For all cases, the optimum injection rate (Case H) gave the maximum present worth for that particular case. Comparing every case, the maximum present worth is $966,000 for Case IV-H. This is followed closely by Case V-H with $956,000. For Case IV and Case V, the injection started at the 15th and 20th year, respectively. Most likely, the true maximum occurs when injection starts between 15 and 20 years of the field's operation. Injecting earlier than the 15th year requires capital expenditures that are earlier than necessary. Injecting later than the 20th year requires higher injection rates; thus, higher capital expenditures for the injection facilities. Furthermore, there will be loss of opportunity to produce at peak rate because steam production from the field starts to decline after 19 years.

4. OPTIMIZATION OF INJECTION

To look at the economics for the whole geothermal field, Case IV-H was used as an example. This case injected with a rate of 1,750 klb/h (140% of peak production rate) starting in the 15th year. The injection facility was comprised of a 2,318 kW electric pump, 10 miles of 12-inch diameter water pipeline, and six injection wells. The undiscounted cost of the six wells was $9 million. The undiscounted capital cost for the pump and pipeline was $16.93 million. Injecting up to the 50th year (35 years total), the total undiscounted operating expense was about $59 million. The incremental electricity generation in this case was about 13.36×10^6 MWh. The undiscounted incremental gross income was about $334 million. The present value of the total capital expense was $10.45 million. The present value of the net income (gross income minus operating expense) was $58.74 million. The benefit-to-cost ratio of the injection project was about 5.62.

5. Conclusions

This study investigated the effects of adsorption and capillary pressure in the exploitation of vapor-dominated geothermal reservoirs. Based on the understanding gained from the preliminary studies, the most effective injection strategy to sustain the reservoir's productivity was determined.

This study showed that adsorption and capillary pressure are major factors governing the behavior of a vapor-dominated geothermal reservoir. These mechanisms affect both the resource size estimation (mass and heat in-place) and the production performance of the field.

Geothermal reservoir simulators that account for adsorption and curved interface thermodynamics are now available. Reservoir simulation codes with formulations based on either adsorption isotherm or capillary pressure yielded similar results. There are two issues that are still needed to be addressed in available simulators. One issue is the hysteresis of adsorption isotherm and capillary properties in response to production and injection operations. The second issue pertains to scaling with respect to temperature of the adsorption and capillary properties.

The effectiveness of water injection programs to sustain the geothermal field's productivity is affected by adsorption and capillary pressure. Water injection into vapor-dominated reservoirs may increase the prevailing reservoir pressure. Although this improves field's productivity, it also increases the water retention capacity of the reservoir rocks through adsorption and capillary condensation. Increasing the water injection rate will result in a greater fraction of injectate remaining unproduced when the same pressure drawdown is imposed.

Delaying the injection breakthrough in the production area until the end of the project life is an effective criterion for optimizing steam production and economic value resulting from an injection project.

5. CONCLUSIONS

Comparable energy yield can be attained for injection programs that are initiated at various stages of the field's development. Higher injection rate is desirable when injection starts later in the life of the field.

Considering the economics of the injection project, it is best to implement the injection program during the later stages of the field's development. Most probably, the point in the project's history at which the production goes into decline is the best time to begin injection. This way, a greater fraction of the injectate can become available for production and at the same time optimize the present worth of the project.

Appendices

A. TETRAD Data Deck for Dual Porosity Evaluation Model

```
'NOMESS'
'COMMENT'  '     '
'COMMENT'  'BASE CASE DATA DECK                    '
'COMMENT'  'RUN THIS DECK USING TETRAD VERSION 12    '
'COMMENT'  '     '
'COMMENT'  'THIS IS A GEOTHERMAL DUAL POROSITY MODEL'
'COMMENT'  'ONE-QUARTER OF A 5-SPOT PATTERN (HORIZONTAL 2-D)'
'COMMENT'  'WITH ADSORPTION AND VAPOR-PRESSURE LOWERING'
'COMMENT'  '     '
'COMMENT'  '     '
'TYPE'  4  1  1 0.0  0.0
'COMMENT'  '          '
'COMMENT'  '*********  CHANGE DIMENSION STATEMENT TO PROBLEM SIZE ***'
'COMMENT'  '          '
'DIMEN'     5   5  1    500
'COMMENT'  '          '
'COMMENT'  '*********  INTERSIM INPUT FILE   ******************'
'COMMENT'  '          '
'ISREAD'  0   'DUAL.IS'
'DUAL' 0 10. 6. 1.E-06 1.E-08 0 0 0 0
'FROCK'  0.15
'COMMENT'  '          '
'COMMENT'  '*********  ACTIVATE FOR GRID REFINEMENT ****'
'COMMENT'  '          '
'COMMENT'  'REFAIS'
'COMMENT'  '          '
'COMMENT'  '          '
'COMMENT'  '*********  OUTPUT FILE CONTROLS  ******************'
'COMMENT'  '          '
'UNITS' 0 1 0 1
'PRINT' 0 0 0 1 0
'OUTFUN' 1 2 0 0 0 0 0 8 0 0
'OUTGEO' 2 1 2 2 2 2 2 0 0 0
'OUTMISC' 0 2 0 0 1 0 0 0 0 0
'GVWRITE'  0 3
3  'P'  'SG'  'T'
'COMMENT'  '          '
'COMMENT'  '******************  NUMERICAL CONTROLS  ****************'
'COMMENT'  '          '
'TMSTEP',,,250. 10000 10.0,,,,,,,
'NORM' 250 0.02 .2 50
'COMP' 0.5E-06 400.  1.E-09 450.
'PROPERTY'
```

APPENDIX A: TETRAD DUAL POROSITY MODEL

```
'COMMENT' '          '
'COMMENT' '***  RELATIVE PERM CURVES AND CAPILLARY PRESSURE ******'
'COMMENT' '          '
'RELGW' 1 21 1 .01 0.0
.005 0.0 1.0  83436.0
.011 0.0 1.0  64131.0
.017 0.0 1.0  52838.0
.024 0.0 1.0  44826.0
.032 0.0 1.0  38611.0
.040 0.0 1.0  33533.0
.050 0.0 1.0  29239.0
.061 0.0 1.0  25520.0
.074 0.0 1.0  22240.0
.089 0.0 1.0  19305.0
.107 0.0 1.0  16651.0
.128 0.0 1.0  14227.0
.154 0.0 1.0  11998.0
.185 0.0 1.0   9934.0
.226 0.0 1.0   8012.0
.280 0.0 1.0   6215.0
.355 2.44E-9 0.9859 4526.0
.464 0.00090 0.6582 2934.0
.642 0.04080 0.2418 1429.0
.980 0.88380 5.54E-5   0.0
1.00 1.00000 0.0       0.0
'COMMENT' '            '
'RELANAL' 21 3 0 1.0
445. 445. .01 .0 .01 .0
0.35 1.0 4.0
0.0 0.0 2.0 0. 2.0
0.0 4.0 3.0
0.0  0.0 2.0 0. 2.0
'RELANAL' 21 2 0 1.0
445. 445. .01 .0 .01 .0
0.35 1.0 4.0
0.0 0.0 2.0 0. 2.0
0.0 4.0 3.0
0.0  0.0 2.0 0. 2.0
'COMMENT' '          '
'COMMENT' '******* VAPOR PRESSURE LOWERING **********'
'VPL' 1.0
'COMMENT' '****** CORRECT FRACTURE TEMPERATURE ******'
'TEMPMOD' 1 25 1 466.3
'COMMENT' '            '
'LIQDEN'
62.43 3.2E-6 5.0E-4 14.7 68.0
'COMMENT' '          '
'RKREG' 1 25 1 2
'RKREG' 26 50 1 1
 'DENCS'   62.43
 1
```

APPENDIX A: TETRAD DUAL POROSITY MODEL

```
 18.02
'LIQSH' 0.245 0. 60. 165.
0.967452 3.63374E-4 60. 0. 0.

'GASSH'
0.56 0.  0.  0.  0.
'LIQTCON' 33.6 0. 170.
9.2,,,
'GASTCON'
0.7,,,
'COMMENT'  '          '
'COMMENT'  '          '
'PRES'  400.  2050 0.005976
'COMMENT'  '          '
'COMMENT'  '          '
'COMMENT'  '          '
'COMMENT'  '          '
'COMMENT'  '          '
'RECUR'
'COMMENT'  '******** PRODUCTION WELL IN FRACTURE BLOCK *******'
'PRODUCER' 'PROD1'         1        3
      1,
0.133 0.3 0. 0.
,
2050.0,,,
'COMMENT'  '*** OBSERVATION WELL IN MATRIX BLOCK OF PROD WELL ***'
'PRODUCER' 'OBS1'          1        3
      26,
0.133 0.3 0. 0.
,
2050.0,,,
'COMMENT'  '*** OBSERVATION WELL IN MATRIX BLOCK OF INJ WELL ***'
'PRODUCER' 'OBS2'          1        3
      50,
0.133 0.3 0. 0.
,
2050.0,,,
'COMMENT'  '******** INJECTION WELL IN FRACTURE BLOCK *********'
'INJECTOR' 'INJ1'          1        3
      25,
0.133 0.3 0. 0.
,
2050.0 0.38 0,
,,
120. 0.
,,
'COMMENT'  '          '
'TIMEYR' 0
'TIME' 0.0 1.0
'P'  'PROD1' 0.    100.  0.4167
'I'  'INJ1'  0.   1000.  0.0
```

```
'C'  'OBS1'
'C'  'OBS2'
'PLOT' 1 0
7 'PBHW' 'QTOTMASS' 'CTOTMASS' 'QTOTENER' 'CTOTENER' 'TAV' 'SGAV'
'TIME' 10000. 0
```

DUAL.IS: INTERSIM Input File for TETRAD

```
Base Case
  14   1   0   0   0   0
   5
   5
   1
DX
        200         200         200         200         200
        200         200         200         200         200
        200         200         200         200         200
        200         200         200         200         200
        200         200         200         200         200
DY
        200         200         200         200         200
        200         200         200         200         200
        200         200         200         200         200
        200         200         200         200         200
        200         200         200         200         200
Top
       2000        2000        2000        2000        2000
       2000        2000        2000        2000        2000
       2000        2000        2000        2000        2000
       2000        2000        2000        2000        2000
       2000        2000        2000        2000        2000
Thickness
        100         100         100         100         100
        100         100         100         100         100
        100         100         100         100         100
        100         100         100         100         100
        100         100         100         100         100
PORFR
        .01         .01         .01         .01         .01
        .01         .01         .01         .01         .01
        .01         .01         .01         .01         .01
        .01         .01         .01         .01         .01
        .01         .01         .01         .01         .01
PORMA
        .04         .04         .04         .04         .04
        .04         .04         .04         .04         .04
        .04         .04         .04         .04         .04
        .04         .04         .04         .04         .04
        .04         .04         .04         .04         .04
```

APPENDIX A: TETRAD DUAL POROSITY MODEL

kXfr

100	100	100	100	100
100	100	100	100	100
100	100	100	100	100
100	100	100	100	100
100	100	100	100	100

kXma

.01	.01	.01	.01	.01
.01	.01	.01	.01	.01
.01	.01	.01	.01	.01
.01	.01	.01	.01	.01
.01	.01	.01	.01	.01

kYfr

100	100	100	100	100
100	100	100	100	100
100	100	100	100	100
100	100	100	100	100
100	100	100	100	100

kYma

.01	.01	.01	.01	.01
.01	.01	.01	.01	.01
.01	.01	.01	.01	.01
.01	.01	.01	.01	.01
.01	.01	.01	.01	.01

kZfr

100	100	100	100	100
100	100	100	100	100
100	100	100	100	100
100	100	100	100	100
100	100	100	100	100

kZma

.01	.01	.01	.01	.01
.01	.01	.01	.01	.01
.01	.01	.01	.01	.01
.01	.01	.01	.01	.01
.01	.01	.01	.01	.01

PFR

400	400	400	400	400
400	400	400	400	400
400	400	400	400	400
400	400	400	400	400
400	400	400	400	400

PMA

400	400	400	400	400
400	400	400	400	400
400	400	400	400	400
400	400	400	400	400
400	400	400	400	400

SGFR

1	1	1	1	1
1	1	1	1	1

APPENDIX A: TETRAD DUAL POROSITY MODEL

```
        1       1       1       1       1
        1       1       1       1       1
        1       1       1       1       1
SGMA
      .7129   .7129   .7129   .7129   .7129
      .7129   .7129   .7129   .7129   .7129
      .7129   .7129   .7129   .7129   .7129
      .7129   .7129   .7129   .7129   .7129
      .7129   .7129   .7129   .7129   .7129
TFR
        445     445     445     445     445
        445     445     445     445     445
        445     445     445     445     445
        445     445     445     445     445
        445     445     445     445     445
TMA
        445     445     445     445     445
        445     445     445     445     445
        445     445     445     445     445
        445     445     445     445     445
        445     445     445     445     445
Trans Mods
  0
  0
  0
Wells
  0
```

B. GSS Data Deck for Dual Porosity Evaluation Model

```
%
TITLE     Quarter of a 5-Spot Pattern with Adsorption and Vapor Pressure Lowering
%
MODEL 1  % model 1 = GeoThermal model (default)
%
%       Nx  Ny  Nz  Option 1: input DX, DY, DZ by array
DIMN     5   5   1      %   X, Y, Z (or R, Theta, Z) Dimensions
%
DX       5*200.
DY       5*200.
DZ        100.
%
DEPTH     25*2000.    % Nx values of top of model
%
DUAL  1  1  5  1  5  1  1
%
FRACTYPE   25*3
%
FWIDTH     25*50.
%
PREF       14.7      % Reference pressure for porosity, psia
%
POROSITY   25*0.04  % matrix
POROSITY   25*0.01  % fracture
%
%  Permeability array, millidarcy
%
PERMX      25*0.01    % matrix
PERMX      25*100.0    % fracture
%
%       rock-compressibility  (1/psi)
COMPR    0.0
%
%       Rock Thermal conductivity (BTU/day/ft/F)
%       value@T-ref  slope   T-ref
TCONR      33.6        0.0    170.
%
%       Specific heat capacity of rock (BTU/lbm/F)
%       value@T-ref  slope   T-ref
HCAPR    0.245         0.0    170.
%
%
% Corey type relative permeability, Swc=0.35, Sgc=0.0, see Sorey (1980)
%  krl=Sw**4   krv=(1-Sw**2)(1-Sw)**2,  Sw=normalized
%
KRTABLE    1
%    Sl       krl        krv       Pc
```

```
KR   0.0      0.0        1.0       0.0
KR   0.35     0.00000    1.00000   0.0
KR   0.40     0.00004    0.84703   0.0
KR   0.45     0.00056    0.69903   0.0
KR   0.50     0.00284    0.56020   0.0
KR   0.55     0.00896    0.43391   0.0
KR   0.60     0.02188    0.32268   0.0
KR   0.65     0.04538    0.22818   0.0
KR   0.70     0.08407    0.15126   0.0
KR   0.75     0.14341    0.09191   0.0
KR   0.80     0.22972    0.04930   0.0
KR   0.85     0.35013    0.02174   0.0
KR   0.90     0.51262    0.00672   0.0
KR   0.95     0.72602    0.00088   0.0
KR   1.00     1.0        0.0       0.0
%
%       Densities at standard conditions (only rock dens. is used for now)
%           Water  Steam   Rock (lbm/cu-ft)
STDRHO      62.4     5.     165.
%
% Note: Arrange sorption table in order of DECREASING pressure (p/po)
%
%   Langmuir isotherm, c= 0.1
%         TABLE#    Po
DESTABLE     1    500.
%
SORPTION  1.00   0.012800
SORPTION  0.95   0.008386
SORPTION  0.90   0.006063
SORPTION  0.85   0.004630
SORPTION  0.80   0.003657
SORPTION  0.75   0.002954
SORPTION  0.70   0.002422
SORPTION  0.65   0.002005
SORPTION  0.60   0.001670
SORPTION  0.55   0.001394
SORPTION  0.50   0.001164
SORPTION  0.45   0.000968
SORPTION  0.40   0.000800
SORPTION  0.35   0.000654
SORPTION  0.30   0.000526
SORPTION  0.25   0.000413
SORPTION  0.20   0.000312
SORPTION  0.15   0.000222
SORPTION  0.10   0.000141
SORPTION  0.05   0.000067
SORPTION  1.E-6  0.000000
%
%       Value  Fr. Nx to Nx    Fr. Ny to Ny   Fr Nz to Nz
DREGION   1         1    5          1    5       1     1
%       Value = 0 => no sorption / flat surface thermodynamics (default)
```

APPENDIX B: GSS DUAL POROSITY MODEL

```
%             1 => use this sorption table # for the identified blocks
%
%  Specify initial P, T and Sl arrays, Use option 1 for init
%
PARRAY     50*400.      % Initial pressure array, psia
TARRAY     50*466.3     % deg-F, ignore if saturated 2-phase steam
SLARRAY    25*0.2871    % SL ignored if sorption is applied
%
DATE  0     % default option, time start from 0.
%
TIMER   0   % TIME and TIMESTEP to be specified in days (default)
%  TIMER   1   % TIME and TIMESTEP to be specified in seconds
%  TIMER   2   % TIME and TIMESTEP to be specified in years
%
% -------------- Producer ----------------------------------------------
%
%     WellName  Type  Nx  Ny  Nz  IHor  BHPDatum
WELL  'PRODUCER'   1    1   1   1    1     2050.
%
WPERF   1   % perforate in layer 1 only
%
%         rw  skin  w-index      wellfg
WINDEX   0.30   0.0    3000.        0.0
%
% -------------- Injector ----------------------------------------------
%
%     WellName  Type  Nx  Ny  Nz  IHor  BHPDatum
WELL  'INJECTOR'   1    5   5   1    1     2050.
%
WPERF   1   % perforate in layer 1 only
%
%         rw  skin  w-index      wellfg
WINDEX   0.30   0.0     1.0       0.0
%
%
INIT     1   % Option 1 : to use user supplied p, T and sl
           % Option 0 : auto, requires p, T at datum
%
% ------------------------- RECURRENT DATA -----------------------------
%
%    MaxIter   NRtolerence   ResidualTolerence
TOL      10        1.E-3        .001
%
%  Specify maximum changes over a time step, zero values are ignored
%       DPMAX  DSMAX  DHMAX  DZMAX
CHANGE   200.   0.10   500.    0.25
%
MAPS  1  % turn parameter map printing: 1=on 0=off.
%
%  Specify observation blocks (p, T, Sl, h) will be printed in filename.sum
%       Nx  Ny  Nz
```

APPENDIX B: GSS DUAL POROSITY MODEL

```
OBSERVE   1   1   1
%
%          start       min       max    Increment factor
TIMESTEP    1.E-4      1.E-6     1.00    1.5
%
%    Well control modes: 1=rate,  2=bhp
%    Units:  rate:lb/day    bhp:psia  Tinj: deg-F
%
%             Primary         2ndary
%    WellName  Mode    Value  Mode    Value    Tinj  Inj.SteamQuality
RATE  'INJECTOR'  1       -0.   2     3000.      120.        0.0
%
RATE  'PRODUCER'  2      100.    1    10000.      144.        1.0
%
%  Note: 1) Use NEGATIVE rate to indicate injection
%        2) in RATE card, Tinj and Steam quality inputs are necessary. These
%           values are used when injecting, use dummy values otherwise.
%
TIME      10
%    MaxIter   NRtolerance   ResidualTolerance
TOL       15        1.E-3        0.0001
TIMESTEP    1.00    1.E-6        5.0      1.5
TIME      100.
TIMESTEP    5.00    1.E-6       25.0      1.5
TIME     1000.
TIMESTEP   25.00    1.E-6       25.0      2.0
TIME     2000.
TIMESTEP   25.00    1.E-6       25.0      2.0
TIME     3000.
TIMESTEP   25.00    1.E-6       25.0      2.0
TIME     4000.
TIMESTEP   25.00    1.E-6       25.0      2.0
TIME     5000.
TIMESTEP   25.00    1.E-6       25.0      2.0
TIME     6000.
TIMESTEP   25.0     1.E-6       25.0      2.0
TIME     7000.
TIMESTEP   25.00    1.E-6       25.0      2.0
TIME     8000.
TIMESTEP   25.00    1.E-6       25.0      2.0
TIME     9000.
TIMESTEP   25.00    1.E-6       25.0      2.0
TIME    10000.
END
```

C. TETRAD Data Deck for 1-D Evaluation Model

```
'NOMESS'
'COMMENT'  '     '
'COMMENT'  'MODIFIED DATA DECK (1)                    '
'COMMENT'  'RUN THIS DECK USING TETRAD VERSION 12    '
'COMMENT'  '     '
'COMMENT'  'THIS IS A GEOTHERMAL SINGLE POROSITY MODEL'
'COMMENT'  '1-DIMENSIONAL HORIZONTAL, CARTESIAN GRID'
'COMMENT'  'WITH VAPOR-PRESSURE LOWERING AND CAPILLARY PRESSURE'
'COMMENT'  '     '
'COMMENT'  '     '
'TYPE'  4  1  1 0.0  0.0
'COMMENT'  '          '
'COMMENT'  '**********  CHANGE DIMENSION STATEMENT TO PROBLEM SIZE ***'
'COMMENT'  '          '
'DIMEN'     5    1    1    500
'COMMENT'  '          '
'COMMENT'  '********** DEFINE GRIDS **********'
'DELX',,
,5*200
'DELY',,
,1*200
'DELZ',,
,100
'FTOPS' 1,,
1 2000.0
'LEASE'  1 1 1 1
'LEASE'  2 2 1 2
'LEASE'  3 3 1 3
'LEASE'  4 4 1 4
'LEASE'  5 5 1 5
'PORMOD' 1 5  1 0.05
'PERMMOD' 1 5  1 20.008 20.008 20.008
'COMMENT'  '          '
'COMMENT'  '**********  OUTPUT FILE CONTROLS  ******************'
'COMMENT'  '          '
'UNITS' 0 1 0 1
'PRINT' 10 0 0 0 0
'OUTFUN' 2 0 3 0 0 0 0 8 0 0
'OUTGEO' 0 0 1 1 0 0 1 0 1 0
'OUTMISC' 4 2 0 0 1 0 0 0 0 0
'GVWRITE' 0 3
3 'P' 'SG' 'T'
'COMMENT'  '          '
'COMMENT'  '******************  NUMERICAL CONTROLS  ****************'
'COMMENT'  '          '
'TMSTEP',,,500. 10000.0 10.0,,,,,,,
'NORM' 50.0 0.1 .2 50.0
```

APPENDIX C: TETRAD 1-D EVALUATION MODEL

```
'COMP' 0.5E-06 400.  1.E-09 450.
'COMMENT'  '          '
'PROPERTY'
'COMMENT'  '          '
'COMMENT'  '*** RELATIVE PERM CURVES AND CAP PRESSURE ******'
'COMMENT'  '          '
'RELGW' 1 21 0 .01 0.0
.005 0.0     1.0   83436.0
.011 0.0     1.0   64131.0
.017 0.0     1.0   52838.0
.024 0.0     1.0   44826.0
.032 0.0     1.0   38611.0
.040 0.0     1.0   33533.0
.050 0.0     1.0   29239.0
.061 0.0     1.0   25520.0
.074 0.0     1.0   22240.0
.089 0.0     1.0   19305.0
.107 0.0     1.0   16651.0
.128 0.0     1.0   14227.0
.154 0.0     1.0   11998.0
.185 0.0     1.0    9934.0
.226 0.0     1.0    8012.0
.280 0.0     1.0    6215.0
.355 2.44E-9 0.9859 4526.0
.464 0.00090 0.6582 2934.0
.642 0.04080 0.2418 1429.0
.980 0.88380 5.54E-5   0.0
1.00 1.00000 0.0       0.0
'COMMENT' '           '
'COMMENT' '           '
'COMMENT' '******* VAPOR PRESSURE LOWERING **********'
'VPL' 1.0
'PRES' 400.0 2050.0 0.005976
'SATMOD' 1 5 1 0.70 0.0
'COMMENT' '           '
'LIQDEN'
62.43 3.2E-6 5.0E-4 14.7 68.0
'COMMENT' '          '
'RKREG' 1 5 1 1
'DENCS'   62.43
 1
 18.02
'LIQSH' 0.245 0. 60. 165.
0.967452 3.63374E-4 60. 0. 0.
'GASSH'
0.56 0.  0.  0.  0.
'LIQTCON' 33.6 0. 170.
9.2,,,
'GASTCON'
0.7,,,
'COMMENT'  '          '
```

APPENDIX C: TETRAD 1-D EVALUATION MODEL

```
'RECUR'
'COMMENT'  '******** PRODUCTION WELL  *******'
'PRODUCER' 'PROD1'          1        3
     5,
0.133 0.3 0. 0.
,
2050.0,,,
'PRODUCER' 'OBS2'          1        3
     2,
0.133 0.3 0. 0.
,
2050.0,,,
'PRODUCER' 'OBS3'          1        3
     3,
0.133 0.3 0. 0.
,
2050.0,,,
'PRODUCER' 'OBS4'          1        3
     4,
0.133 0.3 0. 0.
,
2050.0,,,
'PRODUCER' 'OBS5'          1        3
     5,
0.133 0.3 0. 0.
,
2050.0,,,
'COMMENT'  '******** INJECTION WELL  *********'
'INJECTOR' 'INJ1'          1        3
     1,
0.133 0.3 0. 0.
,
2050.0 0.38 0,
,,
120. 0.
,,
'COMMENT'  '          '
'TIMEYR' 0
'TIME' 0.0 1.0
'C'  'PROD1' 0.    100.  0.1
'I'  'INJ1'  0.   1000.  0.02
'PLOT' 1 0
7 'PBHW' 'QTOTMASS' 'CTOTMASS' 'QWPMASS' 'CTOTENER' 'TAV' 'SGAV'
'TIME' 10000.0 -1.0
'C'  'PROD1' 0.    100.  0.1
'I'  'INJ1'  0.   1000.  0.02
'PLOT' 1 0
7 'PBHW' 'QTOTMASS' 'CTOTMASS' 'QWPMASS' 'CTOTENER' 'TAV' 'SGAV'
'TIME' 50000. 0
```

D. TETRAD Data Deck for 2-D Radial Evaluation Model

```
'NOMESS'
'COMMENT' '     '
'COMMENT'  'MODIFIED DATA DECK (1)                    '
'COMMENT'  'RUN THIS DECK USING TETRAD VERSION 12    '
'COMMENT' '     '
'COMMENT'  'THIS IS A GEOTHERMAL SINGLE POROSITY MODEL'
'COMMENT'  '2-D HORIZONTAL, RADIAL GRID GEOMETRY'
'COMMENT'  'WITH VAPOR-PRESSURE LOWERING AND CAPILLARY PRESSURE'
'COMMENT' '     '
'COMMENT' '     '
'TYPE'  4  1  1 0.0  0.0
'COMMENT' '          '
'COMMENT'  '*********  CHANGE DIMENSION STATEMENT TO PROBLEM SIZE ***'
'COMMENT' '          '
'DIMEN'     5    8   1     500
'COMMENT' '          '
'COMMENT'  '********** DEFINE GRIDS **********'
'DELX' 2
1 100.0
4 4*100.0
'DELZ',,
,100.0
'RADIAL'  0  0.3
'DELANGLE'  1
,8*45.0
'FTOPS' 1,,
1 2000.0
'PORMOD' 1 40 1 0.05
'PERMMOD' 1 40 1 20.008 20.008 20.008
'COMMENT' '          '
'COMMENT'  '*********  OUTPUT FILE CONTROLS  *****************'
'COMMENT' '          '
'UNITS' 0 1 0 1
'PRINT' 0 0 0 1 0
'OUTFUN' 1 2 0 0 0 0 0 8 0 0
'OUTGEO' 2 1 2 2 2 2 2 0 0 0
'OUTMISC' 0 2 0 0 1 0 0 0 0 0
'COMMENT' '          '
'COMMENT'  '******************  NUMERICAL CONTROLS  ***************'
'COMMENT' '          '
'TMSTEP',,,250. 10000 10.0,,,,,,,
'NORM' 250 0.02 .2 50
'COMP' 0.5E-06 400.  1.E-09 450.
'COMMENT' '          '
'PROPERTY'
'COMMENT' '          '
'COMMENT'  '***  RELATIVE PERM CURVES AND CAP PRESSURE ******'
```

APPENDIX D: TETRAD 2-D RADIAL EVALUATION MODEL

```
'COMMENT' '          '
'RELGW' 1 21 0 .01 0.0
.005 0.0    1.0   83436.0
.011 0.0    1.0   64131.0
.017 0.0    1.0   52838.0
.024 0.0    1.0   44826.0
.032 0.0    1.0   38611.0
.040 0.0    1.0   33533.0
.050 0.0    1.0   29239.0
.061 0.0    1.0   25520.0
.074 0.0    1.0   22240.0
.089 0.0    1.0   19305.0
.107 0.0    1.0   16651.0
.128 0.0    1.0   14227.0
.154 0.0    1.0   11998.0
.185 0.0    1.0    9934.0
.226 0.0    1.0    8012.0
.280 0.0    1.0    6215.0
.355 2.44E-9 0.9859 4526.0
.464 0.00090 0.6582 2934.0
.642 0.04080 0.2418 1429.0
.980 0.88380 5.54E-5   0.0
1.00 1.00000 0.0       0.0
'COMMENT' '          '
'RELANAL' 21 3 0 1.0
445. 445. .01 .0 .01 .0
0.35 1.0 4.0
0.0 0.0 2.0 0. 2.0
0.0 4.0 3.0
0.0  0.0 2.0 0. 2.0
'RELANAL' 21 2 0 1.0
445. 445. .01 .0 .01 .0
0.35 1.0 4.0
0.0 0.0 2.0 0. 2.0
0.0 4.0 3.0
0.0  0.0 2.0 0. 2.0
'COMMENT' '          '
'COMMENT' '******* VAPOR PRESSURE LOWERING **********'
'VPL' 1.0
'PRES' 400.0 2050.0 0.005976
'PRESMOD' 1 40 1 400.0
'SATMOD' 1 40 1 0.70 0.0
'COMMENT' '          '
'LIQDEN'
62.43 3.2E-6 5.0E-4 14.7 68.0
'COMMENT' '          '
'RKREG' 1 40 1 1
'DENCS'   62.43
 1
 18.02
'LIQSH' 0.245 0. 60. 165.
```

```
0.967452 3.63374E-4 60. 0. 0.
'GASSH'
0.56 0.  0.  0.  0.
'LIQTCON' 33.6 0. 170.
9.2,,,
'GASTCON'
0.7,,,
'COMMENT'  '          '
'COMMENT'  '          '
'COMMENT'  '          '
'COMMENT'  '          '
'COMMENT'  '          '
'COMMENT'  '          '
'COMMENT'  '          '
'RECUR'
'COMMENT'  '******** PRODUCTION WELL *******'
'PRODUCER' 'PROD1'         1        3
     1,
0.152 0.3 0. 0.
,
2050.0,,,
'COMMENT'  '******** OBSERVATION WELLS **********'
'PRODUCER' 'OBS2'          1        3
     2,
0.14 0.3 0. 0.
,
2050.0,,,
'PRODUCER' 'OBS3'          1        3
     3,
0.14 0.3 0. 0.
,
2050.0,,,
'PRODUCER' 'OBS4'          1        3
     4,
0.14 0.3 0. 0.
,
2050.0,,,
'PRODUCER' 'OBS5'          1        3
     5,
0.134 0.3 0. 0.
,
2050.0,,,
'COMMENT'  '******** INJECTION WELL *********'
'INJECTOR' 'INJ1'          1        3
     1,
0.152 0.3 0. 0.
,
2050.0 0.38 0,
,,
120. 0.
,,
```

APPENDIX D: TETRAD 2-D RADIAL EVALUATION MODEL

```
'COMMENT' '  '
'TIMEYR' 0
'TIME' 0.0 1.0
'C' 'PROD1' 0.  100.  0.05
'C' 'INJ1' 0.  1000.  0.05
'PLOT' 1 0
7 'PBHW' 'QTOTMASS' 'CTOTMASS' 'QWPMASS' 'CTOTENER' 'TAV' 'SGAV'
'TIME' 5000.0 -1.0
'C' 'PROD1' 0.  100.  0.05
'I' 'INJ1' 0.  1000.  0.3
'PLOT' 1 0
7 'PBHW' 'QTOTMASS' 'CTOTMASS' 'QWPMASS' 'CTOTENER' 'TAV' 'SGAV'
'TIME' 10000.0 -1.0
'C' 'PROD1' 0.  100.  0.05
'C' 'INJ1' 0.  1000.  0.05
'PLOT' 1 0
7 'PBHW' 'QTOTMASS' 'CTOTMASS' 'QWPMASS' 'CTOTENER' 'TAV' 'SGAV'
'TIME' 15000.0 -1.0
'P' 'PROD1' 0.  401.  0.3
'C' 'INJ1' 0.  1000.  0.05
'PLOT' 1 0
7 'PBHW' 'QTOTMASS' 'CTOTMASS' 'QWPMASS' 'CTOTENER' 'TAV' 'SGAV'
'TIME' 20000.0 -1.0
'P' 'PROD1' 0.  401.  0.3
'C' 'INJ1' 0.  1000.  0.05
'PLOT' 1 0
7 'PAV' 'QTOTMASS' 'CTOTMASS' 'QWPMASS' 'CTOTENER' 'TAV' 'SGAV'
'TIME' 30000. 0
```

E. TETRAD Data Deck for 3-D Field Scale Model

```
'NOMESS'
'COMMENT'  '     '
'COMMENT'  'MODIFIED AND EXPANDED DATA DECK (1)                '
'COMMENT'  'RUN THIS DECK USING TETRAD VERSION 12    '
'COMMENT'  '     '
'COMMENT'  'THIS IS A GEOTHERMAL SINGLE POROSITY MODEL'
'COMMENT'  'ONE-QUARTER OF A 5-SPOT PATTERN (3-D)'
'COMMENT'  'WITH VAPOR-PRESSURE LOWERING AND CAPILLARY PRESSURE'
'COMMENT'  '     '
'TYPE'  4  1  1 0.0  0.0
'COMMENT'  '          '
'COMMENT'  '**********  CHANGE DIMENSION STATEMENT TO PROBLEM SIZE ***'
'COMMENT'  '          '
'DIMEN'     7   7   9    500
'COMMENT'  '          '
'COMMENT'  '********** DEFINE GRIDS **********'
'DELX',,
,7*200
'DELY',,
,7*200
'DELZ',,
,9*400
'FTOPS' 1,,
1 2000.0
'PORMOD' 1 441 1 0.05
'PERMMOD' 1 441 1 40.008 40.008 20.004
'COMMENT'  '          '
'COMMENT'  '*********  OUTPUT FILE CONTROLS  ******************'
'COMMENT'  '          '
'UNITS' 0 1 0 1
'PRINT' 0 0 0 0 0
'OUTFUN' 1 2 0 0 0 0 0 8 0 0
'OUTGEO' 2 1 2 2 2 2 2 0 0 0
'OUTMISC' 0 2 0 0 0 0 0 0 0 0
'COMMENT'  '          '
'COMMENT'  '******************  NUMERICAL CONTROLS  ****************'
'COMMENT'  '          '
'TMSTEP',,,250. 10000 10.0,,,,,,,
'NORM' 250 0.02 .2 50
'COMP' 0.5E-06 400.  1.E-09 450.
'COMMENT'  '          '
'PROPERTY'
'COMMENT'  '          '
'RELGW' 1 21 0 .01 0.0
.005 0.0     1.0   83436.0
.011 0.0     1.0   64131.0
.017 0.0     1.0   52838.0
```

```
.024 0.0     1.0   44826.0
.032 0.0     1.0   38611.0
.040 0.0     1.0   33533.0
.050 0.0     1.0   29239.0
.061 0.0     1.0   25520.0
.074 0.0     1.0   22240.0
.089 0.0     1.0   19305.0
.107 0.0     1.0   16651.0
.128 0.0     1.0   14227.0
.154 0.0     1.0   11998.0
.185 0.0     1.0    9934.0
.226 0.0     1.0    8012.0
.280 0.0     1.0    6215.0
.355 2.44E-9 0.9859 4526.0
.464 0.00090 0.6582 2934.0
.642 0.04080 0.2418 1429.0
.980 0.88380 5.54E-5   0.0
1.00 1.00000 0.0       0.0
'COMMENT' '              '
'COMMENT' '******* VAPOR PRESSURE LOWERING **********'
'VPL' 1.0
'COMMENT' '              '
'PRES' 400.0 3800 0.005976
'SATMOD' 1 441 1 0.65 0.0
'COMMENT' '              '
'LIQDEN'
62.43 3.2E-6 5.0E-4 14.7 68.0
'COMMENT' '              '
'RKREG' 1 441 1 1
'DENCS'   62.43
 1
 18.02
'LIQSH' 0.245 0. 60. 165.
0.967452 3.63374E-4 60. 0. 0.
'GASSH'
0.56 0.  0.  0.  0.
'LIQTCON' 33.6 0. 170.
9.2,,,
'GASTCON'
0.7,,,
'COMMENT'  '              '
'RECUR'
'COMMENT'  '******** PRODUCTION WELL *******'
'PRODUCER' 'PROD1'          3         3
      148,,,
0.133 0.3 0. 0.
,,,,
,,,,
'COMMENT'  '*** OBSERVATION WELL ***'
'PRODUCER' 'OBS1'           1         3
      221,
```

APPENDIX E: TETRAD 3-D FIELD SCALE MODEL

```
0.140 0.3 0. 0.
,
,,,,
'COMMENT'  '******** INJECTION WELL *********'
'INJECTOR' 'INJ1'          1        3
       245,
0.133 0.3 0. 0.
,
,0.38 0,
,,
80. 0.
,,
'COMMENT'  '           '
'TIMEYR' 0
'TIME' 0.0 1.0
'P'  'PROD1' 0.    100.  25.0
'I'  'INJ1'  0.   1000.   0.0
'C'  'OBS1'
'PLOT' 1 0
7 'PBHW' 'QTOTMASS' 'CTOTMASS' 'QWPMASS' 'CTOTENER' 'TAV' 'SGAV'
'TIME' 18250.0 -1.0
'P'  'PROD1' 0.    100.  25.0
'I'  'INJ1'  0.   1000.   0.0
'C'  'OBS1'
'PLOT' 1 0
7 'PBHW' 'QTOTMASS' 'CTOTMASS' 'QWPMASS' 'CTOTENER' 'TAV' 'SGAV'
'TIME' 20000. 0
```

F. Result Plots of Case I

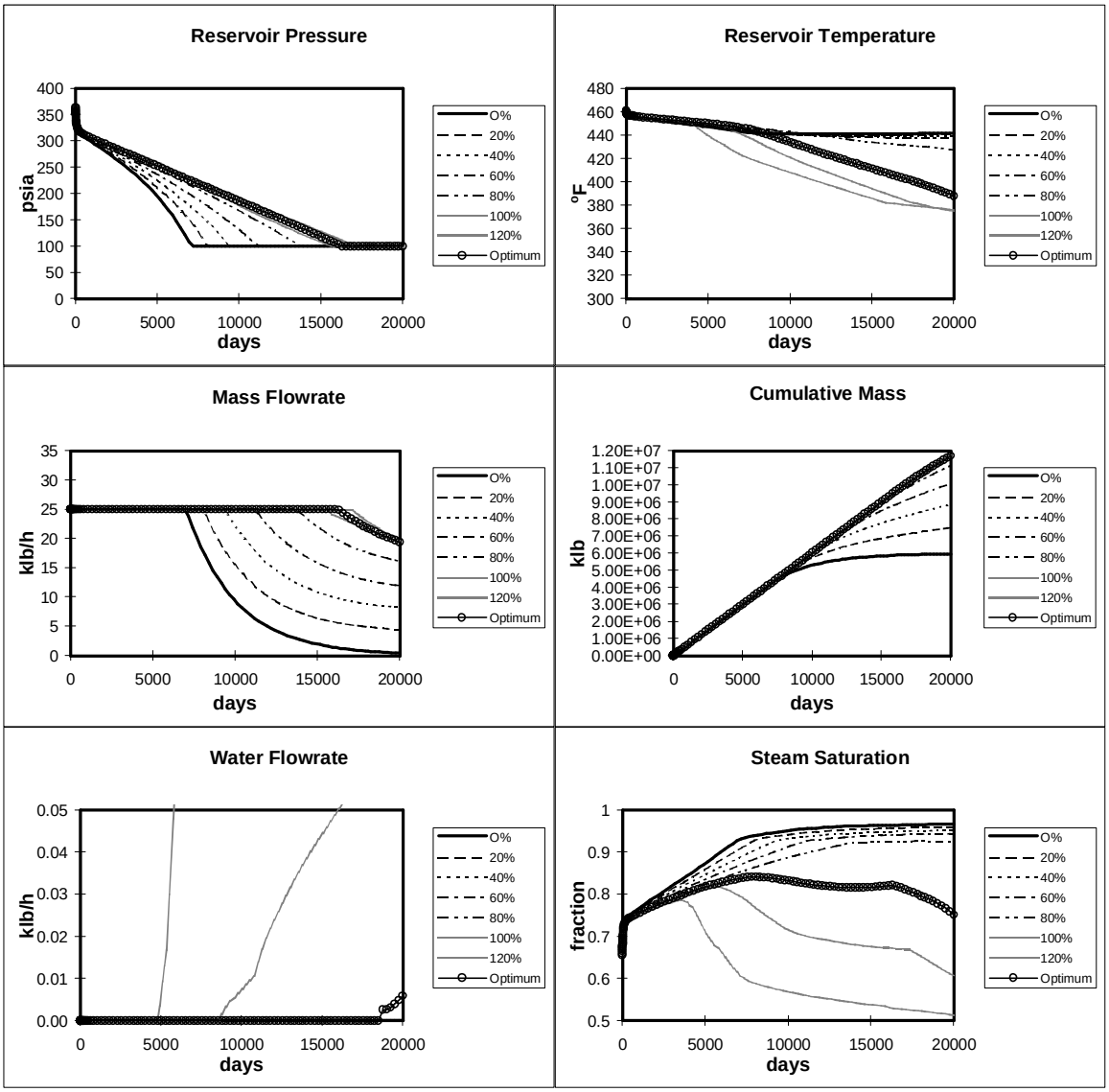

Case I: Injection starts at t=0 years. Properties measured in the production gridblock.

APPENDIX F: RESULTS OF CASE I

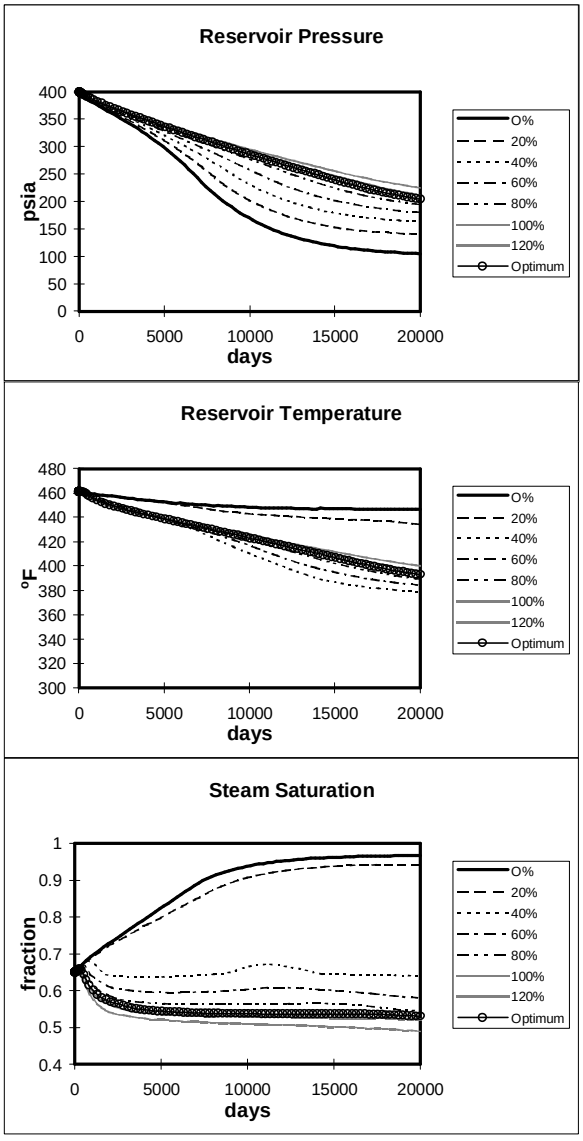

Case I: Injection starts at t=0 years. Properties measured in the observation gridblock.

G. Result Plots of Case II

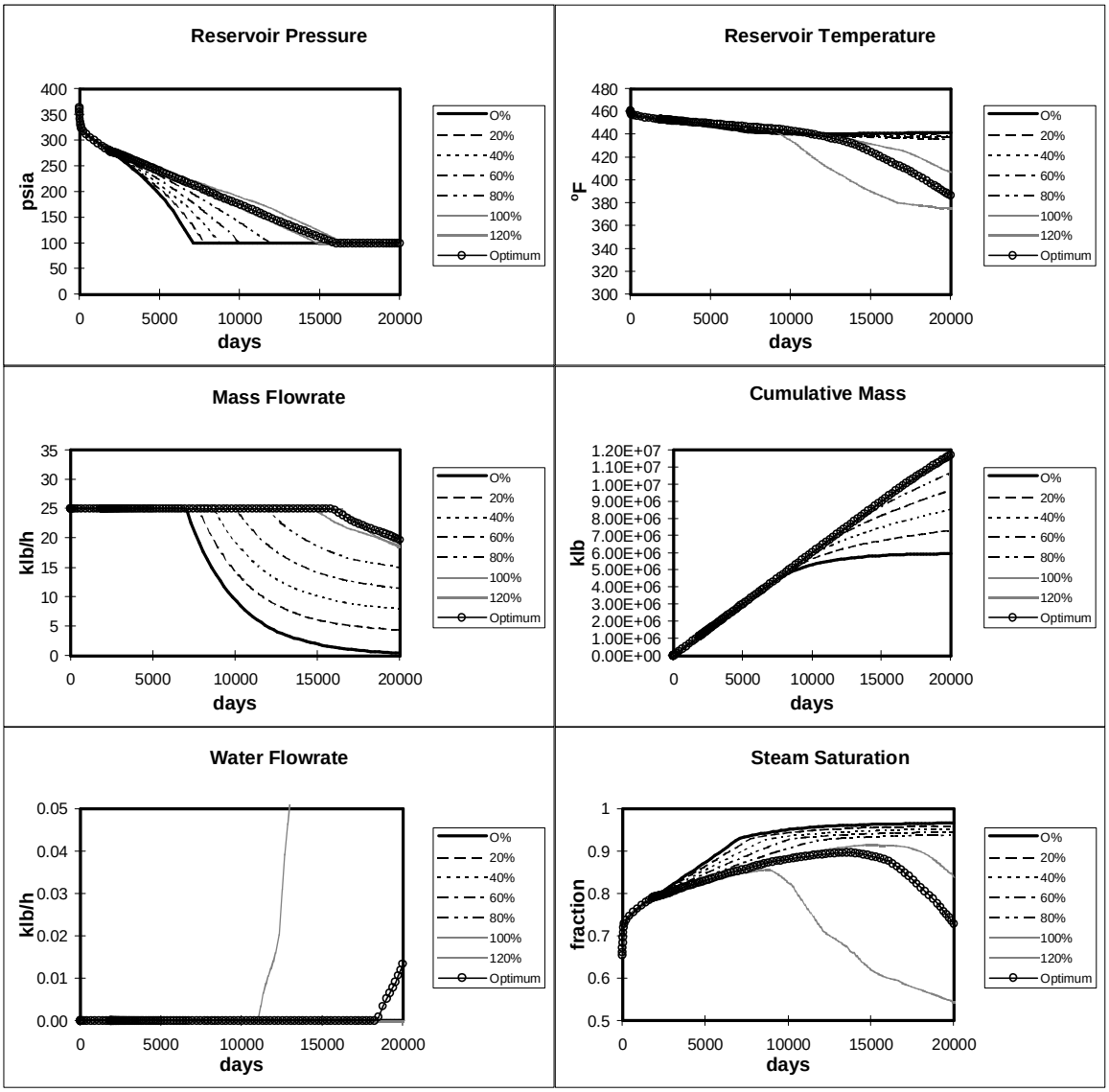

Case II: Injection start @ t=5 years. Properties measured in the production gridblock.

APPENDIX G: RESULTS OF CASE II

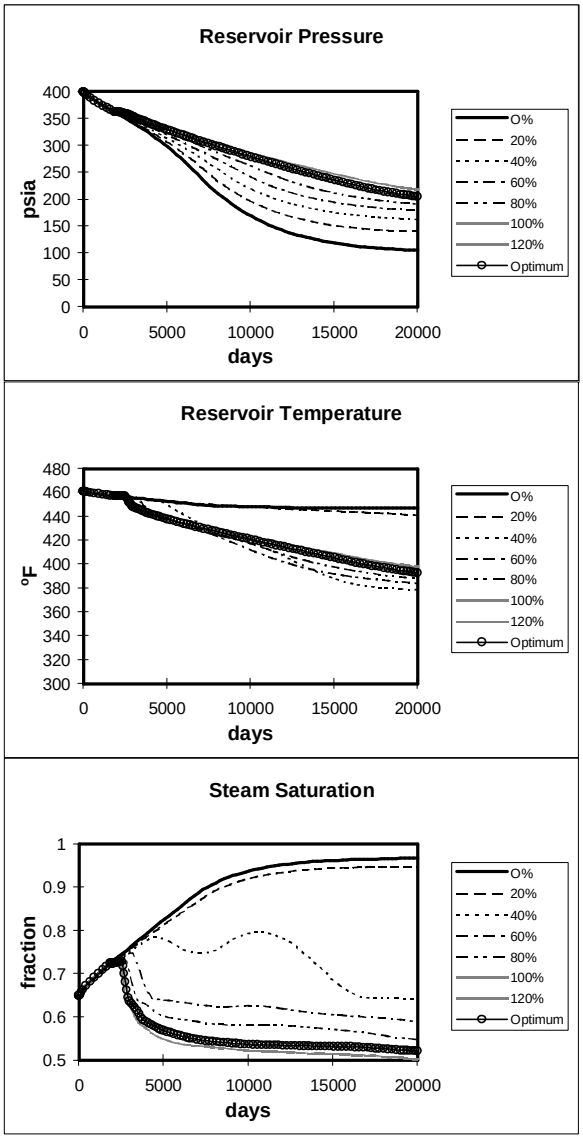

Case II: Injection start @ t=5 years. Properties measured in the observation gridblock.

H. Result Plots of Case III

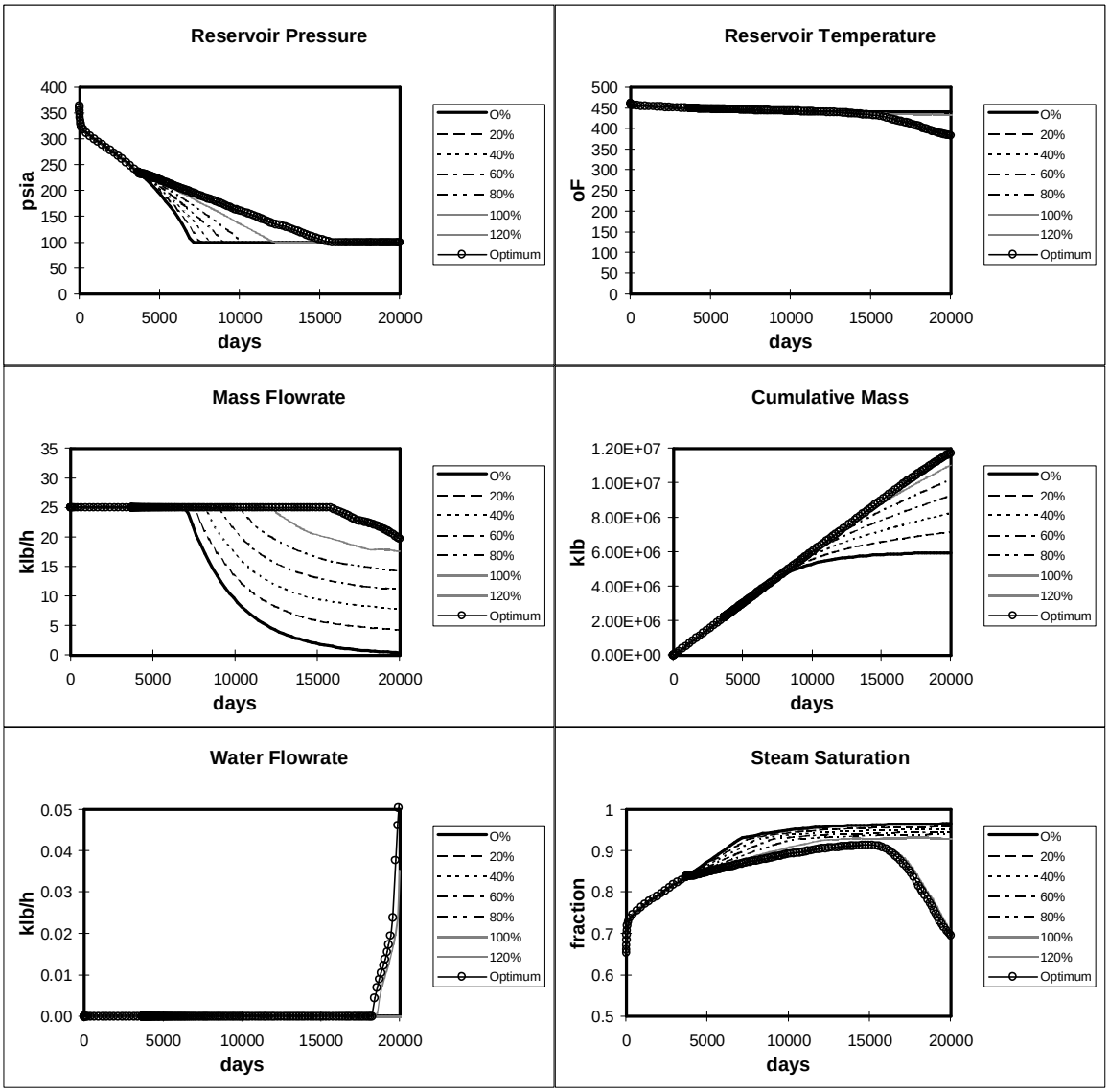

Case III: Injection starts at t=10 years. Properties measured in the production gridblock.

APPENDIX H: RESULTS OF CASE III

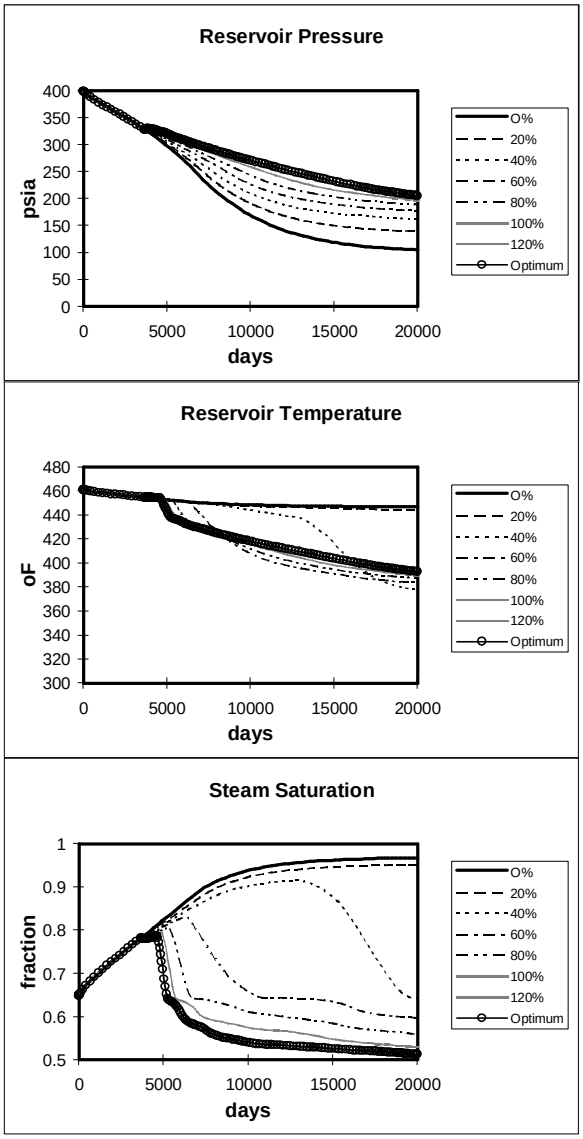

Case III: Injection starts at t=10 years. Properties measured in the observation gridblock.

I. Result Plots of Case IV

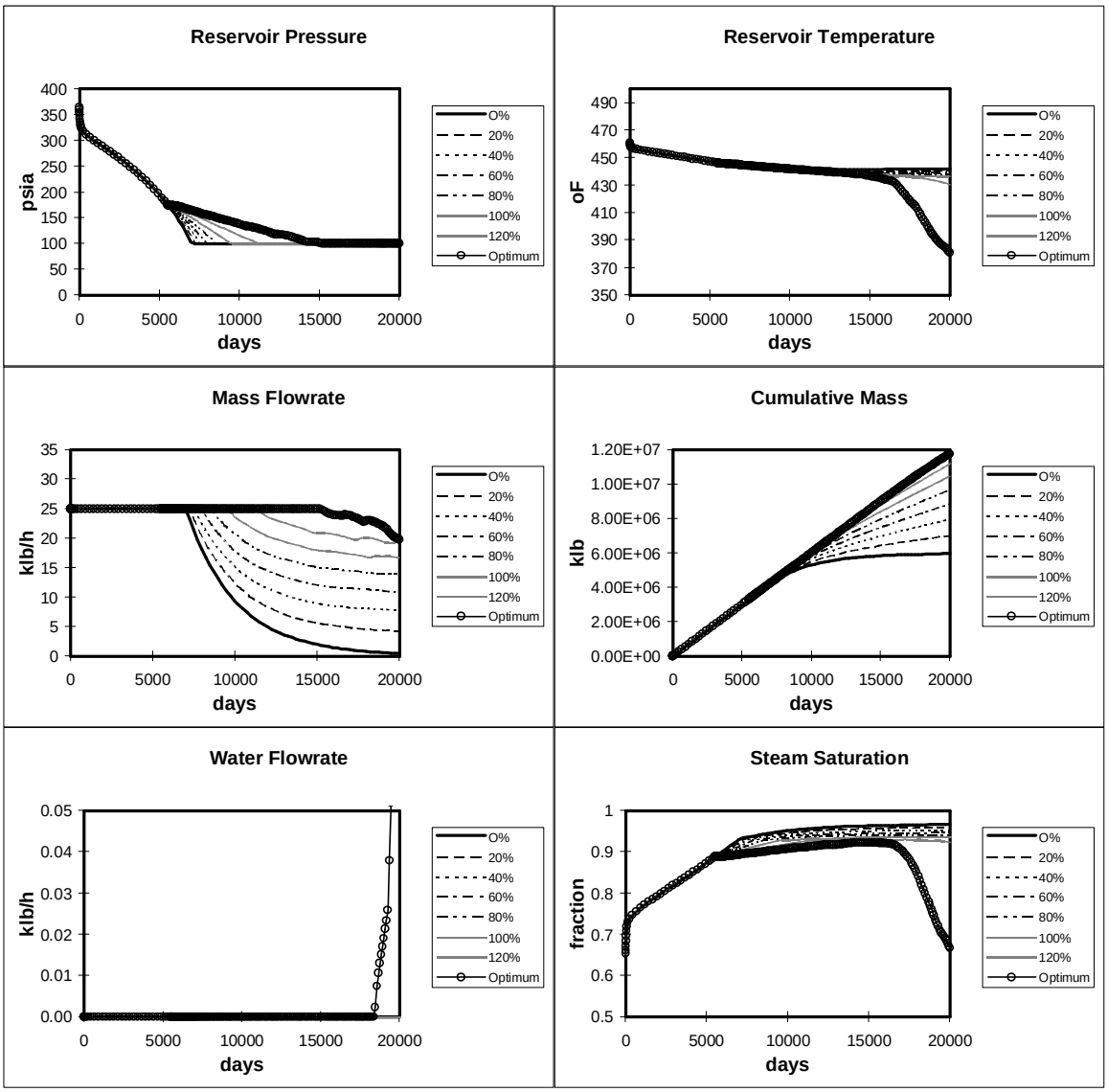

Case IV: Injection starts at t=15 years. Properties measured in the production gridblock.

APPENDIX I: RESULTS OF CASE IV

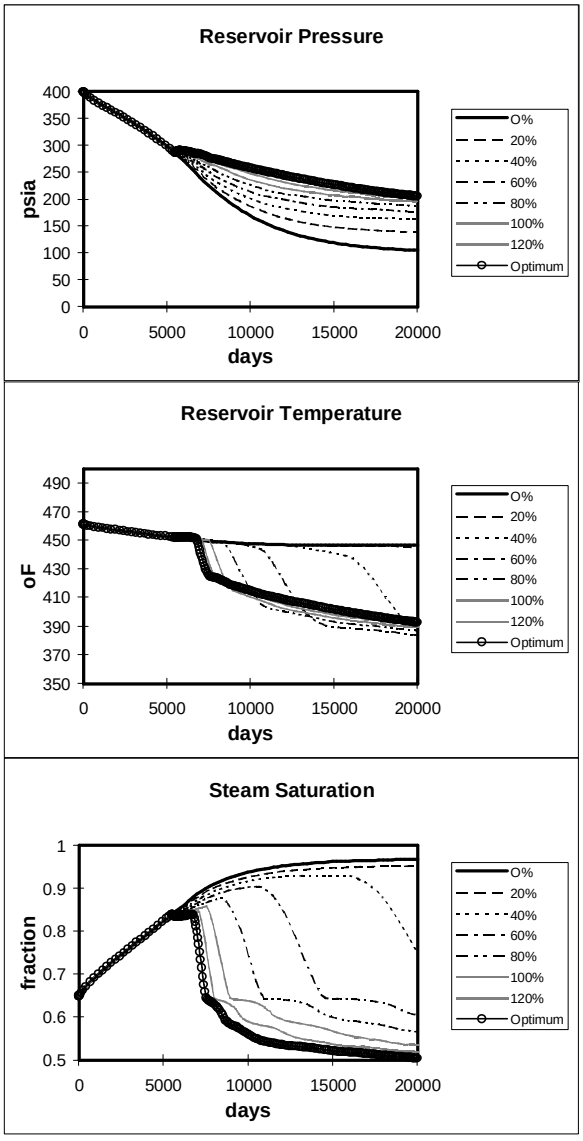

Case IV: Injection starts at t=15 years. Properties measured in the observation gridblock.

J. Result Plots of Case V

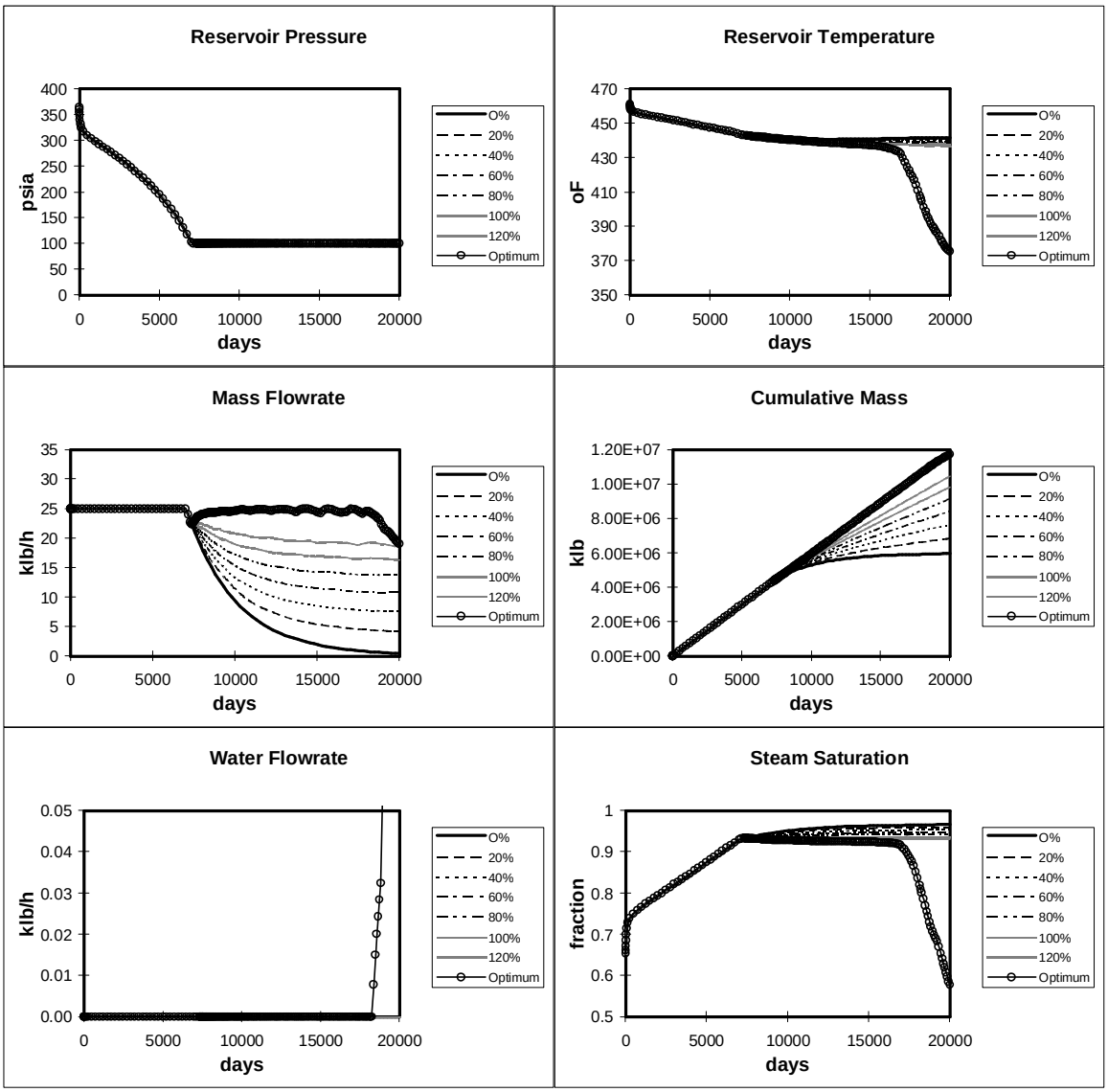

Case V: Injection starts at t=20 years. Properties measured in the production gridblock.

APPENDIX J: RESULTS OF CASE V

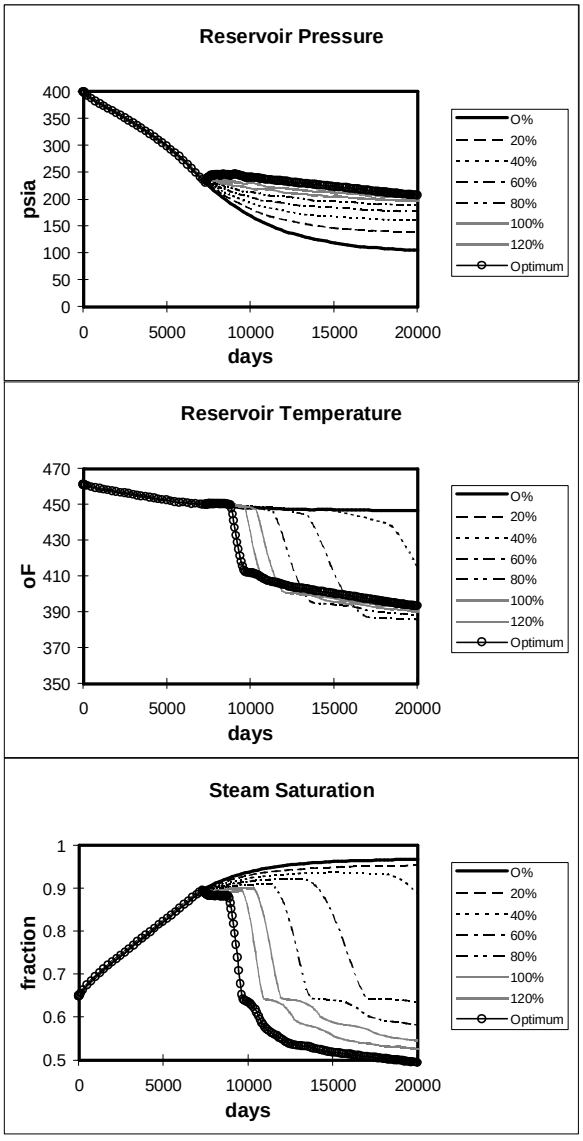

Case V: Injection starts at t=20 years. Properties measured in the observation gridblock.

K. Result Plots of Case VI

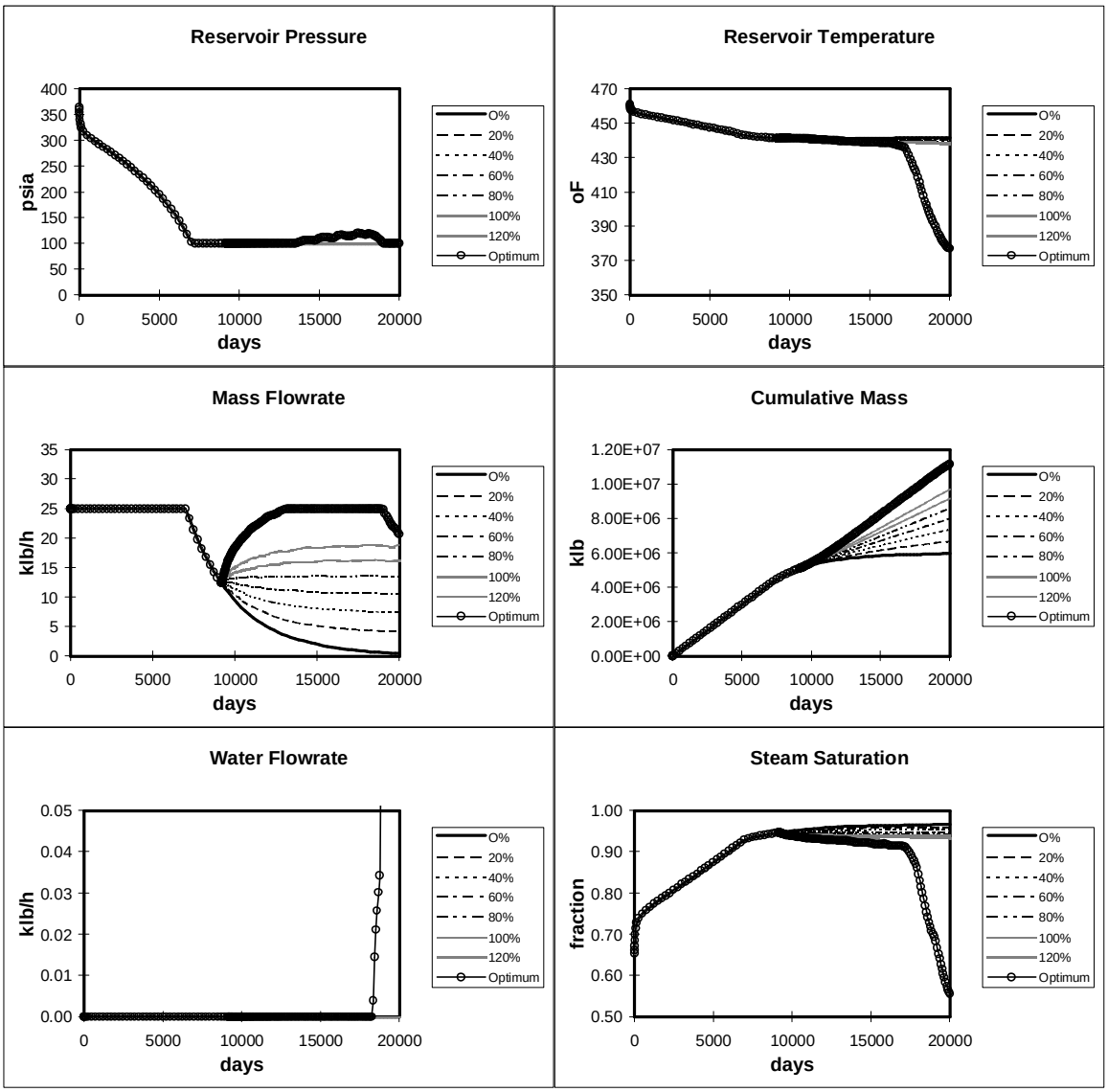

Case VI: Injection starts at t=25 years. Properties measured in the production gridblock.

APPENDIX K: RESULTS OF CASE VI

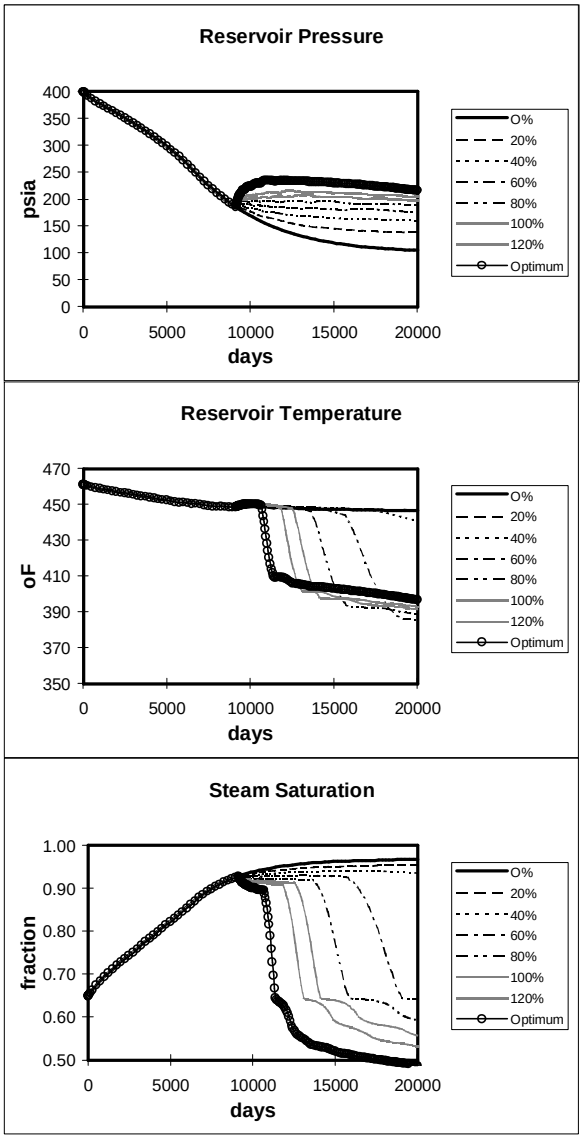

Case VI: Injection starts at t=25 years. Properties measured in the observation gridblock.

L. Result Plots of Case VII

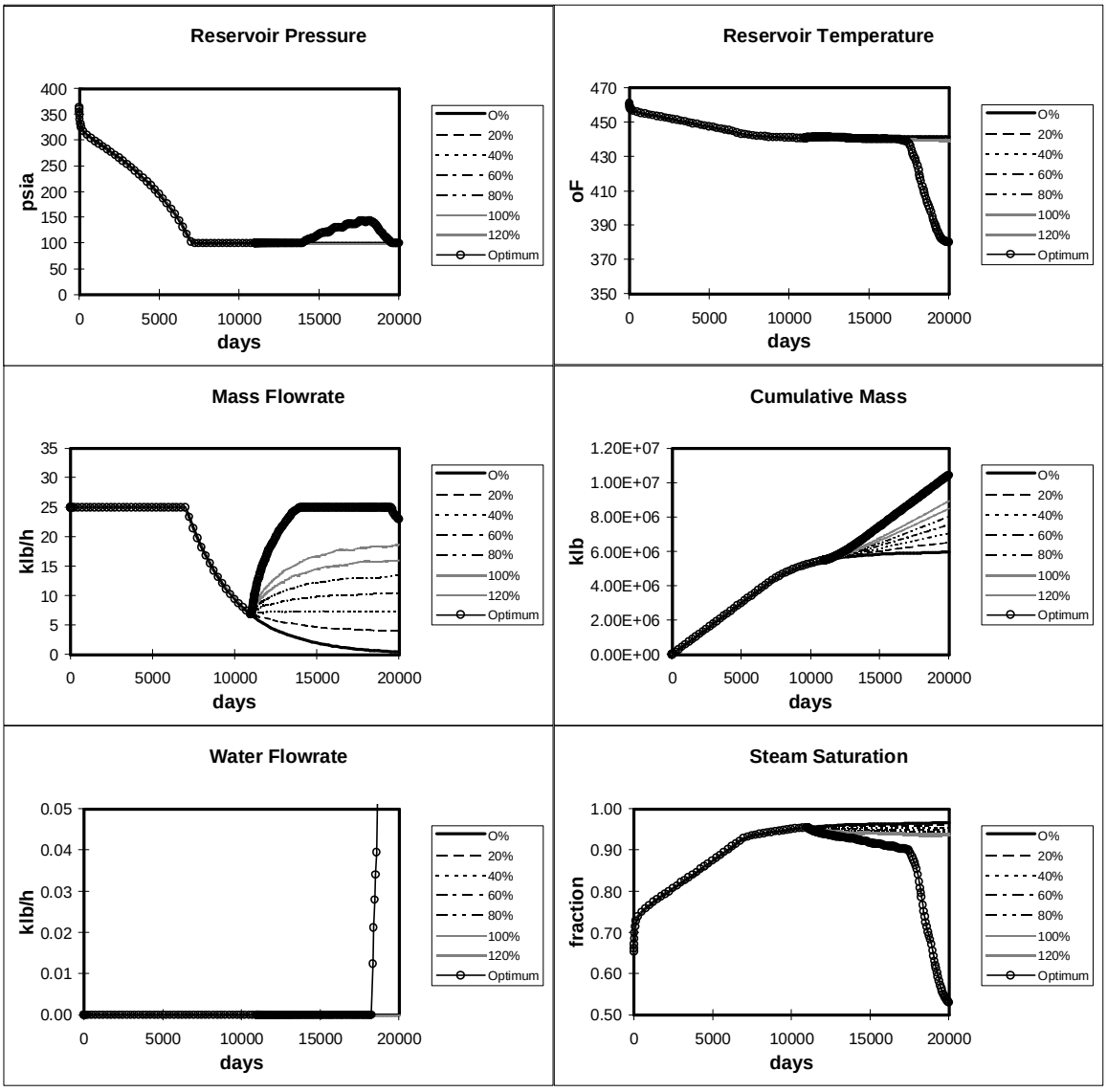

Case VII: Injection starts at t=30 years. Properties measured in the production gridblock.

APPENDIX L: RESULTS OF CASE VII

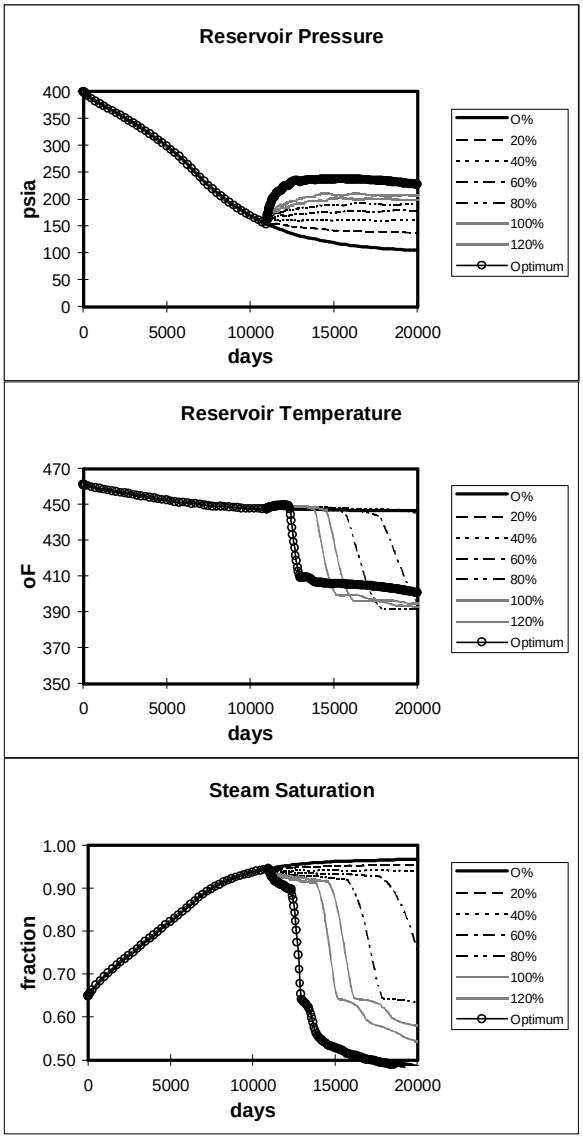

Case VII: Injection starts at t=30 years. Properties measured in the observation gridblock.

M. Injectate Recovery for Various Cases

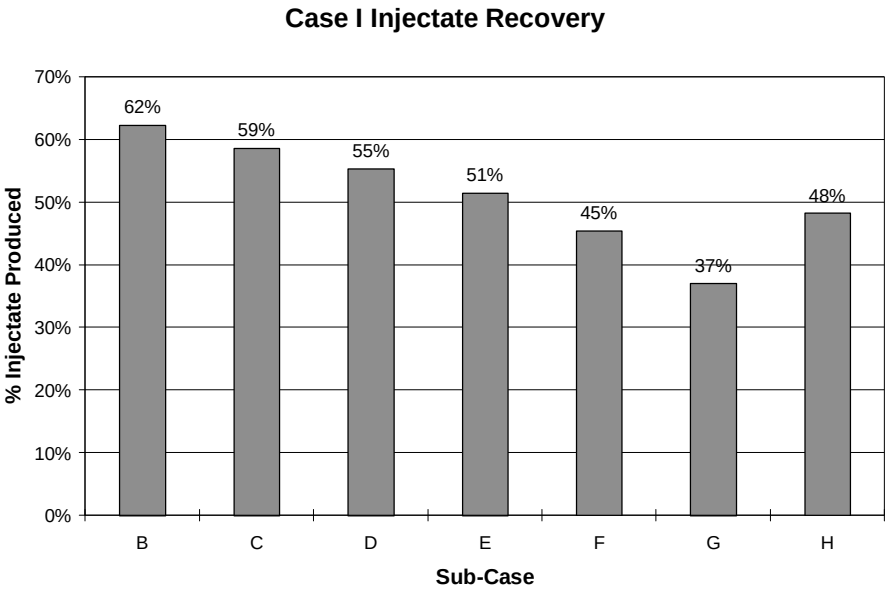

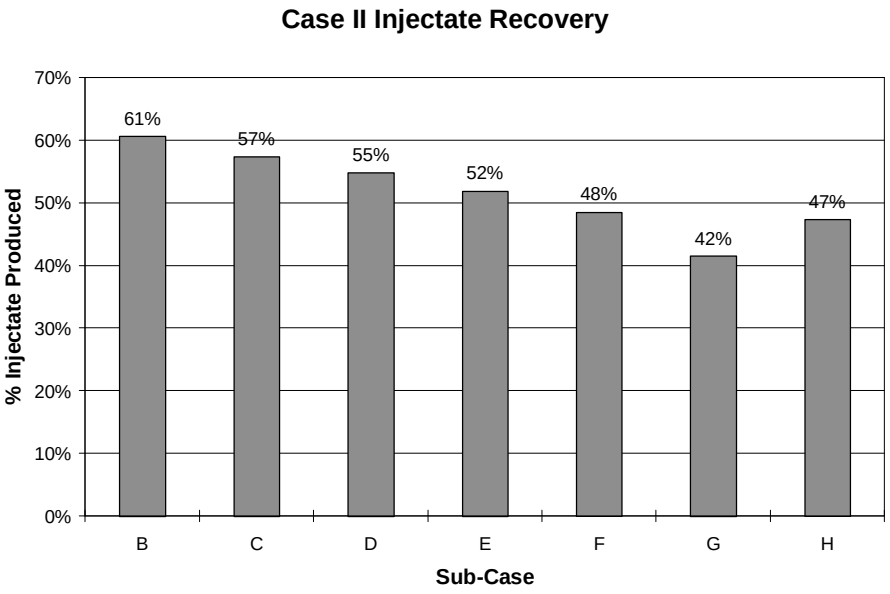

APPENDIX M: INJECTATE RECOVERY FOR VARIOUS CASES

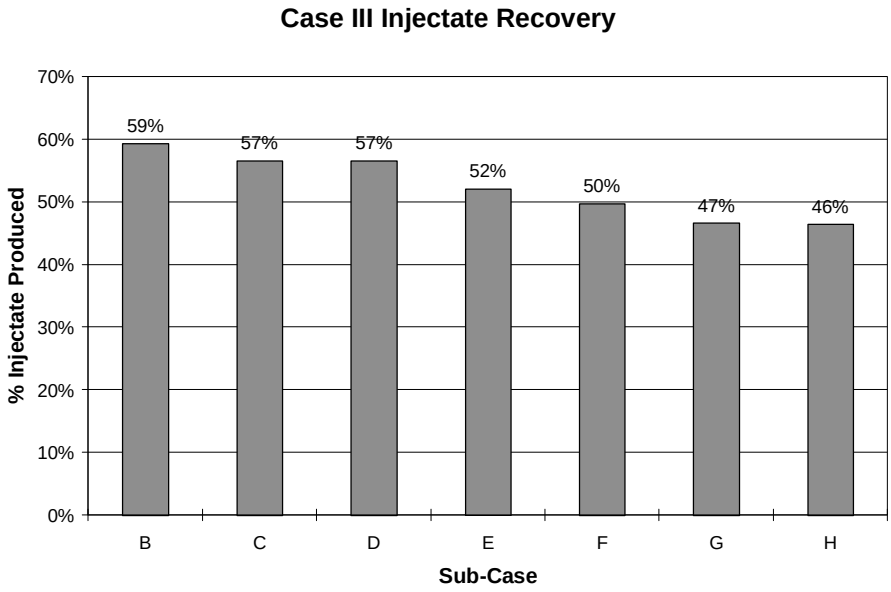

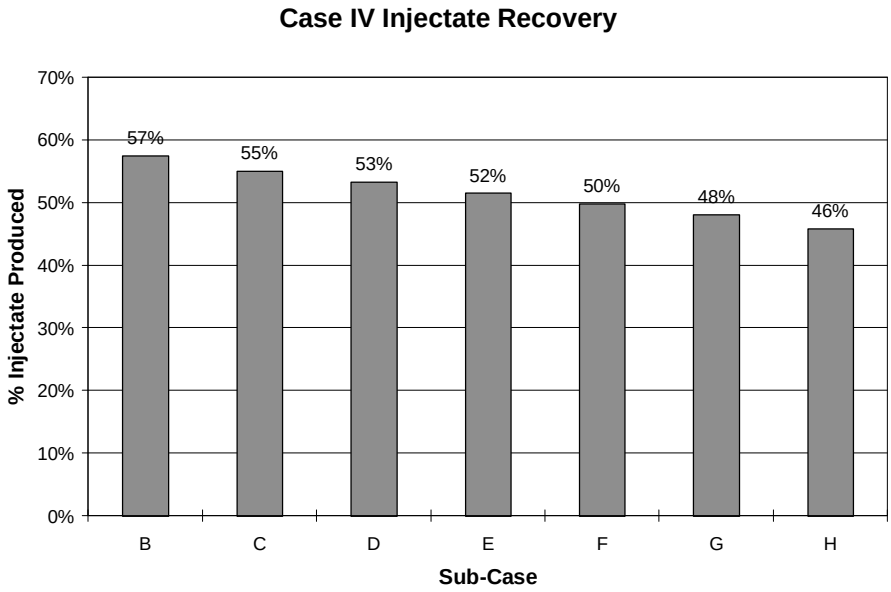

APPENDIX M: INJECTATE RECOVERY FOR VARIOUS CASES

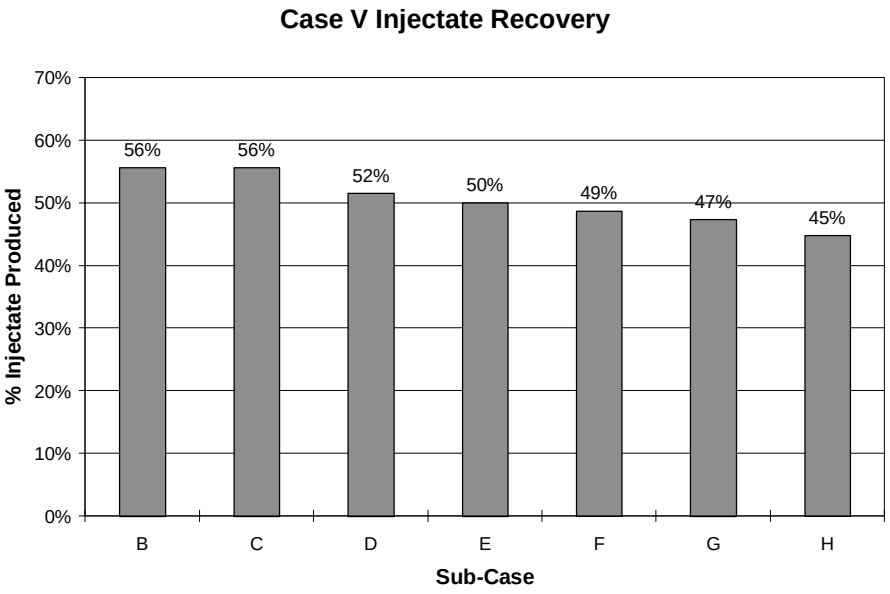

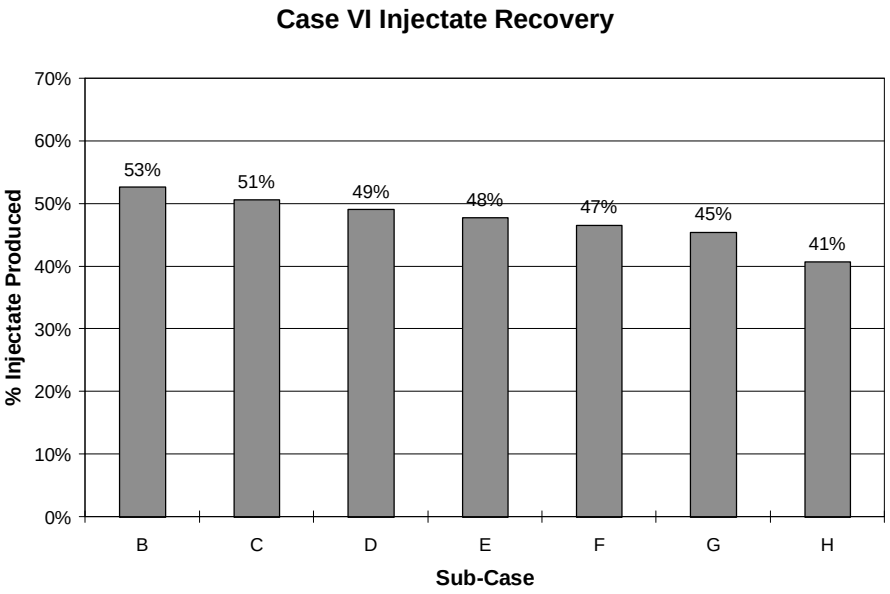

APPENDIX M: INJECTATE RECOVERY FOR VARIOUS CASES

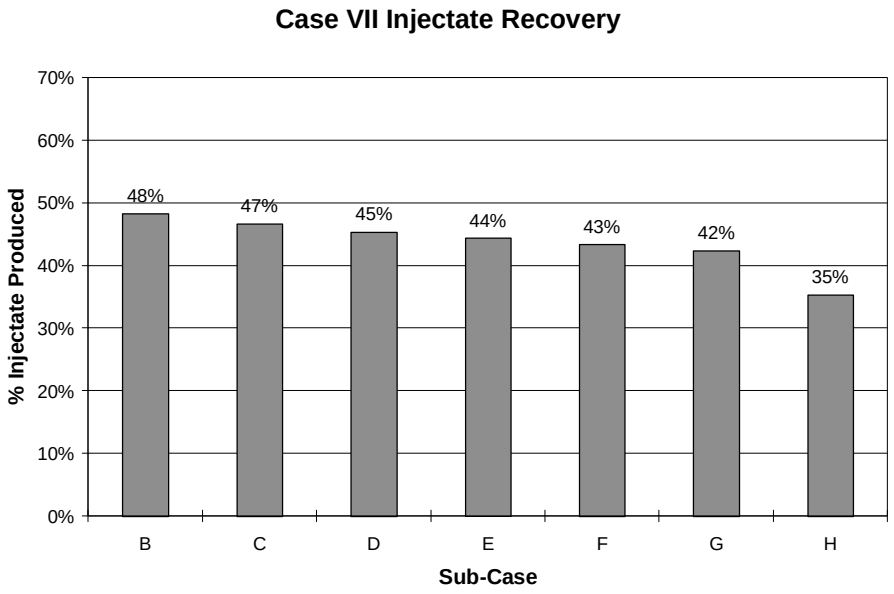

N. Injectate Recovery for Various Injection Rates

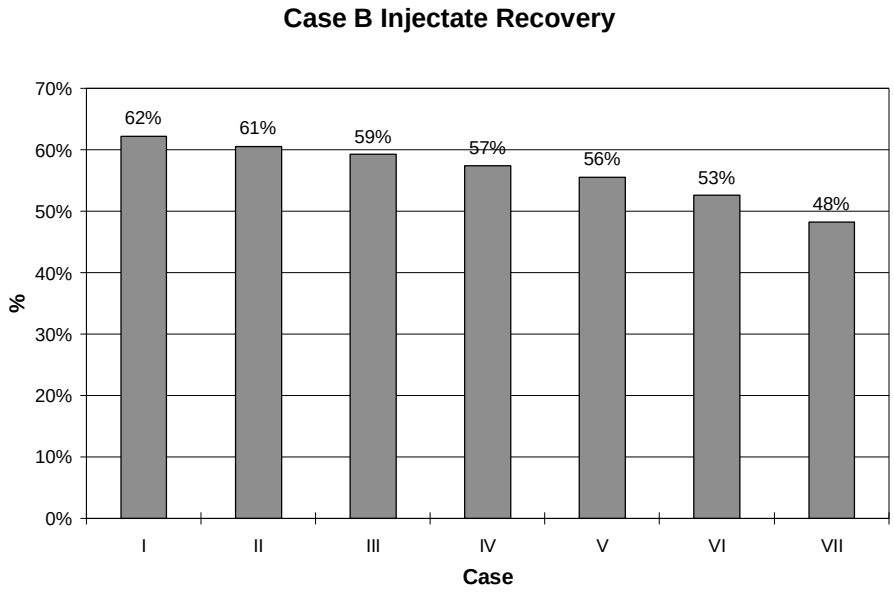

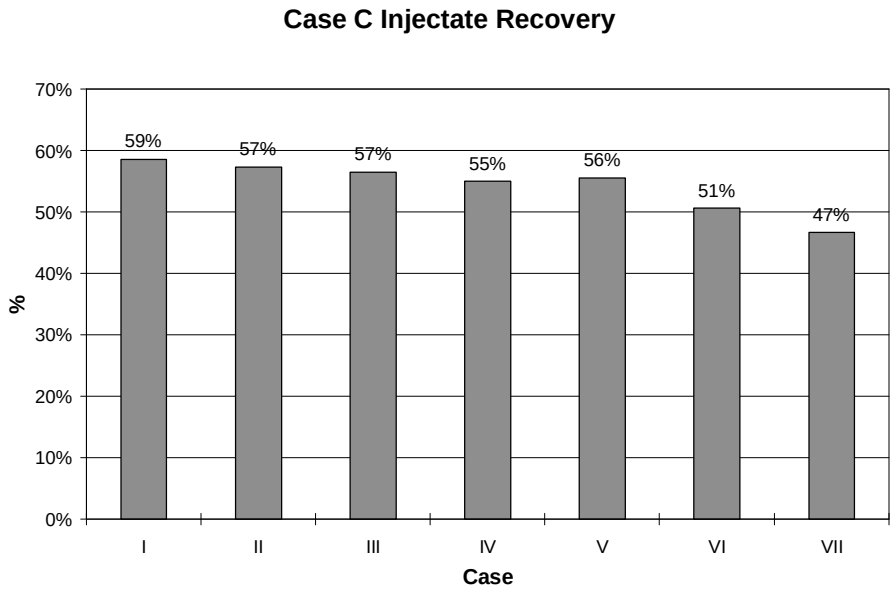

APPENDIX N: INJECTATE RECOVERY FOR VARIOUS INJECTION RATES

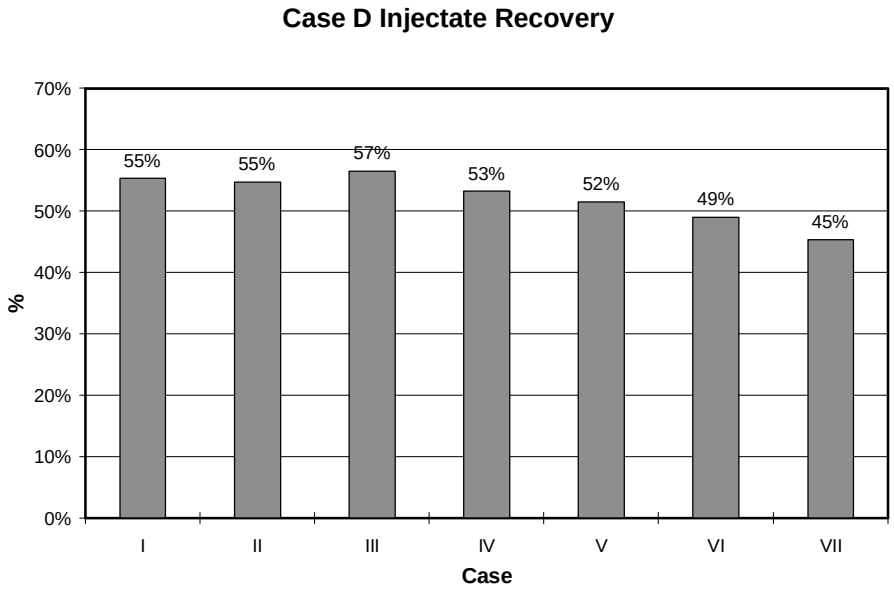

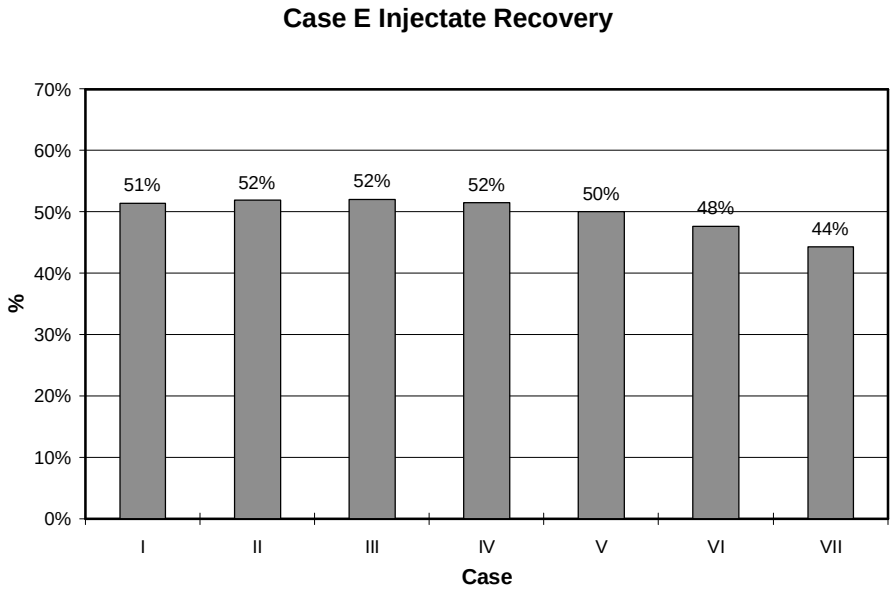

APPENDIX N: INJECTATE RECOVERY FOR VARIOUS INJECTION RATES

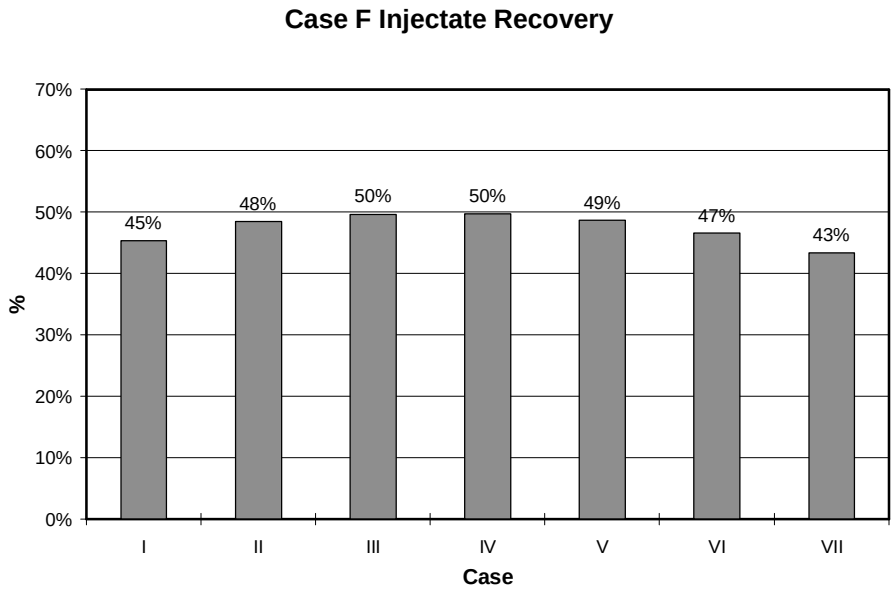

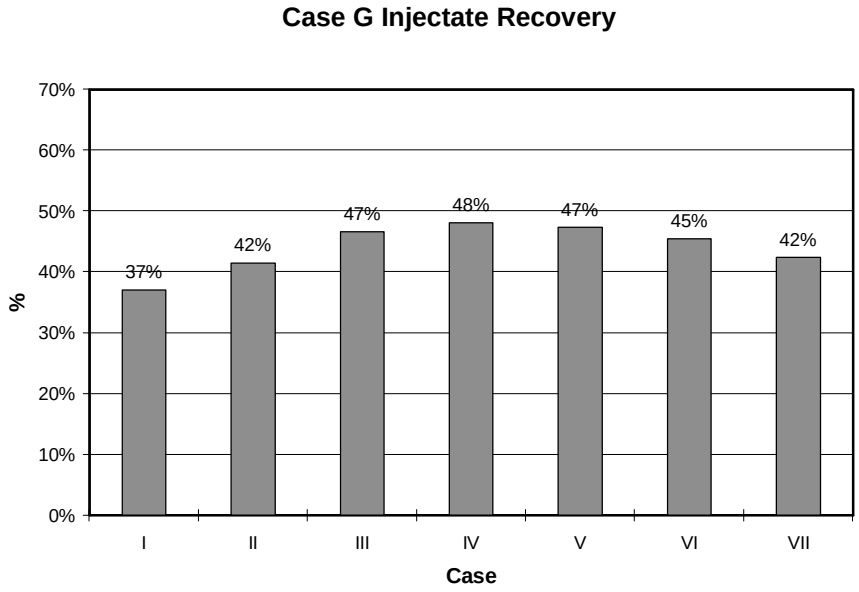

APPENDIX N: INJECTATE RECOVERY FOR VARIOUS INJECTION RATES

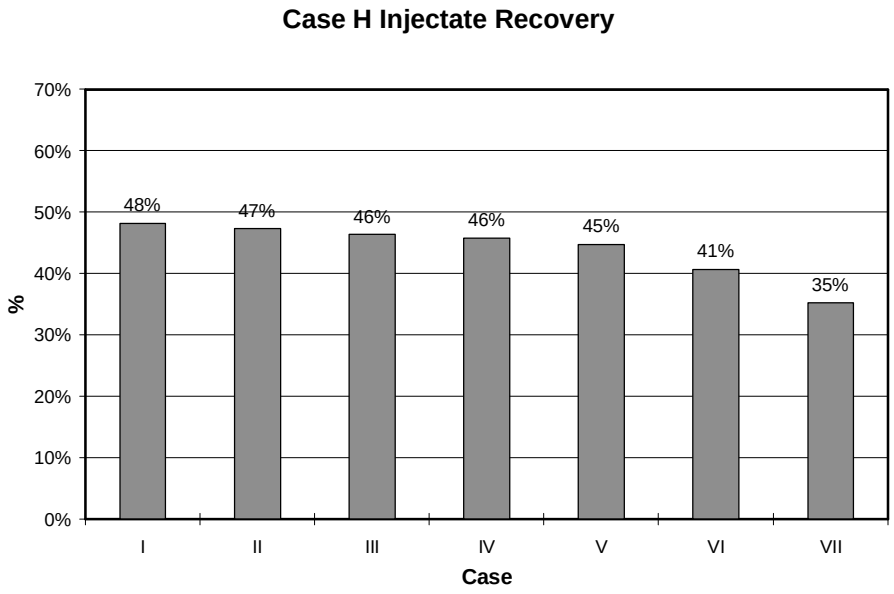

O. Present Worth of Injection Project

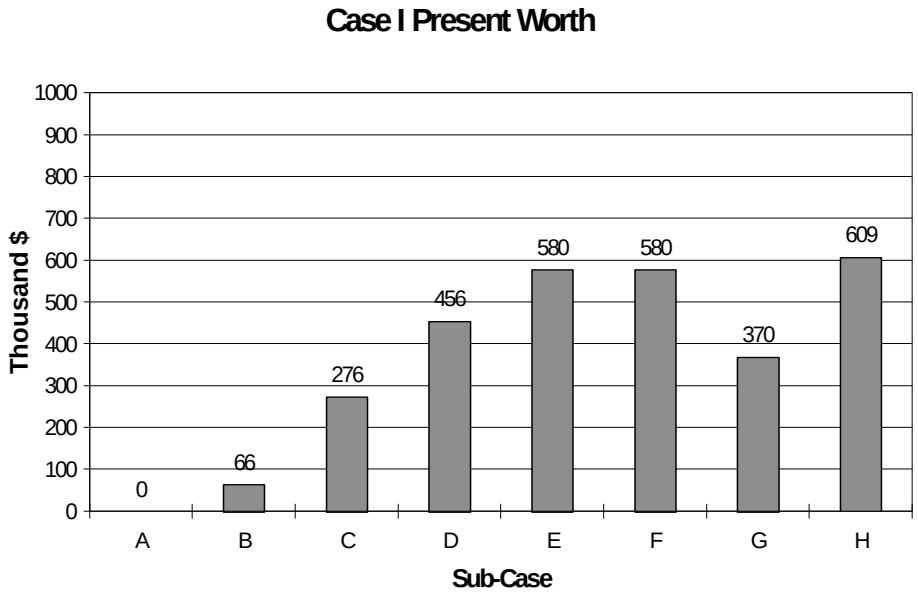

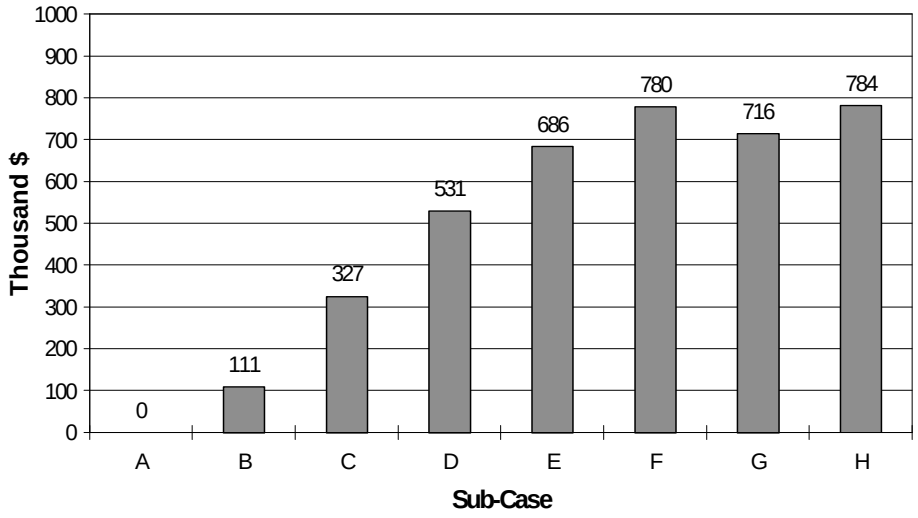

APPENDIX O: PRESENT WORTH OF INJECTION PROJECT

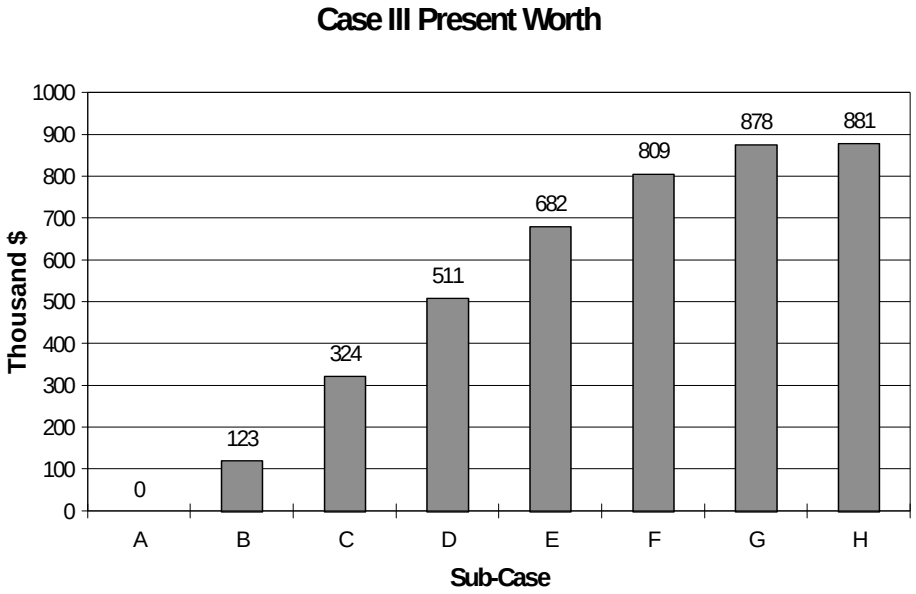

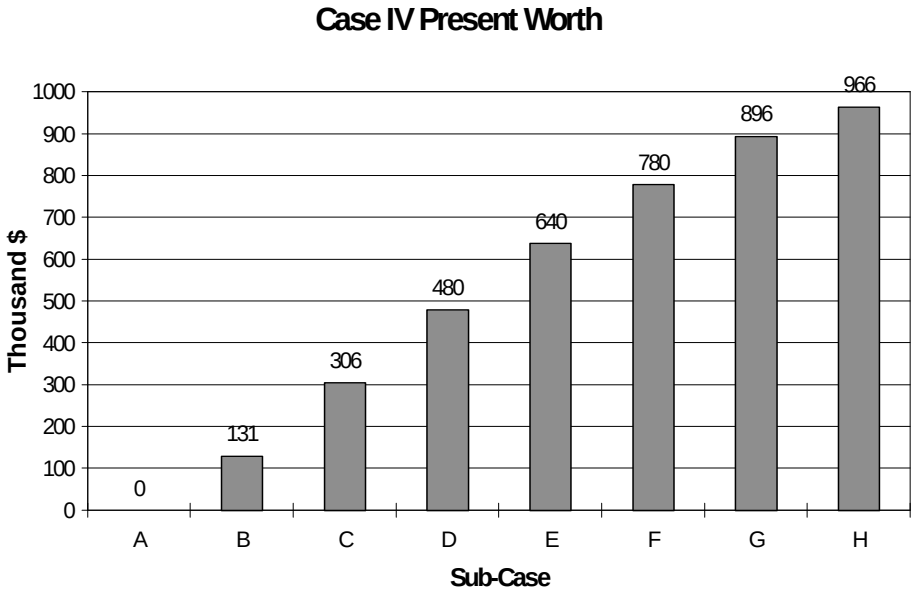

APPENDIX O: PRESENT WORTH OF INJECTION PROJECT

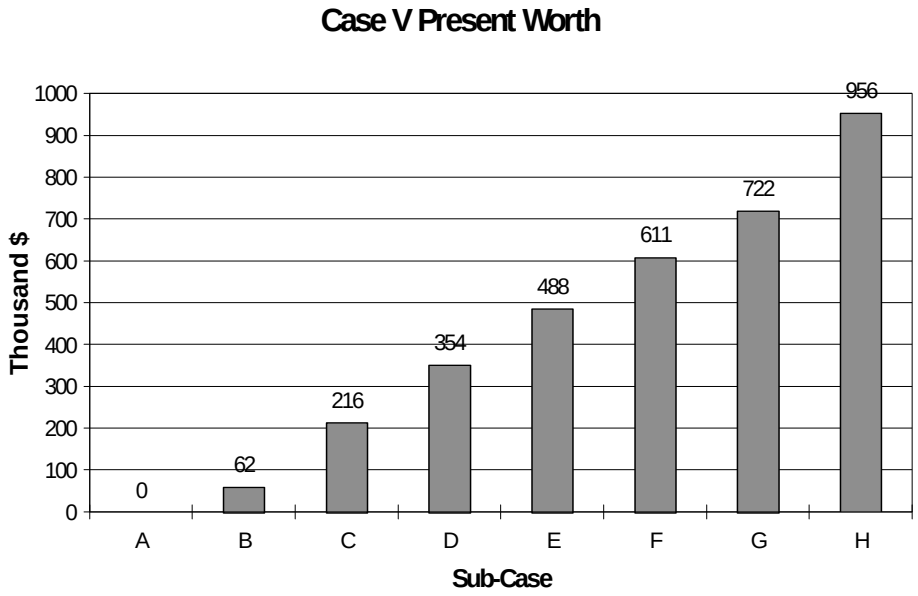

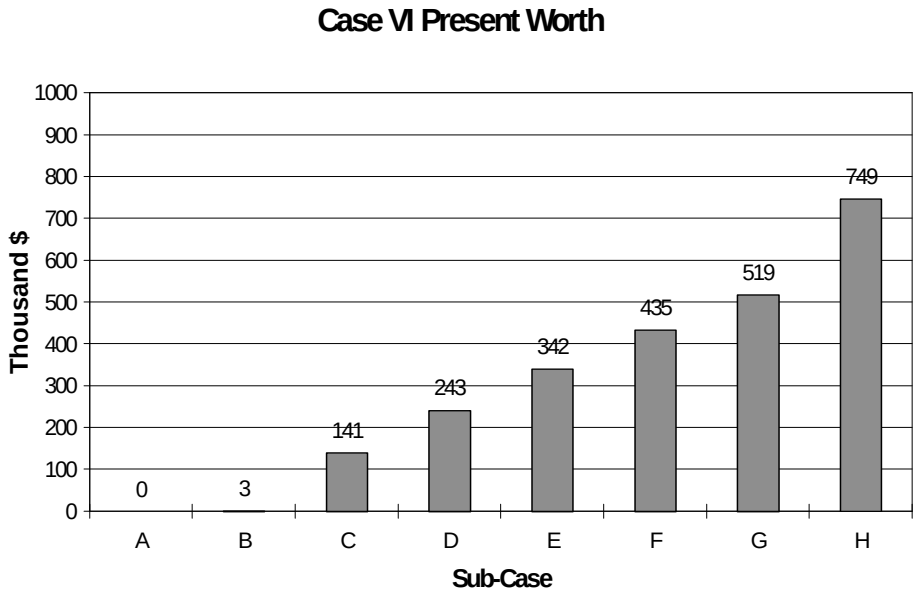

APPENDIX O: PRESENT WORTH OF INJECTION PROJECT

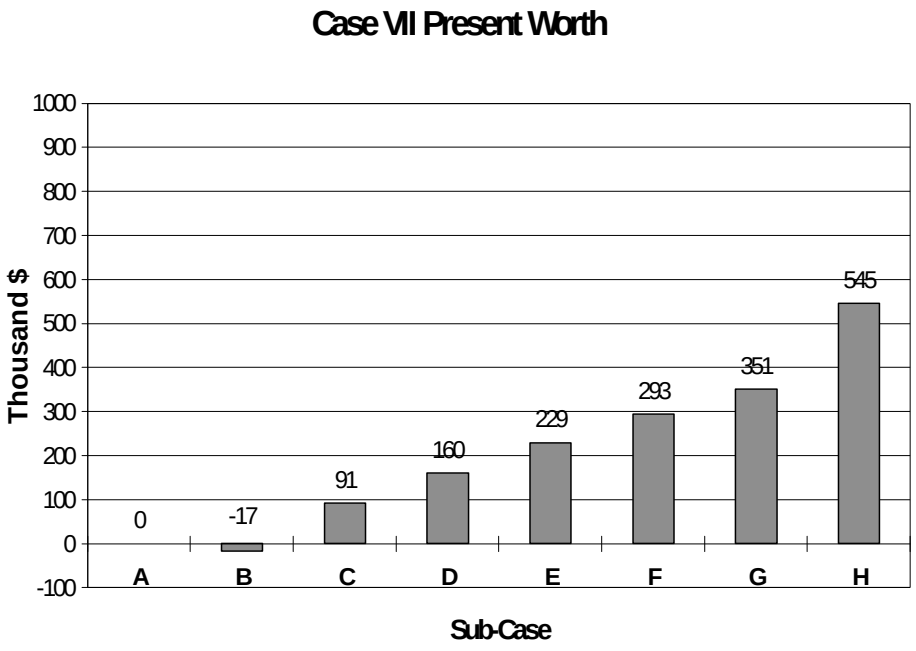

References

1. Barker, B.J., Gulati, M.S., Bryan, M.A., and Riedel, K.L., "Geysers Reservoir Performance", Geothermal Resources Council, Monograph on the Geysers Geothermal Field, Special Report No. 17, 1991.

2. Enedy, S.L., Enedy, K.L., and Maney, J., "Reservoir Response to Injection in the Southeast Geysers", Geothermal Resources Council, Monograph on the Geysers Geothermal Field, Special Report No. 17, 1991.

3. Holt, R., and Pingol, A., "Adding Adsorption to a Geothermal Simulator", Proc. of the 17th Annual Workshop on Geothermal Reservoir Engineering, Stanford University, California, January 1992.

4. Hornbrook, J. W., "The Effects of Adsorption on Injection Into and Production From Vapor-Dominated Geothermal Reservoirs", Ph.D. thesis, Stanford University, California, 1994.

5. Hornbrook, J. W., and Horne, R. N., "The Effects of Adsorption on Injection Into Geothermal Reservoirs", Proc. of the 19th Annual Workshop on Geothermal Reservoir Engineering, Stanford University, California, January 1994.

6. Horne, R., Ramey, H. Jr., Shang, S., Correa, A., and Hornbrook, J., "The Effects of Adsorption and Desorption on Production and Reinjection in Vapor-Dominated Geothermal Fields", Proc. of the World Geothermal Congress 1995, Florence, Italy, May 1995, pp. 1973-77.

7. Hsieh, C.H., and Ramey, H.J. Jr., "Vapor-Pressure Lowering in Geothermal Systems", Society of Petroleum Engineers Journal, February 1983.

8. Lim, K-T., "Simulation of Fractured Reservoir with Sorption and Applications to Geothermal Reservoir", Ph.D. thesis, Stanford University, California, March 1995.

REFERENCES

9. Pruess, K., and O'Sullivan M., "Effects of Capillarity and Vapor Adsorption in the Depletion of Vapor-Dominated Geothermal Reservoirs", Proc. of the 17th Annual Workshop on Geothermal Reservoir Engineering, Stanford University, California, January 1992.

10. Pruess, K., "Numerical Simulation of Water Injection into Vapor-Dominated Reservoirs", Proc. of the World Geothermal Congress 1995, Florence, Italy, May 1995, pp. 1673-79.

11. Shang, S., Horne, R., and Ramey, H. Jr., "Experimental Study of Water Adsorption On Geysers Reservoir Rocks", Proc. of the 18th Annual Workshop on Geothermal Reservoir Engineering, Stanford University, California, January 1993.

12. Shook, M., "Generalization of Vapor Pressure Lowering Effects in an Existing Geothermal Simulator", Idaho National Engineering Laboratory Report, Idaho, June 1993.

13. Shook, M., "Effects of Adsorption on Exploitation of Geothermal Reservoirs", Geothermal Resource Council TRANSACTIONS, Vol. 18, October 1994.

14. Sorey, M.L., "Nonlinear Effects in Two-Phase Flow to Wells in Geothermal Reservoirs", Water Resources Research, Vol. 16, No. 4, August 1980.

15. Sta.Maria, R., and Pingol, A., "Simulating the Effects of Adsorption and Capillary Forces in Geothermal Reservoirs", Proc. of the 21st Annual Workshop on Geothermal Reservoir Engineering, Stanford University, January 1996.